Abstract

Title of Dissertation: Stability Exchange in Parameter-Dependent Constrained Variational Principles with Applications to Elastic Rod Models of DNA Minicircles

Kathleen Ann Rogers, Doctor of Philosophy, 1997

Dissertation directed by: Professor J. H. Maddocks
Department of Mathematics

Novel techniques are developed that exploit certain special features of one-dimensional calculus of variations problems in order to determine the index of critical points. The first technique concerns isoperimetrically constrained problems. It extends Jacobi's theory of unconstrained conjugate points in such a way that an isoperimetric index can be defined by counting certain isoperimetric conjugate points. An associated efficient numerical implementation is also described. The second technique is concerned with unconstrained parameter-dependent calculus of variations problems, in which the parameter-dependence appears in the boundary conditions. The variational structure and parameter-dependence is exploited to predict changes in index at folds in a certain distinguished bifurcation diagram. The third technique determines the appropriate distinguished diagram for parameter-dependent calculus of variations problems involving isoperimetric constraints.

The development of all three of these techniques was motivated by an application in molecular biology. Recently, elastic rods have become a widely accepted model of DNA minicircles. In this model, the rod is twisted and bent into a closed loop, which is mathematically described by an isoperimetrically constrained one-dimensional calculus of variations problem in which the parameter enters through the boundary conditions. The general techniques for computation of a constrained index are then applied to both an idealized problem in which the unstressed shape is straight, and to a model with experimentally motivated parameters. Finally, motivated by numerical calculations of distinguished diagrams, we use a local perturbation expansion to show that certain bifurcating branches in the idealized problem shift between subcritical and supercritical depending on the ratio of the twisting stiffness to the bending stiffness.

Stability Exchange in Parameter-Dependent Constrained Variational Principles with Applications to Elastic Rod Models of DNA Minicircles

by

Kathleen Ann Rogers

Dissertation submitted to the Faculty of the Graduate School of the
University of Maryland at College Park in partial fulfillment
of the requirements for the degree of
Doctor of Philosophy
1997

Advisory Committee:

Professor J. H. Maddocks, Chairman/Advisor
Professor S. S. Antman
Professor L. Greenberg
Professor R. B. Kellogg
Professor P. Wolfe
Associate Professor A. R. Baden

Dedication

For my parents.

Acknowledgements

This thesis has benefited from the advice and support from more people than I could possibly list here. I am indebted to my advisor, Prof. John H. Maddocks, who guided my dissertation research through its many pitfalls and crises. His numerous ideas made this project comprehensive and taught me the nuances of scientific research. I acknowledge Prof. Lee Zia, my undergraduate advisor and mentor, for first introducing me to mathematical research and for his continued support and enthusiasm.

I am grateful to the past and present members of the Laboratory for Computation and Visualization in Mechanics (LCVM) for their help and support. Special thanks go to Dr. Robert Manning, my co-author, whose insight and advice were invaluable; Randy Paffenroth, whose expertise lies behind the many graphics in this dissertation; Stefan Kehrbaum for reading preliminary drafts of this manuscript; and Dr. Donald Dichmann for extensive discussions on Euler parameters.

I am also indebted to my friends and colleagues in the Mathematics Department. Without their strength and support, I would not have advanced to the thesis stage of the program. I thank Tom Frohman, Katie Gurski, Deb Heicklen, Mary Jacobsen, Navin Keswani, Tammy Kolda, Joe Previte, Michelle Previte, Eugene Xia, and especially Bob Hoffman.

Finally, I cannot begin to express my gratitude to my family and friends in NH especially Dad, Mom, Kim, Shane and Karyn, who have always been there for me, especially through my years in graduate school. I thank them for their unwavering confidence in my abilities. This dissertation is as much for them as because of them.

This research was supported by an AASERT Award from ONR.

Table of Contents

List of Tables

List of Figures

Chapter 1

Introduction

Many problems have the structure of a variational principle that allows stability analysis of the equilibria to be reduced to the classic question of characterizing which critical points are actually local minima (in an appropriate sense). A necessary condition for a critical point to be a (local) minimum of a functional is that the second variation be non-negative over an appropriate admissible set of variations. In the problems that follow, we define an *index*, which quantifies the dimension of a space on which the second variation can be made negative, and a critical point will be called *stable* if it has index zero. In a *constrained* variational principle, the admissible set includes only variations on the tangent space to the constraint manifold. Accordingly, a *constrained index* is defined to measure the dimension of a subspace of this tangent space on which the second variation is negative, and as before, stable equilibria are defined to be equilibria with constrained index zero.

The motivation for adopting the adjective stable to describe critical points satisfying the appropriate second variation necessary conditions, is the expectation that this property can in turn be related to dynamic stability of an associated evolutionary system (damped or undamped, linear or nonlinear). We do not pursue a detailed investigation of this connection here, but instead defer to the discussion and citations in Antman [1, p. 170]. Certainly, a purely static characterization of stability has a venerable history, and can be fully justified in many contexts.

The study of the second variation is, of course, a classic subject. In this dissertation, new results are obtained for three different classes of one-dimensional calculus of variations problems. The first technique determines the constrained index in isoperimetrically constrained calculus of variations problems. The second technique exploits parameter-dependence of unconstrained calculus of variations problems when the parameter enters in the boundary conditions. The third technique addresses isoperimetrically constrained, parameter-dependent calculus of variations problems.

The first technique for determining the index of an isoperimetric critical point is a generalization of the classic formulation of conjugate point theory. For unconstrained calculus of variations problems, the absence of a conjugate point on an extremal (Jacobi's condition) is a well-known necessary condition for the extremal to be an unconstrained local minimum [16, p.112]. Morse [47] later introduced the notion of counting conjugate points of the second variation operator to determine an index. The notion of constrained conjugate points appropriate to isoperimetric calculus of variations problems is considerably more obscure. Weierstrass, Kneser, and Bolza (see [7, p. 220]) proposed a definition of constrained conjugate points and derived a test analogous to Jacobi's (unconstrained) condition for a constrained local minimum based on the absence of any isoperimetric conjugate point. In Chapter 2, we set forth an alternative derivation of isoperimetric conjugate points, which proves conducive to defining an isoperimetric index, based on counting the number of isoperimetric conjugate points for an appropriately projected second variation operator. Our formulation also leads naturally to an efficient algorithm for numerical calculation of isoperimetric conjugate points. This algorithm is based on calculations of the determinant of a *constrained stability matrix* whose entries are solutions to appropriate initial value problems.

The second technique addresses unconstrained, but parameter-dependent calculus of variations problems in which the bifurcation parameter appears in the boundary conditions. One-parameter variational principles produce families of extremals whose stability properties can be related to the shapes of the solution curves. Standard bifurcation theory [24, p. 22] predicts that folds in bifurcation diagrams correspond to stability exchanges, i.e. changes in index. Further, in a *distinguished bifurcation diagram*, i.e. a particular projection of the solution set, the index can be shown to change in a known direction. Thus, distinguished diagrams can be used to determine which solutions have index greater than zero, and which therefore do not correspond to minima. Maddocks [42] calculated the abscissa and ordinate of a distinguished diagram for a variational problem whose parameter is present in the integrand of the functional. This dissertation extends these ideas to variational problems in which the bifurcation parameter is present not in the integrand, but instead in the boundary conditions.

The third technique considers parameter-dependent isoperimetrically constrained problems. The constraints impose a restriction on the domain of the second-order operator associated with the second variation, thus, the eigenvalue problem which is appropriate for distinguished diagram theory contains a projection. In previous work by Maddocks [42], the Lagrange multipliers arise naturally as the only bifurcation parameter, but for the class of problems of interest here, the bifurcation parameter is in addition to the multipliers. Understanding the role of the multipliers, in particular in regards to the domain restriction due to the constraints, required new ideas. Perhaps surprisingly, the abscissa and ordinate of the distinguished diagram for the isoperimetrically constrained problem are the same as in the unconstrained problem.

The techniques described here can be used to determine the constrained index, and thus, the stability properties, of twisted elastic rods. Specifically, we first consider a uniform, transversely isotropic, twisted elastic rod and seek equilibrium configurations when this rod is twisted and then closed upon itself to form a stressed loop (see Figure 5.1). This problem can be formulated as an isoperimetrically constrained calculus of variations problem with nonhomogeneous boundary conditions containing the bifurcation parameter, namely the angle by which one end of the rod is twisted relative to the other.

Following Dichmann [10, 11] and Li & Maddocks [37], Euler parameters or quaternions, which relate the orientation of the rod to a fixed coordinate system in space, are used to parametrize $SO(3)$. The equilibrium equations can be written in polynomial form in terms of Euler parameters in contrast to more cumbersome trigonometric expressions which arise with the traditional choice of Euler angles to parametrize $SO(3)$. Although parametrizing $SO(3)$ by Euler parameters is computationally more convenient, it causes unforeseen difficulties in the stability analysis. For instance, the variational problem which describes elastic rods is homogeneous in the Euler parameters, which implies that the second variation vanishes in many directions. Since this phenomenon is an artifact of the representation, it is of no interest in the stability analysis. We show that provided the variations are properly projected, these flat directions can be eliminated straightforwardly.

Additionally, for the idealized elastic loop problem described in Chapter 6, the projection of the Euler parameters can also be chosen so that Jacobi's accessory equation will have constant coefficients when evaluated on the trivial circular solutions. This particular projection leads to a three-dimensional variation whose components correspond to infinitesimal rotations about the tangent, the in-plane normal and the out-of-plane normal components of the body frame. This correspondence is consistent with the three-dimensional stability analysis of planar equilibria presented by Maddocks [40] in terms of Euler angles.

The stability analysis of the twisted elastic loop naturally separates into two categories: the analysis of the planar circular equilibria and the analysis of the nonplanar equilibria. An explicit calculation of the constrained index is possible on the trivial branches because the appropriate projection of Jacobi's accessory equation has constant coefficients. These calculations reveal that the trivial branch comprising single-covered circles is stable until the first bifurcation point and then unstable with the constrained index increasing by two at every bifurcation point. The trivial branches consisting of n-covered circles, $n > 1$, are unstable. At zero twist the index of the n-covered circle is $2(n-1)$ and increases by 2 at each bifurcation point.

For the nontrivial branches, which consist of nonplanar equilibria, stability is determined based on the shape of a distinguished diagram, in accordance with the third general technique described above. As a fold opening to the left is traversed from the lower to upper branch in the twist moment vs. angle projection of the bifurcation diagram, the critical eigenvalue changes sign from negative to positive. In order to be able to fully classify the index everywhere, the index of only one critical point on each branch must be known. The planar analysis at the bifurcation point provides the necessary information in this example. Bifurcations that are supercritical from a stable branch consist of stable equilibria (at least locally) and subcritical nontrivial branches correspond to unstable equilibria. The results reveal both subcritical and supercritical behavior depending on the value of a parameter γ, namely the ratio of the twist stiffness to the bending stiffness.

Motivated by the numerically observed switch between subcritical and supercritical behavior, we present a perturbation expansion of the Euler-Lagrange equations which analytically determines the value of γ at which a subcritical bifurcation point becomes supercritical. The value of γ at which the m^{th} bifurcation point on the trivial branch corresponding to the n-covered circle switches behavior from subcritical to supercritical is

$$\gamma = 1 + \frac{3n^2}{2(n+m)^2}.$$

These analytical results are in concordance with the numerical evidence of the onset of stable equilibria on the first nontrivial branch.

The twisted elastic loop is an accepted model of DNA minicircles (cf. the extensive survey articles by Schlick [54] and Olson [49]). Minicircles are DNA molecules of approximately 150 base-pairs in which the double helix closes upon itself to form a twisted loop. Although the intrinsically straight elastic rod described previously provides a reasonable approximation of the macrostructure of DNA, a better approximation can be obtained by using a formulation that incorporates experimental information regarding local DNA geometry as input parameters to the model, as was done by Manning et al. [45]. The inherent curvature of actual DNA molecules is represented in the elastic rod model as a curved, twisted, unstressed state. Analytical computations of the constrained index are not possible for such a rod model, thus, distinguished diagram theory is ultimately inconclusive because an index must be computed by other means on each connected component of the solution set. Instead, we apply the constrained conjugate point test to determine the stability properties of the computed DNA minicircle equilibria. The results reveal the presence of at least two stable minicircle configurations for each of the eleven molecules studied in [45] which was an unanticipated conclusion. The stability of the equilibria again depends on γ, the ratio of twisting stiffness to bending stiffness.

To close this introduction, I outline the overall structure of the dissertation. The first two chapters contain a description of the general techniques for determining the constrained index of critical points within the structure of one-dimensional calculus of variations problems. The remaining chapters contain a stability analysis of the twisted elastic loop and an elastic rod model of DNA minicircles, which was the application that inspired the development of the general techniques. In Chapter 2, we describe unconstrained conjugate point theory and index in a manner that is conducive to developing the isoperimetric conjugate point theory, and correspondingly the isoperimetric index. In Chapter 3, we present the distinguished diagram theory for variational principles, both unconstrained and isoperimetrically constrained, in which the bifurcation parameter appears in the boundary conditions. Chapter 4 contains a brief description of the elastic rod model used in the examples presented subsequently. In Chapter 5, we present the variational formulation of an idealized elastic rod, the equilibrium equations and a complete description of the solution set. In Chapter 6, we present a bifurcation and stability analysis of the trivial (planar) and nontrivial (nonplanar) equilibria of the twisted elastic loop. In Chapter 7, a perturbation expansion is used to determine the value of γ for which each bifurcation point switches from a subcritical bifurcation to a supercritical bifurcation with respect to the parameter α. In Chapter 8, we summarize the elastic rod model of DNA developed in [45] and then present the results of applying the isoperimetric conjugate point test developed in Chapter 2 to the model. A detailed summary of our results is presented in Chapter 9, along with a discussion of the relation of our results with the current literature. Appendix A contains remarks about an alternative derivation of distinguished diagrams for isoperimetric problems based upon bordered operators, which are an extension of the finite-dimensional theory of bordered matrices. In Appendix B, we derive a general expression for the Lagrange multiplier which enforces the unit length constraint arising in Euler parameters. In Appendix C, we detail the lengthy computations of a certain partial derivative arising in the second variation of the rod example.

Chapter 2

Variational Principles and Conjugate Points

2.1 Introduction

For unconstrained one-dimensional calculus of variations problems of the standard form (2.1) below, the absence of a conjugate point on an extremal (Jacobi's condition) is a well-known necessary condition for the extremal to actually be a local minimum. The goal of this chapter is to derive an analogous conjugate point test for an isoperimetrically constrained variational principle of the form (2.9). Further, the definition of isoperimetric conjugate point proposed here is conducive to our using the number of conjugate points in the interval to define an isoperimetric index analogous to the index of Morse for unconstrained problems. Additionally, an efficient numerical calculation of the isoperimetric index is presented based on counting isoperimetric conjugate points as zeros of the determinant of a constrained stability matrix.

In Section 2.2.1, we describe a derivation of the standard unconstrained conjugate point theory, but from a particular perspective that is amenable to extension to the isoperimetrically constrained case. In Section 2.2.2, we construct the isoperimetric theory and in Section 2.3, we describe the construction of the constrained stability matrix and the numerical implementation of this technique.

2.2 Conjugate Points and Indices

2.2.1 The Unconstrained Case

In this subsection, we set notation and present a self-contained treatment of the standard conjugate point theory in unconstrained calculus of variations problems from a perspective which makes an extension to isoperimetrically constrained problems most transparent. We consider a functional of the form[1]:

$$\begin{gathered} J[\mathbf{q}] = \int_0^1 W(\mathbf{q}, \mathbf{q}', s)\, ds, \quad \mathbf{q}(s) \in \mathbb{R}^p, \\ \mathbf{q}(0) = \mathbf{f}_0, \quad \mathbf{q}(1) = \mathbf{f}_1. \end{gathered} \tag{2.1}$$

[1] We only consider Dirichlet boundary conditions; conjugate point tests exist for more general boundary conditions, but they can be more complicated.

Most of the results cited here are an established part of the classic unconstrained calculus of variations literature and can be found in many standard texts, e.g. [15, 16, 23, 52]. However, index (or signature) theory appears only in more modern treatments [20, 47].

Critical points $\mathbf{q}_0(s)$ are solutions to the standard Euler-Lagrange equations for the functional J:

$$-\frac{d}{ds}W_{\mathbf{q}'} + W_{\mathbf{q}} = \mathbf{0}, \tag{2.2}$$

which also satisfy the boundary conditions in Equation (2.1). Classification of these critical points involves an analysis of the second variation of (2.1) at $\mathbf{q}_0$, namely

$$\delta^2 J[\boldsymbol{\zeta}] = \frac{1}{2}\int_0^1 \left[\boldsymbol{\zeta}'\cdot\mathbf{P}\boldsymbol{\zeta}' + \boldsymbol{\zeta}'\cdot\mathbf{C}^T\boldsymbol{\zeta} + \boldsymbol{\zeta}\cdot\mathbf{C}\boldsymbol{\zeta}' + \boldsymbol{\zeta}\cdot\mathbf{Q}\boldsymbol{\zeta}\right]\, ds, \tag{2.3}$$

where $\mathbf{P} = W_{\mathbf{q}'\mathbf{q}'}$, $\mathbf{C} = W_{\mathbf{q}\mathbf{q}'}$, and $\mathbf{Q} = W_{\mathbf{q}\mathbf{q}}$ are all $p \times p$ matrices evaluated at $\mathbf{q}_0$. We assume throughout that Legendre's strengthened condition holds

$$\mathbf{P} > 0, \tag{2.4}$$

i.e., the symmetric matrix $\mathbf{P}$ is positive definite. Here, $\boldsymbol{\zeta}$ is a variation in the solution that, due to the boundary conditions on $\mathbf{q}_0$, must lie in the set of admissible variations:

$$\mathcal{A}_d \equiv \left\{\boldsymbol{\zeta} \in \mathcal{H}^2(0,1) : \boldsymbol{\zeta}(0) = \mathbf{0} = \boldsymbol{\zeta}(1)\right\}. \tag{2.5}$$

With these boundary conditions, an alternative form of the second variation is achieved after an integration by parts:

$$\delta^2 J[\boldsymbol{\zeta}] \;=\; \frac{1}{2}\langle\boldsymbol{\zeta}, \mathcal{S}\boldsymbol{\zeta}\rangle$$

where $\mathcal{S}$ is the self-adjoint second-order vector differential operator:

$$\mathcal{S}\boldsymbol{\zeta} \equiv -\frac{d}{ds}\left[\mathbf{P}\boldsymbol{\zeta}' + \mathbf{C}^T\boldsymbol{\zeta}\right] + \mathbf{C}\boldsymbol{\zeta}' + \mathbf{Q}\boldsymbol{\zeta}, \tag{2.6}$$

and the notation $\langle\cdot,\cdot\rangle$ represents the standard L^2 inner product. Standard issues concerning domains of definition of quadratic forms of the type (2.3) and densely defined differential operators of the form (2.6) arise (see, for example [50] Section VIII.6), but are not of primary concern here.

A necessary condition for $\mathbf{q}_0$ to be a local minimum of J is that

$$\delta^2 J[\boldsymbol{\zeta}] \geq 0 \;\; \forall \boldsymbol{\zeta} \in \mathcal{A}_d. \tag{2.7}$$

Given Legendre's strengthened condition (2.4), condition (2.7) is equivalent to Jacobi's necessary condition, namely that $\mathbf{q}_0$ has no *conjugate point.* A conjugate point is defined to be a value $0 < \sigma < 1$ for which there is a nontrivial solution to:

$$\mathcal{S}\boldsymbol{\zeta} = \mathbf{0}, \quad 0 < s < \sigma, \quad \boldsymbol{\zeta}(0) = \boldsymbol{\zeta}(\sigma) = \mathbf{0}.$$

Morse [47] extended Jacobi's condition to use the *number* of conjugate points to define an index which quantifies the maximal dimension of a space on which $\delta^2 J$ is negative; our presentation of the index is not the one given by Morse, but rather an equivalent form suitable for extension to the constrained case. We embed Jacobi's condition into the eigenvalue problem

$$\mathcal{S}\boldsymbol{\zeta} = \rho\boldsymbol{\zeta}, \quad 0 < s < \sigma, \quad \sigma \le 1, \quad \boldsymbol{\zeta}(0) = \boldsymbol{\zeta}(\sigma) = \mathbf{0}. \tag{2.8}$$

The eigenvalues ρ will generally depend on σ, so we denote them $\rho(\sigma)$. Conjugate points are then values of σ for which (2.8) has $\rho(\sigma) = 0$ as an eigenvalue. Using Legendre's strengthened condition, Rayleigh quotients, and other techniques (see, e.g., the proofs in Section 2.2.2 for the constrained case), one can derive the following three properties:

Property 2.1. *For prescribed σ, the operator $\mathcal{S}$ has a countable infinity of isolated eigenvalues $\rho_1(\sigma) \le \rho_2(\sigma) \le \cdots$, each with finite multiplicity.*

Property 2.2. *Each eigenvalue $\rho_j(\sigma)$ is a monotonically decreasing function of σ.*

Property 2.3. *For σ sufficiently close to 0, $\rho_j(\sigma) > 0$ for all j.*

The *index* I is then defined to be the number of eigenvalues $\rho_j(1)$ of (2.8) that are negative. Due to Properties 2.1, 2.2, 2.3, the index is equal to the number of conjugate points $0 < \sigma < 1$, counted according to multiplicity.[2] If $I = 0$, then Jacobi's necessary condition holds, and we shall describe $\mathbf{q}_0$ as *stable.* If $I > 0$, then $\mathbf{q}_0$ is not a local minimum (in any of the standard topologies), and in fact there is a subspace of variations of dimension I on which $\delta^2 J < 0$.

2.2.2 The Isoperimetric Case

The focus of this section is to extend the notion of index to isoperimetrically constrained calculus of variations problems involving functionals of the form:[3]

$$\begin{gathered}\int_0^1 W(\mathbf{q}, \mathbf{q}', s)\, ds, \quad \mathbf{q}(s) \in \mathbb{R}^p, \\ \int_0^1 g_i(\mathbf{q})\, ds = 0, \quad i = 1, \ldots, n, \\ \mathbf{q}(0) = \mathbf{f}_0, \quad \mathbf{q}(1) = \mathbf{f}_1.\end{gathered} \tag{2.9}$$

[2] This conclusion relies on both the isolation of the conjugate points σ and on the continuity of $\rho_j(\sigma)$ with respect to σ. Both these properties are standard in the unconstrained setting; for example, isolation of conjugate points has been proven by Morse [47] and the continuity of ρ follows from an argument based on Green's functions, see e.g. [48, 62].

[3] For convenience, we only consider isoperimetric constraints with integrands of the form $g(\mathbf{q}(s))$, although the analysis can immediately be extended to the more general case $g(\mathbf{q}(s), \mathbf{q}'(s), s)$.

According to the usual multiplier rule, an associated functional

$$J[\mathbf{q}] = \int_0^1 (W + \mathbf{g} \cdot \boldsymbol{\lambda})\ ds$$

is constructed, and constrained critical points $(\mathbf{q}_0(s), \boldsymbol{\lambda}_0)$ of J are solutions of the standard unconstrained Euler-Lagrange equations (2.2) for the functional J, with the multiplier $\boldsymbol{\lambda}_0$ determined by the integral constraints. The second variation $\delta^2 J$, and its associated operator $\mathcal{S}$, take the unconstrained forms (2.3) and (2.6), but now with $\mathbf{Q} = \mathbf{g}_{\mathbf{qq}} \cdot \boldsymbol{\lambda}_0 + W_{\mathbf{qq}}$. The variations $\boldsymbol{\zeta}$ must satisfy the linearized constraints

$$\int_0^1 \boldsymbol{\zeta} \cdot \frac{\partial g_i}{\partial \mathbf{q}}(\mathbf{q}_0)\ ds = 0, \quad i = 1, \ldots, n$$

giving rise to the admissible set of constrained variations:

$$\mathcal{A}_d^{cons} \equiv \left\{ \boldsymbol{\zeta} \in \mathcal{A}_d : \int_0^1 \boldsymbol{\zeta} \cdot \mathbf{T}_i\ ds = 0, \quad i = 1, \cdots, n \right\}, \tag{2.10}$$

where:

$$\mathbf{T}_i \equiv \frac{\partial g_i}{\partial \mathbf{q}}(\mathbf{q}_0).$$

We assume that the $\mathbf{T}_i(s)$ are linearly independent as functions of s on every interval $(0, \sigma)$ for $0 < \sigma < 1$.

A necessary condition for $\mathbf{q}_0$ to realize a constrained local minimum [23, p. 85] is

$$\delta^2 J[\boldsymbol{\zeta}] = \langle \boldsymbol{\zeta}, \mathcal{S}\boldsymbol{\zeta} \rangle \geq 0 \ \ \forall \boldsymbol{\zeta} \in \mathcal{A}_d^{cons}. \tag{2.11}$$

The goal of this section is to use a suitably projected eigenvalue problem $\mathcal{Q}\mathcal{S}\mathcal{Q}\boldsymbol{\zeta} = \rho\boldsymbol{\zeta}$ analogous to (2.8) to define an isoperimetric index that can be determined by counting the number of certain isoperimetric conjugate points. In particular, the absence of an isoperimetric conjugate point will be equivalent to the condition (2.11). In anticipation of the definition of isoperimetric conjugate point, we define a family of projections $\mathcal{Q}(\sigma)$, where $0 < \sigma \leq 1$;

$$\mathcal{Q}(\sigma)\boldsymbol{\zeta} \equiv \boldsymbol{\zeta} - \sum_{i,j=1}^{n} \mathbf{T}_i \xi_{ij} \int_0^\sigma \boldsymbol{\zeta} \cdot \mathbf{T}_j, \tag{2.12}$$

is a self-adjoint orthogonal projection which maps $L^2(\sigma)$, (i.e. the L^2-functions on the interval $(0, \sigma)$), onto

$$\mathcal{T}^\perp(\sigma) \equiv \left\{ \boldsymbol{\zeta} \in L^2(\sigma) : \int_0^\sigma \boldsymbol{\zeta} \cdot \mathbf{T}_i\ ds = 0, i = 1, \ldots, n \right\}. \tag{2.13}$$

The matrix $\mathbf{\Xi} = \{\xi_{ij}\}$ is defined by $\mathbf{\Xi}^{-1} \equiv \{\int_0^\sigma \mathbf{T}_i \cdot \mathbf{T}_j \; ds\}$ (this matrix being nonsingular by virtue of the linear independence of the $\mathbf{T}_i$ on each subinterval $(0, \sigma)$). The kernel of $\mathcal{Q}(\sigma)$ is

$$\mathcal{T} \equiv \operatorname{span}(\mathbf{T}_1, \ldots, \mathbf{T}_n). \tag{2.14}$$

Henceforth, for ease of notation the dependence of the projection on σ will usually be suppressed; therefore, $\mathcal{Q}(\sigma)$ will be denoted $\mathcal{Q}$.

For convenience, we define two additional spaces, namely

$$\mathcal{A}_d(\sigma) \equiv \left\{\boldsymbol{\zeta} \in \mathcal{H}^2(0,\sigma) : \boldsymbol{\zeta}(0) = \mathbf{0} = \boldsymbol{\zeta}(\sigma)\right\}, \tag{2.15}$$

which is a generalization of the space defined in Equation (2.5) and

$$\mathcal{A}_d^{cons}(\sigma) \equiv \left\{\boldsymbol{\zeta} \in \mathcal{A}_d(\sigma) : \int_0^\sigma \boldsymbol{\zeta} \cdot \mathbf{T}_i \; ds = 0, \;\; i = 1, \cdots, n\right\}. \tag{2.16}$$

Other choices of projection $\mathcal{Q}$ could be made. In particular, we remark that $\mathcal{Q}(1)$ does not map $L^2(1)$ onto the space of admissible variations $\mathcal{A}_d^{cons}(1)$, but rather onto $\mathcal{T}^\perp(1)$, because the functions $\mathbf{T}_i(s)$ will, in general, not satisfy the Dirichlet boundary conditions. Nevertheless, the choice of projection operator (2.12) has desirable properties as will be seen later.

To develop a test for condition (2.11), we first trivially equate the quadratic forms $\langle \boldsymbol{\zeta}, \mathcal{S}\boldsymbol{\zeta}\rangle$ and $\langle \boldsymbol{\zeta}, \mathcal{Q}\mathcal{S}\mathcal{Q}\boldsymbol{\zeta}\rangle$ for $\boldsymbol{\zeta} \in \mathcal{A}_d^{cons}(\sigma)$. The sign of $\langle \boldsymbol{\zeta}, \mathcal{Q}\mathcal{S}\mathcal{Q}\boldsymbol{\zeta}\rangle$ for $\boldsymbol{\zeta} \in \mathcal{A}_d^{cons}(\sigma)$ can then be related to the eigenvalues of the densely defined operator $\mathcal{Q}\mathcal{S}\mathcal{Q} : \mathcal{A}_d^{cons} \subset \mathcal{T}^\perp \to \mathcal{T}^\perp$ by means of a Rayleigh quotient. Accordingly, consider the eigenvalue problem analogous to (2.8) in the unconstrained case

$$\mathcal{Q}\mathcal{S}\mathcal{Q}\boldsymbol{\zeta} = \rho(\sigma)\boldsymbol{\zeta}, \quad 0 < s < \sigma, \;\; \boldsymbol{\zeta} \in \mathcal{A}_d^{cons}(\sigma), \tag{2.17}$$

which has the following three properties analogous to Properties 2.1, 2.2, 2.3 in the unconstrained setting:

Property 2.4. *For prescribed σ, the operator $\mathcal{Q}\mathcal{S}\mathcal{Q}$ has at most a countable infinity of isolated eigenvalues $\rho_1(\sigma) \leq \rho_2(\sigma) \leq \cdots$, each with finite (geometric) multiplicity.*

Proof. The fact of central importance is that $\mathcal{Q}\mathcal{S} : \mathcal{A}_d(\sigma) \subset L^2(\sigma) \to L^2(\sigma)$ is a compact perturbation of $\mathcal{S} : \mathcal{A}_d(\sigma) \subset L^2(\sigma) \to L^2(\sigma)$. To show this, we write $\mathcal{Q}$ as $\mathcal{I} - \mathcal{P}$, where $\mathcal{P}$ is the orthogonal projection of $L^2(\sigma)$ onto $\mathcal{T}$, and compute:

$$\mathcal{F} \equiv \mathcal{Q}\mathcal{S} - \mathcal{S} = -\mathcal{P}\mathcal{S}$$

It is thus clear that $\mathcal{F}$ has finite rank (which implies $\mathcal{F}$ is compact), since its range is spanned by $\{\mathbf{T}_1, \cdots, \mathbf{T}_n\}$.

Under the standard assumption that the coefficient matrix $\mathbf{P}$ is positive definite (which is true for the examples presented in this dissertation), it is well-known that the Sturm-Liouville operator $\mathcal{S}$ is bounded below and has a countable infinity of isolated eigenvalues each with finite multiplicity, and hence no essential spectrum (see, e.g. [51]). Because $\mathcal{QS}$ is a compact perturbation of $\mathcal{S}$, it also has no essential spectrum [29, p. 244]. Hence $\mathcal{QS}$ has only isolated eigenvalues with finite multiplicity.

Let $(\rho, \boldsymbol{\zeta})$ with $\boldsymbol{\zeta} \in \mathcal{A}_d(\sigma)$ be an eigenpair for $\mathcal{QS}$, i.e.

$$\mathcal{QS}\boldsymbol{\zeta} = \rho\boldsymbol{\zeta}, \quad \boldsymbol{\zeta} \in \mathcal{A}_d(\sigma). \tag{2.18}$$

If $\rho \neq 0$, then we may rewrite this expression as

$$\boldsymbol{\zeta} = \mathcal{QS}(\boldsymbol{\zeta}/\rho)$$

and thus conclude that $\boldsymbol{\zeta}$ is in the range of $\mathcal{Q}$, i.e. $\boldsymbol{\zeta} \in \mathcal{T}^{\perp}(\sigma)$. Since $\mathcal{Q}$ is the identity on $\mathcal{T}^{\perp}(\sigma)$, we may rewrite the equation in (2.18) as:

$$\mathcal{QSQ}\boldsymbol{\zeta} = \rho\boldsymbol{\zeta}.$$

Further, since $\boldsymbol{\zeta}$ is an element of both $\mathcal{A}_d(\sigma)$ and $\mathcal{T}^{\perp}(\sigma)$, we have $\boldsymbol{\zeta} \in \mathcal{A}_d^{cons}(\sigma)$.

We have thus shown that any solution to the $\mathcal{QS}$ eigenvalue problem (2.18) with $\rho \neq 0$ is also a solution to the $\mathcal{QSQ}$ eigenvalue problem (2.17). The multiplicity of $\rho = 0$ for (2.18) and the multiplicity of $\rho = 0$ for (2.17) differ by at most finite number. Therefore, since the spectrum of (2.18) has been shown to satisfy Property 2.4, the spectrum of (2.17) must do so as well. $\square$

The operator $\mathcal{QSQ} : \mathcal{A}_d^{cons}(\sigma) \subset \mathcal{T}^{\perp}(\sigma) \to \mathcal{T}^{\perp}(\sigma)$ is self-adjoint, linear, bounded below, and obeys Property 2.4. Further, $\mathcal{A}_d^{cons}(\sigma)$ is dense in $\mathcal{T}^{\perp}(\sigma)$ (using Lemma 1 on p. 184 of [69] along with the standard fact that $\mathcal{A}_d(\sigma)$ is dense in $L^2(\sigma)$). Therefore, the eigenvalues $\rho_j(\sigma)$ are given by a variational principle [69, p. 6]:

$$\rho_m(\sigma) = \min_{\boldsymbol{\zeta} \in \mathcal{B}_m(\sigma)} \frac{\int_0^\sigma \boldsymbol{\zeta}^T \mathcal{QSQ}\boldsymbol{\zeta}\, ds}{\int_0^\sigma \boldsymbol{\zeta}^T \boldsymbol{\zeta}\, ds} = \min_{\boldsymbol{\zeta} \in \mathcal{B}_m(\sigma)} \frac{\int_0^\sigma \boldsymbol{\zeta}^T \mathcal{S}\boldsymbol{\zeta}\, ds}{\int_0^\sigma \boldsymbol{\zeta}^T \boldsymbol{\zeta}\, ds} \tag{2.19}$$

where the eigenfunctions $\boldsymbol{\zeta}_i(s;\sigma)$ of the operator $\mathcal{QSQ}$ depend on σ and accordingly, the dependence is transfered to the spaces:

$$\mathcal{B}_1(\sigma) \equiv \mathcal{A}_d^{cons}(\sigma),$$

$$\mathcal{B}_m(\sigma) \equiv \left\{ \boldsymbol{\zeta} \in \mathcal{A}_d^{cons}(\sigma) : \int_0^\sigma \boldsymbol{\zeta}(s)^T \boldsymbol{\zeta}_1(s;\sigma)\, ds = \cdots \right.$$
$$\left. \cdots = \int_0^\sigma \boldsymbol{\zeta}(s)^T \boldsymbol{\zeta}_{m-1}(s;\sigma)\, ds = 0 \right\} \; ; \; m > 1.$$

Note that the Rayleigh quotient is invariant to the presence of $\mathcal{Q}$.

Property 2.5. *Each eigenvalue $\rho_j(\sigma)$ is a monotonically decreasing function of σ.*

Proof. Consider $\sigma_1 < \sigma_2$. Let the functions $\boldsymbol{\psi}_i(s), \quad i = 1, \ldots, m$ be defined on $0 \leq s \leq \sigma_2$ by:

$$\boldsymbol{\psi}_i(s) \equiv \begin{cases} \boldsymbol{\zeta}_i(s;\sigma_1) & 0 \leq s \leq \sigma_1 \\ \mathbf{0} & \sigma_1 < s \leq \sigma_2. \end{cases}$$

Now determine a nontrivial linear combination $\sum_{k=1}^m a_k \boldsymbol{\psi}_k(s)$ which is orthogonal to every element of $\mathrm{span}(\boldsymbol{\zeta}_1(s;\sigma_2), \cdots, \boldsymbol{\zeta}_{m-1}(s;\sigma_2))$, and hence an element of $\mathcal{B}_m(\sigma_2)$:

$$\begin{bmatrix} \int_0^{\sigma_2} \boldsymbol{\zeta}_1^T \boldsymbol{\psi}_1 & \int_0^{\sigma_2} \boldsymbol{\zeta}_1^T \boldsymbol{\psi}_2 & \cdots & \int_0^{\sigma_2} \boldsymbol{\zeta}_1^T \boldsymbol{\psi}_m \\ \int_0^{\sigma_2} \boldsymbol{\zeta}_2^T \boldsymbol{\psi}_1 & \int_0^{\sigma_2} \boldsymbol{\zeta}_2^T \boldsymbol{\psi}_2 & \cdots & \int_0^{\sigma_2} \boldsymbol{\zeta}_2^T \boldsymbol{\psi}_m \\ \vdots & \vdots & \ddots & \vdots \\ \int_0^{\sigma_2} \boldsymbol{\zeta}_{m-1}^T \boldsymbol{\psi}_1 & \int_0^{\sigma_2} \boldsymbol{\zeta}_{m-1}^T \boldsymbol{\psi}_2 & \cdots & \int_0^{\sigma_2} \boldsymbol{\zeta}_{m-1}^T \boldsymbol{\psi}_m \end{bmatrix} \begin{bmatrix} a_1 \\ a_2 \\ \vdots \\ \vdots \\ a_m \end{bmatrix} = \mathbf{0}. \tag{2.20}$$

Since the matrix in (2.20) has one more column than rows, a nontrivial solution always exists. For convenience, we rescale so that $\sum_{k=1}^m a_k^2 = 1$.

Inserting $\boldsymbol{\zeta} = \sum_{k=1}^m a_k \boldsymbol{\psi}_k(s)$ into (2.19), we have:

$$\rho_m(\sigma_2) \leq \frac{\int_0^{\sigma_2} \left[\sum_{i=1}^m a_i \boldsymbol{\psi}_i(s)\right]^T \mathcal{Q}(\sigma_2)\mathcal{S}\mathcal{Q}(\sigma_2) \left[\sum_{k=1}^m a_k \boldsymbol{\psi}_k(s)\right] \, ds}{\int_0^{\sigma_2} \left[\sum_{i=1}^m a_i \boldsymbol{\psi}_i(s)\right]^T \left[\sum_{k=1}^m a_k \boldsymbol{\psi}_k(s)\right] \, ds}. \tag{2.21}$$

Now, since $\boldsymbol{\psi}_i \in \mathcal{A}_d^{cons}(\sigma_2)$, we have $\mathcal{Q}(\sigma_2)\boldsymbol{\psi}_i = \boldsymbol{\psi}_i$, so that the projections may be removed from (2.21):

$$\rho_m(\sigma_2) \leq \frac{\int_0^{\sigma_2} \left[\sum_{i=1}^m a_i \boldsymbol{\psi}_i(s)\right]^T \mathcal{S} \left[\sum_{k=1}^m a_k \boldsymbol{\psi}_k(s)\right] \, ds}{\int_0^{\sigma_2} \left[\sum_{i=1}^m a_i \boldsymbol{\psi}_i(s)\right]^T \left[\sum_{k=1}^m a_k \boldsymbol{\psi}_k(s)\right] \, ds}.$$

Since $\mathcal{S}$ is a local operator, both integrands vanish for $\sigma_1 < s < \sigma_2$, so we may change the upper integration limits to σ_1 and replace ψ_i by its restriction to $(0, \sigma_1)$:

$$\rho_m(\sigma_2) \leq \frac{\int_0^{\sigma_1} \left[\sum_{i=1}^m a_i \boldsymbol{\zeta}_i(s;\sigma_1)\right]^T \mathcal{S} \left[\sum_{k=1}^m a_k \boldsymbol{\zeta}_k(s;\sigma_1)\right] \, ds}{\int_0^{\sigma_1} \left[\sum_{i=1}^m a_i \boldsymbol{\zeta}_i(s;\sigma_1)\right]^T \left[\sum_{k=1}^m a_k \boldsymbol{\zeta}_k(s;\sigma_1)\right] \, ds}.$$

Next, we use the fact that $\mathcal{Q}(\sigma_1)\boldsymbol{\zeta}_i(s;\sigma_1) = \boldsymbol{\zeta}_i(s;\sigma_1)$ to introduce $\mathcal{Q}(\sigma_1)$ on either side of $\mathcal{S}$ and then exploit the fact that $\{\boldsymbol{\zeta}_i(s;\sigma_1)\}$ is a set of orthonormal eigenfunctions of $\mathcal{Q}(\sigma_1)\mathcal{S}\mathcal{Q}(\sigma_1)$ to find:

$$\rho_m(\sigma_2) \leq \sum_{i,k=1}^m a_i a_k \rho_k(\sigma_1)\delta_{ik} = \sum_{i=1}^m a_i^2 \rho_i(\sigma_1) \leq \rho_m(\sigma_1).$$

$\square$

Property 2.6. *For σ sufficiently close to 0, $\rho_j(\sigma) \geq 0$, $\forall j$.*

Proof. Standard unconstrained quadratic form theory for Sturm-Liouville operators (see for example [55]) allows us to conclude that for σ sufficiently small,

$$\int_0^{\sigma} \boldsymbol{\zeta} \cdot \mathcal{S}\boldsymbol{\zeta}\; ds \geq 0 \;\; \forall \boldsymbol{\zeta} \in \mathcal{A}_d(\sigma).$$

Since $\mathcal{B}(\sigma) \subset \mathcal{A}_d^{cons}(\sigma) \subset \mathcal{A}_d(\sigma)$ and

$$\int_0^{\sigma} \boldsymbol{\zeta} \cdot \mathcal{QSQ}\boldsymbol{\zeta}\; ds = \int_0^{\sigma} \boldsymbol{\zeta} \cdot \mathcal{S}\boldsymbol{\zeta}\; ds, \; \forall \boldsymbol{\zeta} \in \mathcal{A}_d^{cons},$$

it follows from Equation (2.19) that $\rho_j \geq 0$, $\forall j$. □

An *isoperimetric conjugate point* is defined to be a value $0 < \sigma < 1$ for which

$$\mathcal{QSQ}\boldsymbol{\zeta} = \mathbf{0}, \quad 0 < s < \sigma, \;\; \boldsymbol{\zeta} \in \mathcal{A}_d^{cons}(\sigma), \tag{2.22}$$

has a nontrivial solution. We further define the *isoperimetric index* to be the number of negative eigenvalues $\rho_i(\sigma)$ of (2.17) when $\sigma = 1$, and due to Properties 2.4, 2.5, 2.6, this equals the number of isoperimetric conjugate points $0 < \sigma < 1$.[4]

As in the unconstrained case, if $I = 0$ then the necessary condition (2.11) holds, and we describe $\mathbf{q}_0$ as stable. The analogous idea in the constrained case is illustrated by the following corollary:

Corollary 2.1. *For a given extremal $\mathbf{q}_0$, $\delta^2 J[\boldsymbol{\zeta}] \geq 0$ for all $\boldsymbol{\zeta} \in \mathcal{A}_d^{cons}$ if and only if the extremal contains no isoperimetric conjugate points.*

Proof. By definition, an extremal contains no conjugate points if there is no $0 < \sigma < 1$ for which Eq. (2.22) has a solution. Equivalently, there must be no $0 < \sigma < 1$ with $\rho(\sigma) = 0$ in the eigenvalue problem (2.17). Based on Properties 2.5 and 2.6, this holds if and only if $\rho_1(1)$ is non-negative. Using the variational characterization (2.19), this condition can be written:

$$0 \leq \rho_1(1) = \min_{\boldsymbol{\zeta} \in \mathcal{A}_d^{cons}} \frac{\int_0^1 \boldsymbol{\zeta}^T \mathcal{QSQ}\boldsymbol{\zeta}\; ds}{\int_0^1 \boldsymbol{\zeta}^T \boldsymbol{\zeta}\; ds} = \min_{\boldsymbol{\zeta} \in \mathcal{A}_d^{cons}} \frac{\int_0^1 \boldsymbol{\zeta} \cdot \mathcal{S}\boldsymbol{\zeta}\; ds}{\int_0^1 \boldsymbol{\zeta}^T \boldsymbol{\zeta}\; ds},$$

which is true if and only if

$$\int_0^1 \boldsymbol{\zeta}^T \mathcal{S}\boldsymbol{\zeta}\; ds \geq 0, \;\; \forall \boldsymbol{\zeta} \in \mathcal{A}_d^{cons}.$$

□

Thus, if $I > 0$, $\mathbf{q}_0$ is not a constrained local minimum, and there is a subspace of constrained variations of dimension I on which $\delta^2 J < 0$.

Isoperimetric conjugate points have been previously defined in a different form ([7], p. 220 and Section 2.3 below). The equivalent definition (2.22) has the advantage that it leads naturally to the definition of an index, as demonstrated above.

[4] As in the unconstrained setting, this conclusion relies on the isolation of isoperimetric conjugate points and the continuity of $\rho_j(\sigma)$, both of which we shall assume here since little analysis of such issues has been addressed in the constrained literature. In practice, the failure of either of these assumptions would be readily apparent in numerical implementation and did not occur in the examples we studied.

2.3 Numerical Implementation

As is well known, unconstrained conjugate points can be computed as roots of an appropriate $p \times p$, s-dependent determinant [52]. In this section, we present an analogous algorithm for isoperimetric conjugate points involving a determinant of an augmented $(p+n) \times (p+n)$ matrix.

2.3.1 The Constrained Stability Matrix

We first reformulate the conjugate point condition (2.22) in a more explicit, computationally convenient form.

Lemma 2.1.

$$\mathcal{QSQ}\boldsymbol{\zeta} = \rho\boldsymbol{\zeta}, \quad \boldsymbol{\zeta} \in \mathcal{A}_d^{cons}(\sigma) \tag{2.23}$$

if and only if for some $\breve{c}_i$

$$\begin{gathered} \mathcal{S}\boldsymbol{\zeta} + \sum_{i=1}^{n} \breve{c}_i \mathbf{T}_i = \mathbf{0}, \quad 0 < s < \sigma, \quad \sigma \leq 1, \\ \boldsymbol{\zeta}(0) = \boldsymbol{\zeta}(\sigma) = \mathbf{0}, \quad \int_0^\sigma \boldsymbol{\zeta} \cdot \mathbf{T}_i \, ds = 0, \quad i = 1, \ldots, n. \end{gathered} \tag{2.24}$$

Proof. The equation

$$\mathcal{QSQ}\boldsymbol{\zeta} = \rho\boldsymbol{\zeta}$$

is equivalent to

$$\mathcal{QS}\boldsymbol{\zeta} = \rho\mathcal{Q}\boldsymbol{\zeta}$$

since $\mathcal{Q}$ is the identity on $\mathcal{A}_d^{cons}(\sigma)$. We can rearrange this to the form

$$\mathcal{Q}(\mathcal{S}\boldsymbol{\zeta} - \rho\boldsymbol{\zeta}) = \mathbf{0},$$

which is true if and only if for some constants $\breve{c}_i$

$$\begin{gathered} \mathcal{S}\boldsymbol{\zeta} + \sum_{i=1}^{n} \breve{c}_i \mathbf{T}_i = \mathbf{0}, \quad 0 < s < \sigma, \quad \sigma \leq 1, \\ \boldsymbol{\zeta}(0) = \boldsymbol{\zeta}(\sigma) = \mathbf{0}, \quad \int_0^\sigma \boldsymbol{\zeta} \cdot \mathbf{T}_i \, ds = 0, \quad i = 1, \ldots, n, \end{gathered}$$

since $\mathbf{T}$ is the kernel of $\mathcal{Q}$. □

Thus instead of (2.23) we use the equivalent and computationally more convenient form:

$$\begin{gathered} \mathcal{S}\boldsymbol{\zeta} + \sum_{i=1}^{n} \breve{c}_i \mathbf{T}_i = \mathbf{0}, \quad 0 < s < \sigma, \quad \sigma \leq 1, \\ \boldsymbol{\zeta}(0) = \boldsymbol{\zeta}(\sigma) = \mathbf{0}, \quad \int_0^\sigma \boldsymbol{\zeta} \cdot \mathbf{T}_i \, ds = 0, \quad i = 1, \ldots, n, \end{gathered} \tag{2.25}$$

where $\breve{c}_i$ are arbitrary constants. The goal of this section is to construct a system of linear algebraic equations which is equivalent to (2.25). We first find a general solution to the homogeneous initial value problem:

$$\mathcal{S}\boldsymbol{\zeta} = \mathbf{0}, \quad \boldsymbol{\zeta}(0) = \mathbf{0},$$

which includes p undetermined constants:

$$\boldsymbol{\zeta} = c_1\boldsymbol{\zeta}_1 + c_2\boldsymbol{\zeta}_2 + \cdots + c_p\boldsymbol{\zeta}_p.$$

Similarly, for each i, we find a single solution to the initial value problem

$$\mathcal{S}\breve{\boldsymbol{\zeta}}_i = \mathbf{T}_i, \quad \breve{\boldsymbol{\zeta}}_i(0) = \mathbf{0}.$$

Then, the function

$$\boldsymbol{\zeta} = \sum_{i=1}^{p} c_i\boldsymbol{\zeta}_i - \sum_{i=1}^{n} \breve{c}_i\breve{\boldsymbol{\zeta}}_i$$

is the general solution to

$$\mathcal{S}\boldsymbol{\zeta} = -\sum_{i=1}^{n} \breve{c}_i\mathbf{T}_i, \quad \boldsymbol{\zeta}(0) = \mathbf{0}.$$

The system of two-point BVPs (2.25) will have a solution if and only if there exist constants c_i and $\breve{c}_i$ such that $\boldsymbol{\zeta}(s)$ satisfies the boundary conditions at $s = \sigma$,

$$\sum_{j=1}^{p} c_j\boldsymbol{\zeta}_j(\sigma) - \sum_{j=1}^{n} \breve{c}_j\breve{\boldsymbol{\zeta}}_j(\sigma) = \mathbf{0}, \tag{2.26}$$

along with the (linearized) constraints

$$\int_0^{\sigma} \left[\sum_{j=1}^{p} c_j\boldsymbol{\zeta}_j(\tau) - \sum_{j=1}^{n} \breve{c}_j\breve{\boldsymbol{\zeta}}_j(\tau)\right]^T \mathbf{T}_i(\tau)\, d\tau = 0, \quad i = 1, \ldots, n. \tag{2.27}$$

Equations (2.26) and (2.27) can be written in matrix form:

$$\mathcal{M}(\sigma)\begin{bmatrix}\mathbf{c}\\ -\breve{\mathbf{c}}\end{bmatrix} \equiv \begin{bmatrix}\mathbf{A}(\sigma) & \breve{\mathbf{A}}(\sigma)\\ \mathbf{F}(\sigma) & \breve{\mathbf{F}}(\sigma)\end{bmatrix}\begin{bmatrix}\mathbf{c}\\ -\breve{\mathbf{c}}\end{bmatrix} = \mathbf{0}, \tag{2.28}$$

where

$$\begin{aligned}
\mathbf{c} &\equiv [c_1 \ldots c_p]^T \in \mathbb{R}^p,\\
\breve{\mathbf{c}} &\equiv [\breve{c}_1 \ldots \breve{c}_n]^T \in \mathbb{R}^n,\\
\mathbf{A}(\sigma) &\equiv \begin{bmatrix}\boldsymbol{\zeta}_1(\sigma) & \ldots & \boldsymbol{\zeta}_p(\sigma)\end{bmatrix} \in \mathbb{R}^{p\times p},\\
\breve{\mathbf{A}}(\sigma) &\equiv \begin{bmatrix}\breve{\boldsymbol{\zeta}}_1(\sigma) & \ldots & \breve{\boldsymbol{\zeta}}_n(\sigma)\end{bmatrix} \in \mathbb{R}^{p\times n},\\
\mathbf{F}(\sigma) &\equiv \{f_{ij}(\sigma)\} = \left\{\int_0^{\sigma} \boldsymbol{\zeta}_j(\tau)^T\mathbf{T}_i(\tau)d\tau\right\} \in \mathbb{R}^{n\times p},\\
\breve{\mathbf{F}}(\sigma) &\equiv \left\{\breve{f}_{ij}(\sigma)\right\} = \left\{\int_0^{\sigma} \breve{\boldsymbol{\zeta}}_j(\tau)^T\mathbf{T}_i(\tau)d\tau\right\} \in \mathbb{R}^{n\times n}.
\end{aligned}$$

Equation (2.28), and therefore Equation (2.25), has a nontrivial solution only at values of σ for which the $(p+n)\times(p+n)$ *constrained stability matrix* $\mathcal{M}(\sigma)$ has determinant zero, so that these σ values are precisely the isoperimetric conjugate points and the number of roots of the determinant (counted according to multiplicity) in the interval $0<\sigma<1$ is exactly the isoperimetric index. An analogous test for unconstrained conjugate points is obtained by setting $n=0$ to arrive at $\det \mathbf{A}(\sigma)=0$ ([52], p. 152).

The vanishing of $\det \mathcal{M}$ is Bolza's ([7], p. 220) definition of an isoperimetric conjugate point. In direct analogy with the unconstrained case, Bolza's treatment uses the absence of a constrained conjugate point to rewrite the integrand in the second variation as a complete square, and thus prove its positivity. Our definition of isoperimetric conjugate points in terms of the eigenvalue problem (2.22) allows the notion of a constrained index to be introduced as in Section 2.2.2, while the equivalent relation (2.28) is more suitable for computation.

2.3.2 Computing Homogeneous and Nonhomogeneous Solutions

As shown in Section 2.3.1, construction of the matrix $\mathcal{M}$ requires the computation of a basis of p solutions $\boldsymbol{\zeta}_1,\ldots,\boldsymbol{\zeta}_p$ of the homogeneous equation

$$-\frac{d}{ds}\left[\mathbf{P}\boldsymbol{\zeta}'+\mathbf{C}^T\boldsymbol{\zeta}\right]+\mathbf{C}\boldsymbol{\zeta}'+\mathbf{Q}\boldsymbol{\zeta}=\mathbf{0},\quad \boldsymbol{\zeta}(0)=\mathbf{0}, \tag{2.29}$$

and one solution $\breve{\boldsymbol{\zeta}}_i$ for each of the n non-homogeneous equations

$$-\frac{d}{ds}\left[\mathbf{P}\boldsymbol{\zeta}'+\mathbf{C}^T\boldsymbol{\zeta}\right]+\mathbf{C}\boldsymbol{\zeta}'+\mathbf{Q}\boldsymbol{\zeta}=\mathbf{T}_i,\quad \boldsymbol{\zeta}(0)=\mathbf{0}. \tag{2.30}$$

These solutions can be computed with appropriate initial value problems (IVPs), as outlined here. We first rewrite the second-order differential equations (2.29) and (2.30) as first-order systems, by defining

$$\mathbf{v}\equiv\mathbf{P}\boldsymbol{\zeta}'+\mathbf{C}^T\boldsymbol{\zeta}.$$

Solving for $\boldsymbol{\zeta}'$ in terms of $\mathbf{v}$ and $\boldsymbol{\zeta}$ leads to the first-order systems:

$$\begin{aligned}\boldsymbol{\zeta}'&=\mathbf{P}^{-1}(\mathbf{v}-\mathbf{C}^T\boldsymbol{\zeta}),\\ \mathbf{v}'&=\mathbf{C}\boldsymbol{\zeta}'+\mathbf{Q}\boldsymbol{\zeta}=\mathbf{C}\mathbf{P}^{-1}(\mathbf{v}-\mathbf{C}^T\boldsymbol{\zeta})+\mathbf{Q}\boldsymbol{\zeta},\\ \boldsymbol{\zeta}(0)&=\mathbf{0},\end{aligned} \tag{2.31}$$

and

$$\begin{aligned}\breve{\boldsymbol{\zeta}}'&=\mathbf{P}^{-1}(\breve{\mathbf{v}}-\mathbf{C}^T\breve{\boldsymbol{\zeta}}),\\ \breve{\mathbf{v}}'&=\mathbf{C}\breve{\boldsymbol{\zeta}}'+\mathbf{Q}\breve{\boldsymbol{\zeta}}-\mathbf{T}_i=\mathbf{C}\mathbf{P}^{-1}(\breve{\mathbf{v}}-\mathbf{C}^T\breve{\boldsymbol{\zeta}})+\mathbf{Q}\breve{\boldsymbol{\zeta}}-\mathbf{T}_i,\\ \breve{\boldsymbol{\zeta}}(0)&=\mathbf{0}.\end{aligned} \tag{2.32}$$

Finally, we need to specify the appropriate initial conditions for $\mathbf{v}$. For the homogeneous case, a basis of solutions to (2.31) is provided by using p linearly independent initial values for $\mathbf{v}(0)$, e.g.

$$\mathbf{v}_i(0) = \mathbf{e}_i, \quad i = 1, \dots, p.$$

For the nonhomogeneous solutions, any initial conditions on $\mathbf{v}$ will suffice, and we use $\check{\mathbf{v}}(0) = \mathbf{0}$. The resulting $\check{\boldsymbol{\zeta}}_j$ will be linearly independent, since we have assumed that the $\mathbf{T}_i(s)$ are linearly independent on all intervals $(0, \sigma)$.

2.3.3 Computing the Integrals in the Constrained Stability Matrix

The sub-blocks $\mathbf{F}$ and $\check{\mathbf{F}}$ of the matrix $\mathcal{M}$ consist of the integrals $f_{ij}(\sigma) \equiv \int_0^\sigma \boldsymbol{\zeta}_j(\tau) \cdot \mathbf{T}_i(\tau) d\tau$ and $\check{f}_{ij}(\sigma) \equiv \int_0^\sigma \check{\boldsymbol{\zeta}}_j(\tau) \cdot \mathbf{T}_i(\tau) d\tau$, which also can be computed by solving an IVP. Assuming that the functions $\boldsymbol{\zeta}_j(\sigma)$ and $\check{\boldsymbol{\zeta}}_j(\sigma)$ have been computed (as described in Sec. 2.3.2), the differential equations for f_{ij} and $\check{f}_{ij}$ are:

$$\begin{aligned} f'_{ij}(\sigma) &= \boldsymbol{\zeta}_j(\sigma) \cdot \mathbf{T}_i(\sigma) \\ \check{f}'_{ij}(\sigma) &= \check{\boldsymbol{\zeta}}_j(\sigma) \cdot \mathbf{T}_i(\sigma), \end{aligned}$$

with $f_{ij}(0) = \check{f}_{ij}(0) = 0$.

2.3.4 Assembling the IVP

In summary, to determine conjugate points, we solve the following system of $(n+p)(n+2p)$ first-order differential equations:

$$\begin{aligned} \boldsymbol{\zeta}_i{}' &= \mathbf{P}^{-1}(\mathbf{q}_0)(\mathbf{v}_i - \mathbf{C}^T(\mathbf{q}_0)\boldsymbol{\zeta}_i), \\ \mathbf{v}_i{}' &= \mathbf{C}(\mathbf{q}_0)\mathbf{P}^{-1}(\mathbf{q}_0)(\mathbf{v}_i - \mathbf{C}^T(\mathbf{q}_0)\boldsymbol{\zeta}_i) + \mathbf{Q}(\mathbf{q}_0)\boldsymbol{\zeta}_i, \\ \check{\boldsymbol{\zeta}}'_i &= \mathbf{P}^{-1}(\mathbf{q}_0)(\check{\mathbf{v}}_i - \mathbf{C}^T(\mathbf{q}_0)\check{\boldsymbol{\zeta}}_i), \\ \check{\mathbf{v}}'_i &= \mathbf{C}(\mathbf{q}_0)\mathbf{P}^{-1}(\mathbf{q}_0)(\check{\mathbf{v}}_i - \mathbf{C}^T(\mathbf{q}_0)\check{\boldsymbol{\zeta}}_i) + \mathbf{Q}(\mathbf{q}_0)\check{\boldsymbol{\zeta}}_i - \mathbf{T}_i(\mathbf{q}_0), \\ f'_{ij} &= \boldsymbol{\zeta}_j \cdot \mathbf{T}_i(\mathbf{q}_0), \\ \check{f}'_{ij} &= \check{\boldsymbol{\zeta}}_j \cdot \mathbf{T}_i(\mathbf{q}_0), \end{aligned} \tag{2.33}$$

with initial conditions

$$\begin{aligned} &\boldsymbol{\zeta}_i(0) = \mathbf{0}, \;\; \mathbf{v}_i(0) = \mathbf{e}_i \quad i = 1, \dots, p, \\ &\check{\boldsymbol{\zeta}}_i(0) = \check{\mathbf{v}}_i(0) = \mathbf{0}, \quad i = 1, \dots, n, \\ &f_{ij}(0) = 0, \quad i = 1, \dots, n, \;\; j = 1, \dots, p, \\ &\check{f}_{ij}(0) = 0, \quad i, j = 1, \dots, n. \end{aligned}$$

In the applications that follow, the equilibria $\mathbf{q}_0(s)$ have already been computed by Li & Maddocks [37] for the idealized rod (cf. Chapter 6) and Manning, Maddocks, Kahn [45] for the model of DNA (cf. Chapter 8). In computing the constrained conjugate points for these examples using (2.33), the appropriate initial conditions on $\mathbf{q}_0(0)$ and $\mathbf{q}_0'(0)$ are used to recover the full solution $\mathbf{q}_0(s)$ by an additional call to an IVP solver.

Chapter 3

Parameter-Dependent Variational Principles

3.1 Introduction

In the previous chapter, Jacobi's theory of conjugate points and Morse's index theory were extended to include isoperimetrically constrained calculus of variations problems. In this chapter, we exploit the additional structure present when calculus of variations problems (both constrained and not) depend on parameters, and consequently families of extremals arise. The fundamental tool we exploit in studying the second variation of parameter-dependent problems is the *distinguished bifurcation diagram*, which is a particular projection of the solution set that encodes stability exchange information into the shape of its branches. Standard bifurcation theory asserts that the stability of solutions changes at folds in a bifurcation diagram, but distinguished diagram theory can further predict the direction the stability changes.

For unconstrained parameter-dependent calculus of variations problems, distinguished diagram results have previously been presented by Maddocks [42] for problems in which the bifurcation parameter appears explicitly in the integrand of the functional. Section 3.2 sets forth the theory a calculus of variations problem in which the bifurcation parameter appears in the boundary conditions. The abscissa and ordinate of the distinguished diagram are determined in Section 3.3 by differentiating the eigenvalue with respect to pseudo-arclength and evaluating at a fold in the solution branch.

In Section 3.4, we develop the theory of isoperimetrically constrained calculus of variations problems that have a parameter in the boundary conditions using the projection $\mathcal{Q}$ introduced in Chapter 2 to obtain an appropriate eigenvalue problem in the constrained setting. As in the unconstrained case, the abscissa and ordinate of the distinguished diagram are determined in Section 3.5 by evaluating the expression for the derivative of the eigenvalue at a fold in the solution branch.

3.2 Unconstrained System

Consider an unconstrained parameter-dependent one-dimensional variational problem

$$J[\mathbf{q}, \alpha] = \int_0^1 W(\mathbf{q}, \mathbf{q}', s, \alpha)\, ds, \tag{3.1}$$

subject to the boundary conditions

$$\mathbf{q}(0) = \mathbf{f}_0(\alpha), \quad \mathbf{q}(1) = \mathbf{f}_1(\alpha), \tag{3.2}$$

where $\mathbf{q}(s) \in \mathbb{R}^p$ are the variables, and $\alpha \in \mathbb{R}^1$ is a parameter. A critical point $\mathbf{q}_0(\alpha)$ of (3.1) is a solution to the Euler-Lagrange equations (2.2) which satisfies the boundary conditions (3.2). The solution set, or *bifurcation diagram* comprises the locally one-dimensional family of critical points $\mathbf{q}_0(\alpha)$. The second variation of (3.1) takes the form (2.3), and the associated second-order differential operator $\mathcal{S}$ is given by (2.6).

3.3 Distinguished Diagram for the Unconstrained System

Stability of equilibria in a parameter-dependent variational setting has been previously addressed by Maddocks [40, 41, 42]. In [42], Maddocks showed that for problems with parameter-dependent integrands and homogeneous boundary conditions, folds in a certain distinguished diagram correspond to stability exchange, and further give the direction of exchange. Here, we focus on the case where the parameter dependence enters through the boundary conditions $\mathbf{q}(0) = \mathbf{0}$, $\mathbf{q}(1) = \mathbf{f}_1(\alpha) \not\equiv \mathbf{0}$, and the integrand of the functional does not explicitly depend on a parameter, i.e., $W(\mathbf{q}, \mathbf{q}', \alpha, s) = W(\mathbf{q}, \mathbf{q}', s)$. The two cases can be combined straightforwardly.

Assume that there exists a branch of solutions $(\mathbf{q}(s,\tau), \alpha(\tau))$ to the Euler-Lagrange equations (2.2) where τ is a pseudo-arclength parametrization of the solution branch such that $\|\dot{\mathbf{q}}\|^2 + \dot{\alpha}^2 = 1$ [12]. The notation $\mathbf{q}'(s,\tau)$ will denote the derivative with respect to the independent variable s and $\dot{\mathbf{q}}(s,\tau)$ will denote the derivative with respect to pseudo-arclength τ along the solution branch. A second-order necessary condition for a critical point to correspond to a minimum is given by Equation (2.7), namely,

$$\delta^2 J[\boldsymbol{\zeta}] \geq 0, \quad \forall\, \boldsymbol{\zeta} \in \mathcal{A}_d.$$

As discussed in Chapter 2, the dimension of the space of variations on which the quadratic form $\delta^2 J$ is negative is measured by the index, that is, the number of negative eigenvalues of

$$\begin{gathered} \mathcal{S}\boldsymbol{\zeta} = \rho\boldsymbol{\zeta}, \\ \boldsymbol{\zeta}(0) = \mathbf{0}, \;\; \boldsymbol{\zeta}(1) = \mathbf{0}. \end{gathered} \tag{3.3}$$

The operator $\mathcal{S}$ given in Equations (2.6) is assumed to have eigenvalues and eigenfunctions that depend smoothly on τ. The coefficients of $\mathcal{S}$, namely the matrices $\mathbf{P}$, $\mathbf{C}$ and $\mathbf{Q}$, depend on α only through the solution $\mathbf{q}(s,\tau)$.

In the previous chapter, the number of negative eigenvalues of (3.3) was determined by using a conjugate point test. In this chapter, we exploit the parameter dependence of the functional to determine when the index changes, i.e. when a negative eigenvalue is gained or lost. Parameter-dependent variational principles give rise to families of extremals; in the case of a single parameter α, a curve of solutions is usually produced. We would like to understand how the eigenvalues ρ of (3.3) change as the curve of solutions is traversed. Standard bifurcation theory recognizes that generically folds (i.e. points on the solution branch with vertical tangents) in the bifurcation parameter correspond to stability exchanges [9, 53, 68]; that is, an eigenvalue of (3.3) changes from positive to negative or vice versa as the fold is traversed. By using the variational structure, we will show that the direction of change can also be predicted by determining the sign of the derivative of the eigenvalue with respect to pseudo-arclength along the branch of solutions.

We begin by demonstrating that the eigenvalue problem (3.3) has a zero eigenvalue $\rho = 0$, whenever $\mathcal{S}$ is evaluated at a solution corresponding to a fold in the bifurcation parameter. Differentiating the Euler-Lagrange equations (2.2) and the nonlinear boundary conditions (3.2) with respect to pseudo-arclength yields the boundary value problem

$$\begin{gathered}\mathcal{S}\dot{\mathbf{q}} = \mathbf{0}, \\ \dot{\mathbf{q}}(0) = \mathbf{0}, \quad \dot{\mathbf{q}}(1) = \frac{d\mathbf{f}}{d\alpha}\dot{\alpha}.\end{gathered} \tag{3.4}$$

A comparison of the eigenvalue problem (3.3) with the boundary value problem (3.4) reveals that equation (3.3) has a zero eigenvalue ($\rho = 0$) when $\dot{\alpha} = 0$, i.e. at a fold point in the bifurcation parameter. We further assume that $\rho = 0$ is a simple eigenvalue at the fold, and thus conclude that $\dot{\mathbf{q}}$ is the corresponding eigenvector.

To obtain an expression for $\dot{\rho}$, we differentiate (3.3) with respect to pseudo-arclength, to get:

$$\begin{aligned}&\mathcal{S}\dot{\boldsymbol{\zeta}} = \dot{\rho}\boldsymbol{\zeta} + \rho\dot{\boldsymbol{\zeta}} - \dot{\mathcal{S}}\boldsymbol{\zeta}, \\ &\dot{\boldsymbol{\zeta}}(0) = \mathbf{0}, \quad \dot{\boldsymbol{\zeta}}(1) = \mathbf{0}.\end{aligned} \tag{3.5}$$

The notation $\dot{\mathcal{S}}\boldsymbol{\zeta}$ should be interpreted as

$$\dot{\mathcal{S}}\boldsymbol{\zeta} = \left(\frac{d}{d\tau}\mathcal{S}\right)\boldsymbol{\zeta} = -\frac{d}{ds}\left[\dot{\mathbf{P}}\boldsymbol{\zeta}' + \dot{\mathbf{C}}^T\boldsymbol{\zeta}\right] + \dot{\mathbf{C}}\boldsymbol{\zeta}' + \dot{\mathbf{Q}}\boldsymbol{\zeta}. \tag{3.6}$$

Taking the L^2-inner product of (3.5) with the eigenvector $\dot{\mathbf{q}}$ gives the expression

$$\langle\dot{\mathbf{q}}, \mathcal{S}\dot{\boldsymbol{\zeta}}\rangle = \dot{\rho}\langle\dot{\mathbf{q}}, \boldsymbol{\zeta}\rangle + \rho\langle\dot{\mathbf{q}}, \dot{\boldsymbol{\zeta}}\rangle - \langle\dot{\mathbf{q}}, \dot{\mathcal{S}}\boldsymbol{\zeta}\rangle. \tag{3.7}$$

Since we are interested in the sign of $\dot{\rho}$ at a fold point, expression (3.7) is evaluated at a fold by substituting $\rho = 0$ for the eigenvalue and $\boldsymbol{\zeta} = \dot{\mathbf{q}}$ for eigenvector to yield

$$\dot{\rho}\langle\dot{\mathbf{q}}, \dot{\mathbf{q}}\rangle = \langle\dot{\mathbf{q}}, \mathcal{S}\dot{\boldsymbol{\zeta}}\rangle + \langle\dot{\mathbf{q}}, \dot{\mathcal{S}}\dot{\mathbf{q}}\rangle. \tag{3.8}$$

Integration by parts will be used to simplify the terms in Equation (3.8):

Observation 3.1. *For two vector-valued functions* $\mathbf{u}$ *and* $\mathbf{v}$*,*

$$\langle\mathbf{u}, \mathcal{S}\mathbf{v}\rangle = -\left.\mathbf{u}\cdot\mathbf{P}\mathbf{v}'\right|_0^1 + \left.\mathbf{u}'\cdot\mathbf{P}\mathbf{v}\right|_0^1 + \left.\mathbf{u}\cdot\mathbf{C}\mathbf{v}\right|_0^1 - \left.\mathbf{u}\cdot\mathbf{C}^T\mathbf{v}\right|_0^1 + \langle\mathcal{S}\mathbf{u}, \mathbf{v}\rangle.$$

Proposition 3.1. $\langle\mathcal{S}\dot{\boldsymbol{\zeta}}, \dot{\mathbf{q}}\rangle = 0$

Proof. Apply Observation 3.1 with $\mathbf{v} = \dot{\boldsymbol{\zeta}}$, $\mathbf{u} = \dot{\mathbf{q}}$ and boundary conditions $\dot{\boldsymbol{\zeta}}(0) = 0, \dot{\boldsymbol{\zeta}}(1) = 0, \dot{\mathbf{q}}(0) = 0, \dot{\mathbf{q}}(1) = \frac{df}{d\alpha}\dot{\alpha}$ to get

$$\langle\dot{\mathbf{q}}, \mathcal{S}\dot{\boldsymbol{\zeta}}\rangle = \frac{df}{d\alpha}\cdot\mathbf{P}\dot{\boldsymbol{\zeta}}(1)\dot{\alpha} + \langle\mathcal{S}\dot{\mathbf{q}}, \dot{\boldsymbol{\zeta}}\rangle.$$

Since $\dot{\mathbf{q}}$ is in the kernel of $\mathcal{S}$, $\mathcal{S}\dot{\mathbf{q}} = 0$, and $\langle\dot{\boldsymbol{\zeta}}, \mathcal{S}\dot{\mathbf{q}}\rangle = 0$. The boundary terms also vanish at a fold point because $\dot{\alpha} = 0$. □

Proposition 3.2. $\langle\dot{\mathcal{S}}\dot{\mathbf{q}}, \dot{\mathbf{q}}\rangle = -\mathbf{P}\dot{\mathbf{q}}'(1)\cdot\frac{df}{d\alpha}\ddot{\alpha}$

Proof. Differentiating (3.4) with respect to pseudo-arclength τ, we find $\langle\dot{\mathcal{S}}\dot{\mathbf{q}}, \dot{\mathbf{q}}\rangle = -\langle\mathcal{S}\ddot{\mathbf{q}}, \dot{\mathbf{q}}\rangle$. Applying Observation 3.1 to $-\langle\mathcal{S}\ddot{\mathbf{q}}, \dot{\mathbf{q}}\rangle$ with $\mathbf{u} = \dot{\mathbf{q}}$ and $\mathbf{v} = \ddot{\mathbf{q}}$ with boundary conditions $\dot{\mathbf{q}}(0) = 0, \dot{\mathbf{q}}(1) = \frac{df}{d\alpha}\dot{\alpha}, \ddot{\mathbf{q}}(0) = 0, \ddot{\mathbf{q}}(1) = \frac{\partial^2\mathbf{f}}{\partial\alpha^2}\dot{\alpha} + \frac{d\mathbf{f}}{d\alpha}\ddot{\alpha}$ and evaluating at a fold ($\dot{\alpha} = 0$), we get

$$\begin{aligned} -\langle\mathcal{S}\ddot{\mathbf{q}}, \dot{\mathbf{q}}\rangle &= -\dot{\mathbf{q}}'(1)\cdot\mathbf{P}\ddot{\mathbf{q}}(1) - \langle\ddot{\mathbf{q}}, \mathcal{S}\dot{\mathbf{q}}\rangle, \\ &= -\dot{\mathbf{q}}'(1)\cdot\mathbf{P}\frac{d\mathbf{f}}{d\alpha}\ddot{\alpha}. \end{aligned}$$

□

If we assume that $\langle\dot{\mathbf{q}}, \dot{\mathbf{q}}\rangle = 1$, the expression for $\dot{\rho}$ at a fold (3.8) becomes

$$\dot{\rho} = -\dot{\mathbf{q}}'(1)\cdot\mathbf{P}\frac{d\mathbf{f}}{d\alpha}\ddot{\alpha}. \tag{3.9}$$

For the functional (3.1), $\mathbf{P} = W_{\mathbf{q}'\mathbf{q}'}$ and at a fold $\dot{\mathbf{q}}(1) = \mathbf{0}$, so

$$\begin{aligned} \dot{\mathbf{q}}'\cdot W_{\mathbf{q}'\mathbf{q}'}(1)\frac{d\mathbf{f}}{d\alpha} &= \dot{\mathbf{q}}'(1)\cdot W_{\mathbf{q}'\mathbf{q}'}\frac{d\mathbf{f}}{d\alpha} + \dot{\mathbf{q}}(1)\cdot W_{\mathbf{q}'\mathbf{q}}\frac{d\mathbf{f}}{d\alpha}, & (3.10) \\ &= \frac{d}{d\tau}\left[W_{\mathbf{q}'}\cdot\frac{d\mathbf{f}}{d\alpha}\right]\Bigg|_{s=1}. & (3.11) \end{aligned}$$

Thus the expression for $\dot{\rho}$ can be written as

$$\dot{\rho} = -\ddot{\alpha} \frac{d}{d\tau} \left[W_{\mathbf{q}'} \cdot \frac{d\mathbf{f}}{d\alpha} \right] \Bigg|_{s=1}. \tag{3.12}$$

Consider the distinguished $\left\{ W_{\mathbf{q}'} \cdot \frac{d\mathbf{f}}{d\alpha} \right\}$ vs. α bifurcation diagram. The sign of $\dot{\rho}$ determines if the eigenvalue is increasing or decreasing as the fold is traversed. The sign of $\ddot{\alpha}$ determines whether the fold opens to the left to the right, and the sign of $\frac{d}{d\tau} \left[W_{\mathbf{q}'} \cdot \frac{d\mathbf{f}}{d\alpha} \right]$ is determined by whether the fold is being traversed upward or downward. Consequently, close to a simple fold opening to the left, the lower branch in the α vs. $\left\{ W_{\mathbf{q}'} \cdot \frac{d\mathbf{f}}{d\alpha} \right\}$ does not represent local minima since ρ is increasing, and $\rho = 0$ at the fold. For example, the distinguished diagram for the twisted elastic loop is twist moment m_3 vs. angle α (cf. Chapter 6) and Figure 3.1 demonstrates how the index, and thus, the eigenvalue changes sign as a fold in the solution branch is traversed.

3.4 Constrained Systems

Consider a constrained one-dimensional calculus of variations problem of minimizing the functional

$$\int_0^1 W(\mathbf{q}, \mathbf{q}', s)\, ds \tag{3.13}$$

subject to the isoperimetric constraints

$$\int_0^1 \mathbf{g}_i(\mathbf{q}) = 0, \quad \text{for} \quad i = 1, ..., n, \tag{3.14}$$

and the boundary conditions

$$\mathbf{q}(0) = \mathbf{0}, \quad \mathbf{q}(1) = \mathbf{f}_1(\alpha), \tag{3.15}$$

where $\mathbf{q}(s) \in \mathbb{R}^p$ are the variables and $\alpha \in \mathbb{R}^1$ is a parameter. Constrained critical points are found using the Lagrange multiplier rule by writing a modified functional

$$J = \int_0^1 W(\mathbf{q}, \mathbf{q}', s) + \boldsymbol{\lambda} \cdot \mathbf{g}(\mathbf{q}), \tag{3.16}$$

subject to the same boundary conditions (3.15). Here $\boldsymbol{\lambda}$ is the n-vector of Lagrange multipliers. A branch of critical points $(\mathbf{q}(\alpha), \boldsymbol{\lambda}(\alpha))$ of (3.16) satisfies the Euler-Lagrange equations (2.2), the boundary conditions (3.15) and the constraints (3.14).

The quadratic form of the second variation of (3.16), is given by

$$\delta^2 J[\boldsymbol{\zeta}] = \int_0^1 \left[\boldsymbol{\zeta}' \cdot \mathbf{P}\boldsymbol{\zeta}' + \boldsymbol{\zeta}' \cdot \mathbf{C}^T \boldsymbol{\zeta} + \boldsymbol{\zeta} \cdot \mathbf{C}\boldsymbol{\zeta} + \boldsymbol{\zeta} \cdot \mathbf{Q}\boldsymbol{\zeta} \right] ds, \tag{3.17}$$

where the $p \times p$ matrices $\mathbf{P}$, and $\mathbf{C}$ are as defined in the unconstrained case and $\mathbf{Q}$ is now $W_{\mathbf{qq}} + \mathbf{g}_{\mathbf{qq}}^T \boldsymbol{\lambda}_0$. The set of admissible variations is $\mathcal{A}_d^{cons}$, as defined in Section 2.2.2. As in the unconstrained case, the derivatives of W are evaluated on the solution $(\mathbf{q}_0, \boldsymbol{\lambda}_0)$, and we define

$$\mathbf{T}_i \equiv (\mathbf{g}_i)_{\mathbf{q}}. \tag{3.18}$$

An integration by parts of the second variation yields the form $\delta^2 J[\boldsymbol{\zeta}] = \langle \boldsymbol{\zeta}, \mathcal{S}\boldsymbol{\zeta} \rangle$, where

$$\mathcal{S}\boldsymbol{\zeta} \equiv -\frac{d}{ds}\left[\mathbf{P}\boldsymbol{\zeta}' + \mathbf{C}^T\boldsymbol{\zeta}\right] + \mathbf{C}\boldsymbol{\zeta}' + \mathbf{Q}\boldsymbol{\zeta}. \tag{3.19}$$

3.5 Distinguished Diagram for the Constrained System

Maddocks [42] previously derived distinguished diagram results for problems of the form (3.13) but with homogeneous boundary conditions ($\mathbf{f}_1(\alpha) \equiv \mathbf{0}$) and constraints of the form $g_i = k_i$, where the data k_i varies forming an n-dimensional manifold of critical points and knowledge of this n-dimensional set of critical points was used to determine the appropriate constrained index. For this case, Lagrange multipliers appear as the only bifurcation parameters. For the case $n = 1$, the distinguished diagram for such a constrained system is $\mathbf{g}_1$ versus $\boldsymbol{\lambda}$. In contrast, the focus of Section 3.5 is to determine the distinguished diagram for isoperimetrically constrained problems where the data is fixed at 0 and there is an additional parameter in the problem. The Lagrange multipliers are therefore regarded as dependent variables. We treat the case where the additional bifurcation parameter appears in the boundary conditions $\mathbf{f}_1(\alpha)$. The case of a parameter in the integrand is analogous, and also original.

As before, the second-order necessary condition [23, p.14] for a critical point $(\mathbf{q}(\alpha), \boldsymbol{\lambda}(\alpha))$ to be a constrained local minimum is

$$\delta^2 J[\boldsymbol{\zeta}] = \langle \boldsymbol{\zeta}, \mathcal{S}\boldsymbol{\zeta} \rangle \geq 0, \quad \forall \boldsymbol{\zeta} \in \mathcal{A}_d^{cons}, \tag{3.20}$$

where $\mathcal{A}_d^{cons}$ is defined by Equation (2.10):

$$\mathcal{A}_d^{cons} \equiv \left\{ \boldsymbol{\zeta} \in \mathcal{A}_d : \int_0^1 \boldsymbol{\zeta} \cdot \mathbf{T}_i \, ds = 0, \quad i = 1, \cdots, n \right\}.$$

Trivially, the condition (3.20) is equivalent to $\langle \boldsymbol{\zeta}, \mathcal{QSQ}\boldsymbol{\zeta} \rangle \geq 0, \quad \forall\, \boldsymbol{\zeta} \in \mathcal{A}_d^{cons}$, where the orthogonal projection operator $\mathcal{Q}$ of $L^2(\sigma)$ onto $\mathcal{T}^{\perp}(\sigma)$ was previously described in Section 2.2.2. Since $\mathcal{QSQ}$ is a densely defined self-adjoint, linear, bounded below, and obeys Property 2.4(cf. Section 2.2.2), [69, p. 6] guarantees that $\mathcal{QSQ}$ has only point spectrum and its eigenvalues are given by a Rayleigh quotient. Accordingly we consider the eigenvalue problem

$$\mathcal{QSQ}\boldsymbol{\zeta} = \rho\boldsymbol{\zeta}. \tag{3.21}$$

Condition (3.20) holds, provided that (3.21) has no negative eigenvalues. Instead of analyzing (3.21), it is computationally convenient to work with

$$\begin{gathered} \mathcal{S}\boldsymbol{\zeta} + \sum_{i=1}^{n} \breve{c}_i \mathbf{T}_i = \mathbf{0}, \quad 0 < s < \sigma, \ \ \sigma \leq 1, \\ \boldsymbol{\zeta}(0) = \boldsymbol{\zeta}(\sigma) = \mathbf{0}, \ \ \int_0^{\sigma} \boldsymbol{\zeta} \cdot \mathbf{T}_i \, ds = 0, \ \ i = 1, \ldots, n. \end{gathered} \tag{3.22}$$

where the equivalence of the two problems is guaranteed by Lemma 2.1.

As in the unconstrained problem, we want to determine how the eigenvalue ρ changes as a fold in a branch of solutions is traversed. We begin by demonstrating that the eigenvalue problem (3.22) has a zero eigenvalue $\rho = 0$ at a fold in the bifurcation parameter. Differentiating the Euler-Lagrange equations (2.2), the integral constraints (3.14) and the nonlinear boundary conditions (3.15) with respect to pseudo-arclength along the branch yields the constrained boundary value problem

$$\begin{gathered} \mathcal{S}\dot{\mathbf{q}} + \sum_{i=1}^{n} \dot{\lambda}_i \mathbf{T}_i = \mathbf{0}, \\ \dot{\mathbf{q}}(0) = 0, \dot{\mathbf{q}}(1) = \frac{d\mathbf{f}}{d\alpha}\dot{\alpha}, \\ \int_0^1 \mathbf{T}_i \cdot \dot{\mathbf{q}} \, ds = 0. \end{gathered} \tag{3.23}$$

We remark that Equation (3.23) evaluated at a fold point is exactly the condition for an isoperimetric conjugate point (cf. Lemma 2.23); that is, the index changes at folds in the bifurcation parameter consistent with traditional stability exchange theory.

Note that the boundary value problem (3.23) is equivalent to the eigenvalue problem (3.22) having a zero eigenvalue $\rho = 0$ provided $\dot{\alpha} = 0$ and $c_i = \dot{\lambda}_i$. We further assume that $\rho = 0$ is a simple eigenvalue at a fold with corresponding eigenvector $\dot{\mathbf{q}}$. Additionally, if we take the derivative of (3.22) with respect to pseudo-arclength, τ, we get

$$\begin{gathered} \dot{\mathcal{S}}\boldsymbol{\zeta} + \mathcal{S}\dot{\boldsymbol{\zeta}} + \sum_{i=1}^{n} \dot{c}_i \mathbf{T}_i + \sum_{i=1}^{n} c_i \dot{\mathbf{T}}_i = \dot{\rho}\boldsymbol{\zeta} + \rho\dot{\boldsymbol{\zeta}}, \\ \dot{\boldsymbol{\zeta}}(0) = 0, \ \ \dot{\boldsymbol{\zeta}}(1) = 0, \end{gathered} \tag{3.24}$$

where the notation $\dot{\mathcal{S}}$ is defined in Equation (3.6). Taking the inner product of equation (3.24) with $\dot{\mathbf{q}}$, yields the following expression

$$\dot{\rho}\langle \dot{\mathbf{q}}, \boldsymbol{\zeta} \rangle + \rho \langle \dot{\mathbf{q}}, \dot{\boldsymbol{\zeta}} \rangle = \langle \dot{\mathbf{q}}, \dot{\mathcal{S}}\boldsymbol{\zeta} \rangle + \langle \dot{\mathbf{q}}, \mathcal{S}\dot{\boldsymbol{\zeta}} \rangle + \sum_{i=1}^{n} \langle \dot{\mathbf{q}}, \dot{c}_i \mathbf{T}_i \rangle + \sum_{i=1}^{n} \langle \dot{\mathbf{q}}, c_i \dot{\mathbf{T}}_i \rangle.$$

If this expression is evaluated at a fold point ($\rho = 0, \boldsymbol{\zeta} = \dot{\mathbf{q}}, c_i = \dot{\lambda}_i$), the following expression for $\dot{\rho}$ arises

$$\dot{\rho} = \langle \dot{\mathbf{q}}, \dot{\mathcal{S}}\dot{\mathbf{q}} \rangle + \langle \dot{\mathbf{q}}, \mathcal{S}\dot{\boldsymbol{\zeta}} \rangle + \sum_{i=1}^{n} \langle \dot{\mathbf{q}}, \dot{c}_i \mathbf{T}_i \rangle + \sum_{i=1}^{n} \langle \dot{\mathbf{q}}, \dot{\lambda}_i \dot{\mathbf{T}}_i \rangle. \tag{3.25}$$

The term involving $\dot{\mathcal{S}}$ can be evaluated by differentiating equation (3.23) with respect to τ:

$$\dot{\mathcal{S}}\dot{\mathbf{q}} + \mathcal{S}\ddot{\mathbf{q}} + \sum_{i=1}^{n} \ddot{\lambda}_i \mathbf{T}_i + \dot{\lambda}_i \dot{\mathbf{T}}_i = 0, \tag{3.26}$$

which when substituted into equation (3.25) yields:

$$\begin{aligned} \dot{\rho} &= \langle \dot{\mathbf{q}}, -(\mathcal{S}\ddot{\mathbf{q}} + \sum_{i=1}^{n} \ddot{\lambda}_i \mathbf{T}_i + \dot{\lambda}_i \dot{\mathbf{T}}_i)\rangle + \langle \dot{\mathbf{q}}, \mathcal{S}\dot{\boldsymbol{\zeta}}\rangle + \sum_{i=1}^{n} \langle \dot{\mathbf{q}}, \dot{c}_i \mathbf{T}_i\rangle + \sum_{i=1}^{n} \langle \dot{\mathbf{q}}, \dot{\lambda}_i \dot{\mathbf{T}}_i\rangle, \\ &= -\langle \dot{\mathbf{q}}, \mathcal{S}\ddot{\mathbf{q}}\rangle - \sum_{i=1}^{n} \langle \dot{\mathbf{q}}, \ddot{\lambda}_i \mathbf{T}_i\rangle + \langle \dot{\mathbf{q}}, \mathcal{S}\dot{\boldsymbol{\zeta}}\rangle + \sum_{i=1}^{n} \langle \dot{\mathbf{q}}, \dot{c}_i \mathbf{T}_i\rangle \end{aligned}$$

Recalling from (3.23) that $\langle \mathbf{T}_i, \dot{\mathbf{q}}\rangle = 0$, the expression for $\dot{\rho}$ becomes the same as in the unconstrained case, namely: $\dot{\rho} = \langle \dot{\mathbf{q}}, \mathcal{S}\dot{\boldsymbol{\zeta}}\rangle - \langle \dot{\mathbf{q}}, \mathcal{S}\ddot{\mathbf{q}}\rangle$. Proposition 3.1 and Proposition 3.2 from Section 3.3 can be applied to conclude that

$$\dot{\rho} = -\ddot{\alpha} \frac{d}{d\tau} \left[W_{\mathbf{q}'} \cdot \frac{d\mathbf{f}}{d\alpha} \right] \Bigg|_{s=1}, \tag{3.27}$$

which is exactly the expression that was found in the unconstrained case. Thus just as in that case, at a simple fold opening to the left, the lower branch in the α vs. $\left\{ W_{\mathbf{q}'} \cdot \frac{d\mathbf{f}}{d\alpha} \right\}$ does not represent local minima since ρ is increasing, and $\rho = 0$ at the fold. Note that the constants c_i can be interpreted as variations in the multipliers in the context of the alternative formulation presented in Appendix A.

While distinguished diagrams provide a convenient framework for summarizing and understanding index changes, they do not provide a complete alternative to explicit calculation of conjugate points for two reasons. First, the distinguished diagram can only predict changes in isoperimetric index, so that the index of at least one critical point in each connected component of solutions must be determined by some other means. Second, as in the standard exchange of stability theory, predictions from a distinguished diagram depend upon certain genericity assumptions (e.g. simplicity of folds). The constrained conjugate point test presented in Chapter 2 is a direct computation of the isoperimetric index that is not subject to either of these limitations. In fact, the two approaches yield an efficacious combination of conclusions.

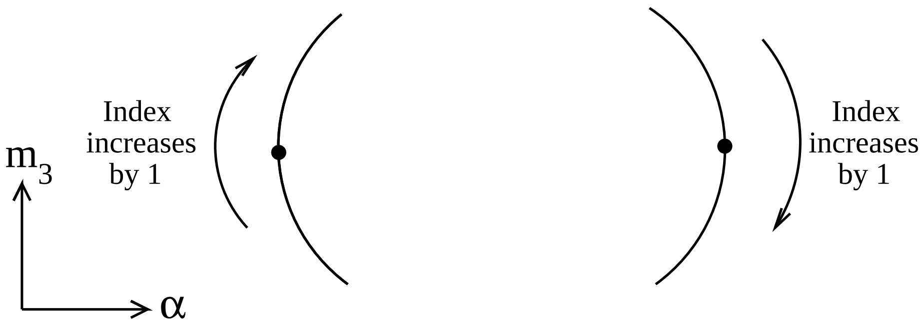

Figure 3.1: The distinguished bifurcation diagram for the twisted elastic loop problem is twist moment m_3 plotted versus angle α. These diagrams predict the direction of the stability exchange at folds (vertical tangents) opening either to the right or to the left. A necessary condition for a minimum is that the index is zero, therefore the portions of the branch which have non-zero index cannot correspond to minima.

Chapter 4

Rod Mechanics

4.1 Introduction

Elastic rods have been the focus of scientific scrutiny since Euler's time. The formulation of the elastic rod that will be exploited in the examples that follow is the special Cosserat theory. The information contained in this chapter is relatively standard and can be found in [1, 10, 11, 37, 38]. In Section 4.2, we present the kinematic equations. In Section 4.3, we state the force and moment balance laws. A discussion of constitutive relations is presented in Section 4.4, and finally Euler parameters, that are used to parametrize the rotation matrices which connect a fixed frame $\{\mathbf{e}_i\}_{i=1}^3$ to the body frame $\{\mathbf{d}_i\}_{i=1}^3$, are described in Section 4.5.

4.2 Kinematics of Rods

An elastic rod consists of a curve in space, denoted $\mathbf{r}(s) : [0, 1] \to \mathbb{R}^3$, and an orthonormal frame of *directors*, denoted $\{\mathbf{d}_i(s)\}_{i=1}^3$ (see Figure 4.1). The kinematic equations

$$\mathbf{r}' = \mathbf{v}, \tag{4.1}$$

$$\mathbf{d}_i' = \mathbf{u} \times \mathbf{d}_i, \quad i = 1, 2, 3, \tag{4.2}$$

where $'$ indicates differentiation with respect to the independent variable s, define the vectors $\mathbf{v}$ and $\mathbf{u}$. The components $u_k(s) \equiv \mathbf{u}(s) \cdot \mathbf{d}_k(s)$ are the strains with respect to bending ($k = 1, 2$) and twisting ($k = 3$). The components $v_k(s) \equiv \mathbf{v}(s) \cdot \mathbf{d}_k(s)$ are the strains associated with shear and stretching. We assume that the rod is unshearable ($v_1 = 0 = v_2$) and inextensible ($v_3 = 1$). Combining these assumptions with the kinematic equation (4.1) yields the equation $\mathbf{r}' = \mathbf{d}_3$, which relates the centerline $\mathbf{r}$ to the frame of directors $\{\mathbf{d}_i\}$.

4.3 Force and Moment Balance Laws

The stresses acting across each material normal cross-section are equivalent to a force and moment applied at the centroid of the cross-section at $\mathbf{r}(s)$; let $\mathbf{n}(s)$ and

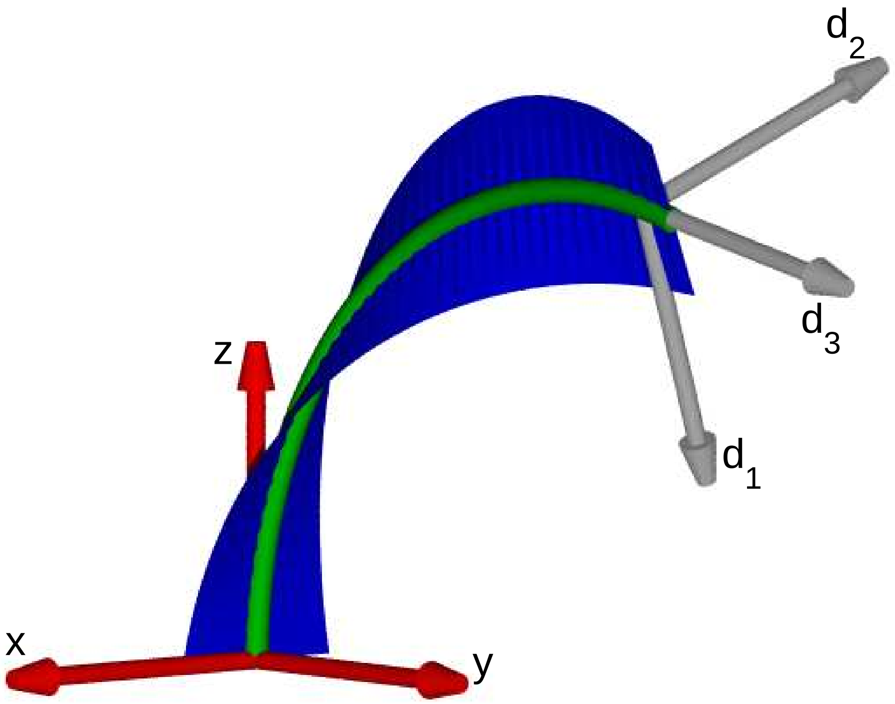

Figure 4.1: The centerline is depicted by a tube and the ribbon traces the path of the director $\mathbf{d}_1$ representing the twist. The director $\mathbf{d}_3$ is tangent to the centerline reflecting the unshearability assumption.

$\mathbf{m}(s)$ denote, respectively, this resultant force and moment (of the material on the side s^+ acting on the material on the side s^-). We will here assume that the only external loads are couples and forces applied at the ends of the rod. Then the force and moment balance laws are

$$\mathbf{n}'(s) = \mathbf{0}, \tag{4.3}$$

and

$$\mathbf{m}'(s) + \mathbf{r}'(s) \times \mathbf{n}(s) = \mathbf{0}. \tag{4.4}$$

4.4 Constitutive Relations

In order to complete the formulation of an elastic rod, constitutive relations between the strains u_i and the moments, $m_i \equiv \mathbf{m} \cdot \mathbf{d}_i$, must be presented. In particular, we consider hyperelastic rods; we assume that there exists a convex, strain energy density function $W(\mathsf{w})$, $\mathsf{w} = (w_1, w_2, w_3)$, such that $W_{\mathsf{w}}(\mathbf{0}) = 0$ and

$$m_i = W_{w_i}(u_i - \hat{u}_i), \quad \text{for} \quad i = 1, 2, 3, \tag{4.5}$$

where $\hat{\mathsf{u}}(s) = (\hat{u}_1(s), \hat{u}_2(s), \hat{u}_3(s))$ is the triplet of strains describing the curvature and twist of the unstressed rod. For the *idealized elastic loop* example presented in Chapter 6, we assume that the intrinsic shape of the rod is straight and untwisted so that $\hat{u}_i = 0$. In Chapter 8, an unstressed state which reflects local DNA geometry is used to adapt the elastic rod to model DNA minicircles.

Although much of the stability analysis in this dissertation can be formulated in terms of general strain energy density functions W, in the specific examples which follow, W is taken to be quadratic in $u_i - \hat{u}_i$. The assumption of diagonal quadratic energy, namely,

$$W(\mathsf{u} - \hat{\mathsf{u}}) = \frac{1}{2} \sum_{i=1}^{3} K_i (u_i - \hat{u}_i)^2, \tag{4.6}$$

defines the linear constitutive relations,

$$m_i = K_i (u_i - \hat{u}_i) \tag{4.7}$$

via equation (4.5). The quadratic energy assumption (4.6) is equivalent to a linear elasticity assumption.

The positive functions $K_i(s)$ in equation (4.6) represent the bending and twisting stiffnesses of the rod. Although generalizations are possible, in all examples presented in this dissertation, we will assume that the elastic rod is uniform, $K_i(s) = K_i$, and transversely isotropic, $K_1 = K_2$.

4.5 Euler Parameters

Rotation matrices in $SO(3)$ connect the body orthonormal frame $\{\mathbf{d}_i\}$ to a set of fixed coordinate axes in space $\{\mathbf{e}_i\}$. There are several ways to parametrize

$SO(3)$, the most common being the three-parameter representation provided by Euler angles. Due to the topology of $SO(3)$, a three-parameter representation cannot be a global representation, but necessarily has a singular direction. In this dissertation, we adopt a four-parameter representation by quaternions (or Euler parameters), which provides a two-fold global cover of $SO(3)$ and avoids the singularity of a three-parameter representation. The expense of these conveniences is the necessity of enforcing of a unit length constraint on the quaternions, which presents several analytical difficulties in the stability analysis of the elastic rod. A comprehensive treatment of Euler angles and Euler parameters can be found in [17, 26, 60], but the presentation in the following section has been adapted from [10, 11, 37].

Euler parameters are described by a vector $\mathbf{q} \in \mathbb{R}^4$, subject to the unit length constraint $|\mathbf{q}|^2 = 1$. Euler's Theorem [17, p.158] asserts that any two coordinate systems in $\mathbb{R}^3$ can be related by a simple rotation about a fixed axis. Let $\mathbf{a} = a_1\mathbf{e}_1 + a_2\mathbf{e}_2 + a_3\mathbf{e}_3$ be the unit vector parallel to this axis, and θ be the angle of rotation. The associated Euler parameters are

$$\begin{aligned} q_1 &= a_1 \sin(\theta/2), \\ q_2 &= a_2 \sin(\theta/2), \\ q_3 &= a_3 \sin(\theta/2), \\ q_4 &= \cos(\theta/2). \end{aligned}$$

Note that $\mathbf{q}$ and $-\mathbf{q}$ correspond to equivalent rotations $(\mathbf{a}, \theta)$ and $(\mathbf{a}, \theta + 2\pi)$, thus giving rise to the double covering of $SO(3)$. This two-to-one correspondence will manifest itself in the stability analysis of the twisted elastic loop.

The directors $\mathbf{d}_i$ can be written with respect to the fixed coordinate system in terms of the Euler parameters in the following manner:

$$\mathbf{d}_1 = \frac{1}{|\mathbf{q}|^2} \begin{pmatrix} q_1^2 - q_2^2 - q_3^2 + q_4^2 \\ 2(q_1q_2 + q_3q_4) \\ 2(q_1q_3 - q_2q_4) \end{pmatrix}, \tag{4.8}$$

$$\mathbf{d}_2 = \frac{1}{|\mathbf{q}|^2} \begin{pmatrix} 2(q_1q_2 - q_3q_4) \\ -q_1^2 + q_2^2 - q_3^2 + q_4^2 \\ 2(q_1q_4 + q_2q_3) \end{pmatrix}, \tag{4.9}$$

$$\mathbf{d}_3 = \frac{1}{|\mathbf{q}|^2} \begin{pmatrix} 2(q_1q_3 + q_2q_4) \\ 2(-q_1q_4 + q_2q_3) \\ -q_1^2 - q_2^2 + q_3^2 + q_4^2 \end{pmatrix}. \tag{4.10}$$

The parametrization of the directors by quaternions involves the normalization factor $|\mathbf{q}|^2$. According to the definition of the Euler parameters, $|\mathbf{q}|^2 = 1$, and any normalization should be equivalent. The choice of normalization factor presented here is deliberate and related to the value of the Lagrange multiplier which enforces the pointwise length constraint (cf. Appendix B). For this choice of normalization, the derivatives of the directors can be expressed elegantly through the following formulas derived by Dichmann [10]:

$$
\begin{aligned}
\left(\frac{\partial \mathbf{d}_1}{\partial \mathbf{q}}\right)^T &= \frac{2}{|\mathbf{q}|^2}\mathbf{B}_3\mathbf{q}\otimes\mathbf{d}_2 - \frac{2}{|\mathbf{q}|^2}\mathbf{B}_2\mathbf{q}\otimes\mathbf{d}_3,\\
\left(\frac{\partial \mathbf{d}_2}{\partial \mathbf{q}}\right)^T &= \frac{2}{|\mathbf{q}|^2}\mathbf{B}_1\mathbf{q}\otimes\mathbf{d}_3 - \frac{2}{|\mathbf{q}|^2}\mathbf{B}_3\mathbf{q}\otimes\mathbf{d}_1,\\
\left(\frac{\partial \mathbf{d}_3}{\partial \mathbf{q}}\right)^T &= \frac{2}{|\mathbf{q}|^2}\mathbf{B}_2\mathbf{q}\otimes\mathbf{d}_1 - \frac{2}{|\mathbf{q}|^2}\mathbf{B}_1\mathbf{q}\otimes\mathbf{d}_2,
\end{aligned}
\tag{4.11}
$$

where $\otimes$ denotes the outer product. The strains u_i can be written in terms of the quaternions via

$$
u_i = \frac{2\mathbf{q}'\cdot\mathbf{B}_i\mathbf{q}}{|\mathbf{q}|^2}, \quad i = 1, 2, 3, \tag{4.12}
$$

where the 4×4 matrices $\mathbf{B}_i$ are

$$
\mathbf{B}_1 = \begin{pmatrix} 0 & 0 & 0 & 1\\ 0 & 0 & 1 & 0\\ 0 & -1 & 0 & 0\\ -1 & 0 & 0 & 0 \end{pmatrix}, \tag{4.13}
$$

$$
\mathbf{B}_2 = \begin{pmatrix} 0 & 0 & -1 & 0\\ 0 & 0 & 0 & 1\\ 1 & 0 & 0 & 0\\ 0 & -1 & 0 & 0 \end{pmatrix}, \tag{4.14}
$$

$$
\mathbf{B}_3 = \begin{pmatrix} 0 & 1 & 0 & 0\\ -1 & 0 & 0 & 0\\ 0 & 0 & 0 & 1\\ 0 & 0 & -1 & 0 \end{pmatrix}. \tag{4.15}
$$

The vectors $\{\mathbf{B}_1\mathbf{q}, \mathbf{B}_2\mathbf{q}, \mathbf{B}_3\mathbf{q}, \mathbf{q}\}$ form an orthonormal basis for $\mathbb{R}^4$ and each vector $\mathbf{B}_i\mathbf{q}$ describes an infinitesimal rotation about the axis $\mathbf{d}_i$ in terms of the quaternions. The vectors which describe an infinitesimal rotation about the axis $\mathbf{e}_i$ are $\mathbf{F}_i\mathbf{q}$, where the matrices $\mathbf{F}_i$ are given by

$$
\mathbf{F}_1 = \begin{pmatrix} 0 & 0 & 0 & 1\\ 0 & 0 & -1 & 0\\ 0 & 1 & 0 & 0\\ -1 & 0 & 0 & 0 \end{pmatrix}, \tag{4.16}
$$

$$
\mathbf{F}_2 = \begin{pmatrix} 0 & 0 & 1 & 0\\ 0 & 0 & 0 & 1\\ -1 & 0 & 0 & 0\\ 0 & -1 & 0 & 0 \end{pmatrix}, \tag{4.17}
$$

$$
\mathbf{F}_3 = \begin{pmatrix} 0 & -1 & 0 & 0 \\ 1 & 0 & 0 & 0 \\ 0 & 0 & 0 & 1 \\ 0 & 0 & -1 & 0 \end{pmatrix}. \tag{4.18}
$$

A set of matrices $\mathbf{D}_j^k$ are defined by

$$
|\mathbf{q}|^2 \mathbf{d}_j \cdot \mathbf{e}_k = \mathbf{q} \cdot \mathbf{D}_j^k \mathbf{q},
$$

and can be written as $\mathbf{D}_j^k = -\mathbf{B}_j \mathbf{F}_k$; explicitly

$$
\mathbf{D}_1^1 = \begin{pmatrix} 1 & 0 & 0 & 0 \\ 0 & -1 & 0 & 0 \\ 0 & 0 & -1 & 0 \\ 0 & 0 & 0 & 1 \end{pmatrix},
$$

$$
\mathbf{D}_1^2 = \begin{pmatrix} 0 & 1 & 0 & 0 \\ 1 & 0 & 0 & 0 \\ 0 & 0 & 0 & 1 \\ 0 & 0 & 1 & 0 \end{pmatrix},
$$

$$
\mathbf{D}_1^3 = \begin{pmatrix} 0 & 0 & 1 & 0 \\ 0 & 0 & 0 & -1 \\ 1 & 0 & 0 & 0 \\ 0 & -1 & 0 & 0 \end{pmatrix},
$$

$$
\mathbf{D}_2^1 = \begin{pmatrix} 0 & 1 & 0 & 0 \\ 1 & 0 & 0 & 0 \\ 0 & 0 & 0 & -1 \\ 0 & 0 & -1 & 0 \end{pmatrix},
$$

$$
\mathbf{D}_2^2 = \begin{pmatrix} -1 & 0 & 0 & 0 \\ 0 & 1 & 0 & 0 \\ 0 & 0 & -1 & 0 \\ 0 & 0 & 0 & 1 \end{pmatrix},
$$

$$
\mathbf{D}_2^3 = \begin{pmatrix} 0 & 0 & 0 & 1 \\ 0 & 0 & 1 & 0 \\ 0 & 1 & 0 & 0 \\ 1 & 0 & 0 & 0 \end{pmatrix},
$$

$$
\mathbf{D}_3^1 = \begin{pmatrix} 0 & 0 & 1 & 0 \\ 0 & 0 & 0 & 1 \\ 1 & 0 & 0 & 0 \\ 0 & 1 & 0 & 0 \end{pmatrix}, \tag{4.19}
$$

$$\mathbf{D}_3^2 = \begin{pmatrix} 0 & 0 & 0 & -1 \\ 0 & 0 & 1 & 0 \\ 0 & 1 & 0 & 0 \\ -1 & 0 & 0 & 0 \end{pmatrix} ,$$

$$\mathbf{D}_3^3 = \begin{pmatrix} -1 & 0 & 0 & 0 \\ 0 & -1 & 0 & 0 \\ 0 & 0 & 1 & 0 \\ 0 & 0 & 0 & 1 \end{pmatrix} .$$

The matrices defined in this section will be especially useful in developing the projection matrix, which is critical to the stability analysis of the twisted elastic loop.

Chapter 5

Variational Formulation of the Elastic Loop

5.1 Introduction

In the previous chapter, we described the formulation of a Cosserat rod. In this chapter, we set forth an associated calculus of variations problem, demonstrate that the Euler-Lagrange derivative corresponds to the equilibrium equations, and describe the equilibrium configurations of the idealized twisted elastic loop. In the next chapter, we discuss the stability properties of these equilibrium configurations using the tests developed in Chapters 2 and 3.

The variational formulation of an elastic rod, which is bent into a loop and twisted by an angle α is described in Section 5.2. In Section 5.3, we calculate the equilibrium equations for this problem. Closed-form expressions for special equilibria, namely, n-covered circles are given in Section 5.4. Finally, in Section 5.5, we describe the complete set of equilibrium configurations of the twisted elastic loop, as determined numerically by parameter continuation in [37].

5.2 Variational Formulation

In this section we develop a variational formulation describing equilibrium configurations of an elastic rod which is bent into a loop and subjected to a prescribed twist (see Figure 5.1). The energy functional which models a twisted elastic rod (cf. Chapter 4) is

$$\int_0^1 W(u_1, u_2, u_3, s)\, ds, \tag{5.1}$$

where W is chosen to be quadratic in the strains as seen in Equation (4.6). The strains, denoted u_i, can be written as functions of the Euler parameters $\mathbf{q}$ and their derivatives $\mathbf{q}'$ (cf. Equation(4.12)); thus W is a function of the Euler parameters $\mathbf{q}$ and their derivative $\mathbf{q}'$.

We would like to minimize (5.1) subject to certain constraints and boundary conditions. The constraints arising from the unshearability and inextensibility assumption $\mathbf{r}' - \mathbf{d}_3 = \mathbf{0}$ are enforced using the Lagrange multiplier $\boldsymbol{\lambda}(s) \in \mathbb{R}^3$. The pointwise constraint associated with the unit length requirement on the quaternions $|\mathbf{q}(s)|^2 = 1$ can also be enforced by a Lagrange multiplier. Actually,

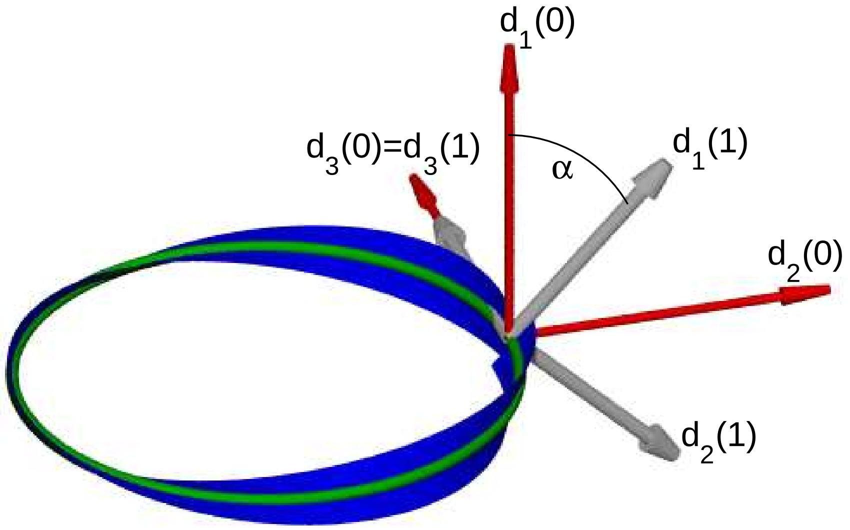

Figure 5.1: The centerline $\mathbf{r}(s)$ is indicated with a tube, and the normal direction $\mathbf{d}_1$ is visualized as a ribbon. At $s = 0$, the frame is oriented along the standard axes. At $s = 1$, the frame is rotated about $\mathbf{d}_3(0)$ by a prescribed angle α. The $s = 0$ frame is drawn darker and at a larger scale in order to distinguish it from the $s = 1$ frame.

instead of enforcing $|\mathbf{q}(s)|^2 = 1$, we choose instead to enforce the derivative of the constraint,

$$\mathbf{q}' \cdot \mathbf{q} = 0 \tag{5.2}$$

via a multiplier $\mu(s) \in \mathbb{R}$. The expression (5.2) is equivalent to $|\mathbf{q}(s)|^2 = 1$ given boundary conditions at $s = 0$ which ensure $|\mathbf{q}(0)|^2 = 1$. Therefore, in accordance with the usual multiplier rule, we consider extremals of the associated functional

$$J[\mathbf{q}, \mathbf{r}] = \int_0^1 [W(u_1, u_2, u_3, s) + \boldsymbol{\lambda} \cdot (\mathbf{r}' - \mathbf{d}_3) + \mu\, \mathbf{q}' \cdot \mathbf{q}]\ ds \tag{5.3}$$

subject to the boundary conditions

$$\mathbf{r}(0) = \mathbf{0}, \quad \mathbf{r}(1) = \mathbf{0}, \tag{5.4}$$

$$\mathbf{q}(0) = (0, 0, 0, 1), \quad \mathbf{q}(1) = \pm(0, 0, \sin(\alpha/2), \cos(\alpha/2)). \tag{5.5}$$

The boundary conditions on $\mathbf{q}$ represent a rotation of the normal directors $\mathbf{d}_1$ and $\mathbf{d}_2$ about the tangent $\mathbf{d}_3$ by an angle α. This can be demonstrated by substituting $\mathbf{q}(0)$ and $\mathbf{q}(1)$ into the expressions for the directors (4.8), (4.9), (4.10). The formulation in terms of Euler parameters produces a curiosity in specifying the boundary conditions. As was noted in Section 4.5, both $\mathbf{q}$ and $-\mathbf{q}$ correspond to the same rotation, thus, the boundary conditions (5.5) have freedom of sign. The linearized boundary conditions are identically zero removing the sign ambiguity.

The functional (5.3), which depends on both $\mathbf{r}$ and $\mathbf{q}$, can be reformulated so that it only depends on $\mathbf{q}$. The variable $\mathbf{r}$ appears only in the term $\int_0^1 \boldsymbol{\lambda}\cdot(\mathbf{r}'-\mathbf{d}_3)$ and the boundary conditions. The Euler-Lagrange derivative of J with respect to $\mathbf{r}$ yields the force balance law $\boldsymbol{\lambda}'=0$ where $\boldsymbol{\lambda}$ represents the force $\mathbf{n}$ in Equation (4.3). Since $\boldsymbol{\lambda}$ is constant, the term $\boldsymbol{\lambda}\cdot\int_0^1(\mathbf{r}'-\mathbf{d}_3)\,ds$ can be integrated to yield

$$\begin{aligned}\boldsymbol{\lambda}\cdot\int_0^1(\mathbf{r}'-\mathbf{d}_3)\,ds &= \boldsymbol{\lambda}\cdot\left(\mathbf{r}(1)-\mathbf{r}(0)-\int_0^1\mathbf{d}_3\,ds\right),\\ &= -\boldsymbol{\lambda}\cdot\int_0^1\mathbf{d}_3\,ds,\end{aligned}$$

where the closure conditions $\mathbf{r}(0)=\mathbf{r}(1)$ have been used. The constraint $\mathbf{r}'-\mathbf{d}_3=0$ can accordingly be replaced by the isoperimetric constraint $\int_0^1\mathbf{d}_3\,ds=0$, which also enforces the closure conditions on the rod because $\int_0^1\mathbf{d}_3\,ds=\int_0^1\mathbf{r}'\,ds=\mathbf{r}(1)-\mathbf{r}(0)=0$. Thus, we study the variational problem:

$$\begin{gathered}J[\mathbf{q}]=\int_0^1\left[W(u_1,u_2,u_3,s)\ -\boldsymbol{\lambda}\cdot\mathbf{d}_3+\mu\,\mathbf{q}\cdot\mathbf{q}'\right]\,ds,\\ \int_0^1\mathbf{d}_3\,ds=0,\\ \mathbf{q}(0)=(0,0,0,1),\quad \mathbf{q}(1)=\pm(0,0,\sin(\alpha/2),\cos(\alpha/2)),\end{gathered}\tag{5.6}$$

where W is given by (4.6), namely

$$W(\mathsf{u})=\frac{1}{2}\sum_{i=1}^{3}K_iu_i^2.\tag{5.7}$$

Given a solution $\mathbf{q}(s)$, the centerline $\mathbf{r}(s)$ of the rod can be recovered using the relation $\mathbf{r}'=\mathbf{d}_3(\mathbf{q})$ and the boundary condition $\mathbf{r}(0)=\mathbf{0}$.

The problem (5.6) is exactly of the general parameter-dependent isoperimetrically constrained form (3.16).

5.3 Equilibrium Equations

A necessary condition for J to have a minimum at $\mathbf{q}_0$ is that $\mathbf{q}_0$ satisfy the Euler-Lagrange equations. In this section, we see that if the four Euler-Lagrange derivatives are projected appropriately, the three moment balance laws (4.4) emerge, with the remaining equation producing an expression for the multiplier μ.

The first-order conditions rely on the chain rule, since the dependence of the strain energy density function W on $\mathbf{q}$ occurs via the strains u_i (cf. Equation (4.12)). The Euler-Lagrange derivative $-\frac{d}{ds}J_{\mathbf{q}'} + J_{\mathbf{q}} = \mathbf{0}$ is

$$\sum_{i=1}^{3} 2m_i' \frac{\mathbf{B}_i\mathbf{q}}{|\mathbf{q}|^2} = \sum_{i=1}^{3} m_i \left[-\left(\frac{4\mathbf{B}_i\mathbf{q}'}{|\mathbf{q}|^2} \right) - 2u_i \frac{\mathbf{q}}{|\mathbf{q}|^2} \right] - \frac{\partial(\mathbf{d}_3 \cdot \boldsymbol{\lambda})}{\partial \mathbf{q}} - \mu' \mathbf{q}, \tag{5.8}$$

where the matrices $\mathbf{B}_j$ are defined by Equations (4.13), (4.14), (4.15). In order to recover the moment balance laws, we project Equation (5.8) onto $\mathbf{B}_j\mathbf{q}$. Taking the inner product of (5.8) with $\mathbf{B}_j\mathbf{q}$, yields

$$2m_j' = \sum_{i=1}^{3} -2m_i u_k \epsilon_{ijk} - \frac{\partial(\mathbf{d}_3 \cdot \boldsymbol{\lambda})}{\partial \mathbf{q}} \cdot \mathbf{B}_j\mathbf{q}, \tag{5.9}$$

where ϵ_{ikj} is the standard permutation symbol. Equation (4.11) allows the last term to be rewritten as

$$\begin{aligned}
\frac{\partial(\mathbf{d}_3 \cdot \boldsymbol{\lambda})}{\partial \mathbf{q}} \cdot \mathbf{B}_j\mathbf{q} &= \frac{2}{|\mathbf{q}|^2} \left[\mathbf{B}_2\mathbf{q}(\mathbf{d}_1 \cdot \boldsymbol{\lambda}) - \mathbf{B}_1\mathbf{q}(\mathbf{d}_2 \cdot \boldsymbol{\lambda}) \right] \mathbf{B}_j\mathbf{q}, \\
&= 2\left[(\mathbf{d}_1 \cdot \boldsymbol{\lambda})\mathbf{e}_2 - (\mathbf{d}_2 \cdot \boldsymbol{\lambda})\mathbf{e}_1 \right], \\
&= 2(\mathbf{d}_i \times \mathbf{d}_3) \cdot \boldsymbol{\lambda},
\end{aligned}$$

so that the equilibrium equations become

$$m_j' = \sum_{i=1}^{3} -m_i u_k \epsilon_{ijk} - (\mathbf{d}_i \times \mathbf{d}_3) \cdot \boldsymbol{\lambda}. \tag{5.10}$$

Explicitly, Equation (5.10) reduces to the moment balance laws

$$\begin{aligned}
m_1' &= -u_2 m_3 + u_3 m_2 + \mathbf{d}_2 \cdot \boldsymbol{\lambda}, \\
m_2' &= u_1 m_3 - u_3 m_1 - \mathbf{d}_1 \cdot \boldsymbol{\lambda}, \\
m_3' &= -u_1 m_2 + u_2 m_1,
\end{aligned}$$

which are equivalent to (4.4), the balance laws in the fixed frame.

The value of the derivative of the Lagrange multiplier μ is determined by taking the inner product of (5.8) with $\mathbf{q}$

$$0 = \sum_{i=1}^{3} m_i \left[-\left(\frac{4\mathbf{q} \cdot \mathbf{B}_i\mathbf{q}'}{|\mathbf{q}|^2}\right) - 2u_i \right] - \frac{\partial(\mathbf{d}_3 \cdot \boldsymbol{\lambda})}{\partial \mathbf{q}} \cdot \mathbf{q} - \mu' = -\frac{\partial(\mathbf{d}_3 \cdot \boldsymbol{\lambda})}{\partial \mathbf{q}} \cdot \mathbf{q} - \mu'.$$

Since the value of μ' depends on the derivative of $\mathbf{d}_3$ with respect to $\mathbf{q}$ which in turn depends on the normalization of $\mathbf{d}_3$, the resulting value of μ' depends on the choice of normalization. The value of μ' for the normalization $|\mathbf{q}|^2$ presented in Section 4.5, is

$$\mu' = \left[\epsilon_{ij3} \frac{2\mathbf{B}_j\mathbf{q}}{|\mathbf{q}|^2} (\mathbf{d}_i \cdot \boldsymbol{\lambda}) \right] \cdot \mathbf{q} = (\mathbf{d}_i \cdot \boldsymbol{\lambda}) \epsilon_{ij3} \frac{2\mathbf{q} \cdot \mathbf{B}_j\mathbf{q}}{|\mathbf{q}|^2} = 0. \tag{5.11}$$

Appendix B calculates the value of μ' for arbitrary normalization of the directors $|\mathbf{q}|^\beta$. Note that $\mu' = 0$ only for the normalization factor $\beta = 2$.

5.4 Trivial Solution

A closed-form solution to the equilibrium equations, which we will call the *trivial solution*, is given by

$$\begin{aligned} q_1(s) &= \sin(n\pi s)\cos(\alpha s/2), \\ q_2(s) &= -\sin(n\pi s)\sin(\alpha s/2), \\ q_3(s) &= \cos(n\pi s)\sin(\alpha s/2), \\ q_4(s) &= \cos(n\pi s)\cos(\alpha s/2). \end{aligned} \tag{5.12}$$

From this solution, an expression for the directors can be calculated using (4.8), (4.9), (4.10), and the centerline

$$\mathbf{r}(s) = \left(0, \frac{\cos(2n\pi s) - 1}{2n\pi}, \frac{\sin(2n\pi s)}{2n\pi}\right)$$

can be recovered using the relation $\mathbf{r}' = \mathbf{d}_3$, and the boundary condition $\mathbf{r}(0) = 0$. The trivial solution corresponds to an n-covered ring lying in the $y-z$ plane with uniform twist α. The solution (5.12) also experiences a shear force $(\lambda_1, 0, 0)$, where $\lambda_1 = 2n\pi\alpha K_3$.

Note that the trivial solution (5.12) only satisfies the boundary conditions up to a sign, depending on the value of n. This quirk of the formulation is an artifact of the double-covering of $SO(3)$ in the Euler parameters representation; that is, both $\mathbf{q}$ and $-\mathbf{q}$ correspond to the same rotations $(\mathbf{d}_1, \mathbf{d}_2, \mathbf{d}_3)$ (cf. Section 4.5).

5.5 Understanding the Solution Set

The full set of equilibria for the idealized elastic loop problem (5.6) was previously calculated in [37] by transforming the constrained Lagrangian formulation to an unconstrained Hamiltonian formulation. The resulting equilibrium equations are a set of fourteen ordinary differential equations with boundary conditions. This boundary value problem (BVP) was numerically solved using AUTO [12], which employs a continuation algorithm to trace out curves of solutions using the n-covered circles as starting points. In the case of an idealized uniform isotropic rod, the (obvious) boundary conditions (5.5) cannot be used to numerically solve the BVP because the solutions are non-isolated due to symmetries of the rod, i.e. for a given value of the parameter α, there is an entire continuum set of symmetry-related equilibria. Instead, Li and Maddocks use an equivalent set of boundary conditions which factor out these symmetries. The effects of using the boundary conditions (5.5), which lead to non-isolated solutions for an idealized rod, appears in the stability analysis in the form of zero eigenvalues of appropriate matrices in the second variation.

The solution set is depicted in Figure 5.2 using the software package PCR [13, 14], which is a visualization tool for two-point boundary values problems. In Figure 5.2, the force λ_1 is plotted against the twisting moment m_3. Only the positive force solutions are shown, since the negative force solutions are symmetrically-related to the positive force solutions. The solution set naturally separates into parts: planar solutions and nonplanar solutions. The n-covered planar circular solutions are represented by the straight lines, whereas the non-planar solutions lie on the arcs which connect the straight lines. The outermost straight lines correspond to single covered circles with positive twist (on the right) and negative twist (on the left). Similarly, the middle and inner set of straight lines correspond to double and triple covered circles, respectively, with the positive twist circles on the right side of the diagram and the negative twist circles on the left side of the diagram. If the bifurcation points on each branch are indexed by m, then each bifurcation point can be labeled by the number of coverings of the circle n, the index m of the bifurcation point, and the sign of the twisting direction $(+,-)$. Symbolically, this is denoted by $(n,m,+)$ or $(n,m,-)$. The branch of nontrivial solutions which connects the bifurcation point $(1,1,+)$ to $(1,1,-)$ we call the *first nontrivial branch*.

We will explore the relationship between the solution set and the corresponding physical configurations. Figure 5.3 contains a sequence of physical configurations lying on the first nontrivial branch. Configuration (a) is a circle with negative twist and corresponds to the $(1,1,-)$ bifurcation point. As the branch is traversed toward $(1,1,+)$, the planar solution deforms to the nonplanar solution (b). The figure-eight solution (c) is the only solution on the first nontrivial branch which has a point of self-contact. Since the formulation of rod equilibria presented here does not account for self-contact forces, the rod simply passes through itself and deforms into configuration (d) which is similar to configuration (b) but with positive twist. Configuration (e) is a single covered circle with positive twist and corresponds to the solution at $(1,1,+)$.

The higher order nontrivial branch which connects $(1,2,+)$ to $(2,1,-)$ contains the three physical configurations depicted in Figure 5.4. Configuration (a) is an unknotted rod with three-fold symmetry. As the branch is traversed, this solution continuously deforms to the self-intersecting trefoil configuration (b). The rod then passes through itself and forms the trefoil knot (c). The physical configurations on higher-order nontrivial branches behave similarly. Although self-contact effects are not accounted for in this formulation, each nontrivial branch contains only one equilibrium with self-intersections, namely the n-foil solution.

The above solution sets were computed for $\hat{u}_i = 0$ and $\gamma = 1$. If solutions for a different value of γ are of interest then the boundary value problem need not be recomputed. Instead, the solution for this different value of γ can be recovered with only a call to an initial value problem solver. Changing the value of γ does not change the centerline of the rod; it only changes the rate at which the $\mathbf{d}_1$ director rotates about the tangent vector [37].

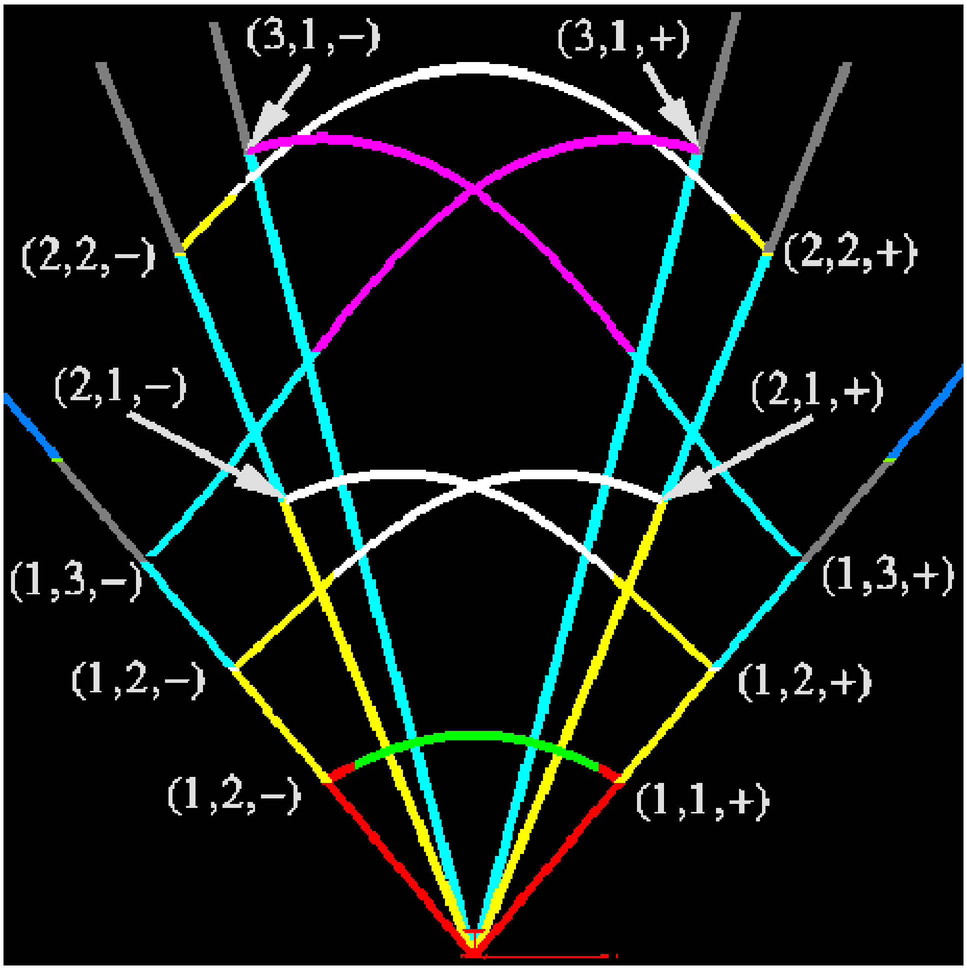

Figure 5.2: The bifurcation diagram for the elastic loop which plots λ_1 versus m_3 consists of straight lines connected by curved segments. The straight lines represent trivial branches of planar circular solutions. The curved arcs represent nontrivial branches of nonplanar equilibria. The diagram is colored by isoperimetric index, with red representing equilibria with isoperimetric index zero, and thus stable. Unstable equilibria are represented by green, yellow, white, cyan, magenta, and gray with corresponding indices 1,2,3,4,5,6, respectively.

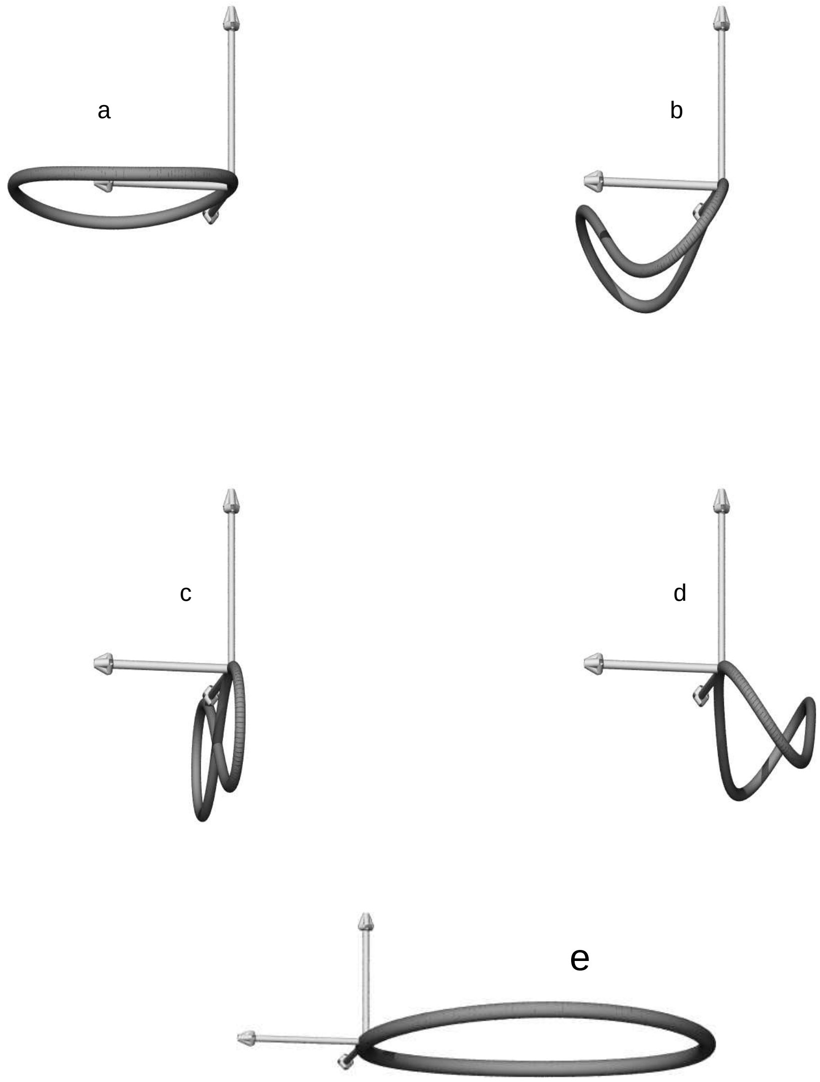

Figure 5.3: This sequence of physical configurations are equilibria which lie on the branch that connects $(1, 1, +)$ to $(1, 1, -)$. Configuration (a) is a circle with negative twist and corresponds to the equilibrium at $(1, 1, -)$. Configuration (b) is a nonplanar solution, which deforms into figure-eight equilibria (c) as the branch is traversed. Configuration (d) is the solution corresponding configuration (b) with positive twist. Configuration (e) is a planar circle with positive twist. (Figures taken from Li & Maddocks [37].)

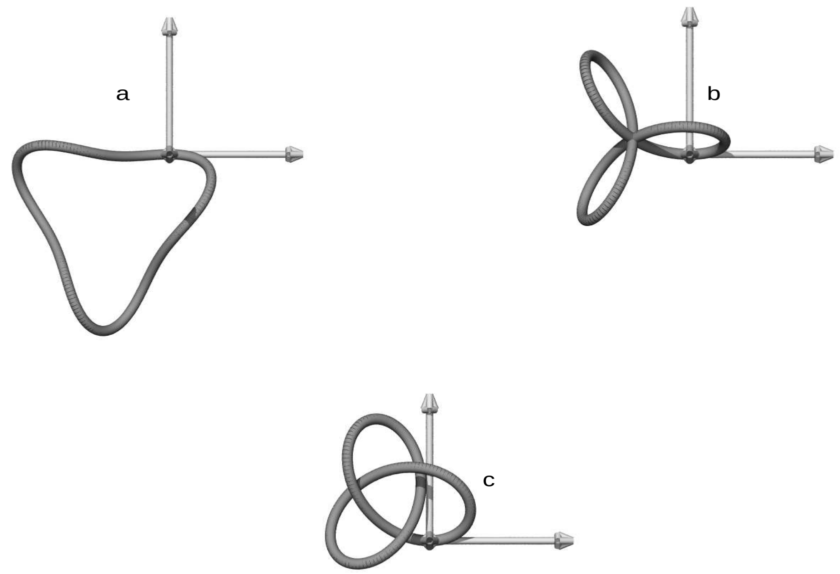

Figure 5.4: The configurations depicted here all lie on the branch which connects $(1, 2, +)$ to $(2, 1, -)$. Configuration (a) is an unknotted nonplanar equilibrium. The trefoil (b) is the only self-intersecting solution on the branch. After the trefoil solution, the rod passes through itself to form a trefoil knot (c). (Figures taken from Li & Maddocks [37].)

Chapter 6

Stability Analysis of the Elastic Loop

6.1 Introduction

The goal of this chapter is to present a bifurcation and stability analysis of the idealized twisted elastic loop. In the previous chapter, we detailed the variational characterization of the problem, presented the equilibrium equations, and described the solution set. In this chapter, the second variation of (5.6) is derived to further determine the constrained index of the equilibrium solutions.

The index of the planar solutions on the trivial branches is determined using a test originating in the theory of restricted quadratic forms [41]. This test determines the constrained index from the number of negative and zero eigenvalues of the (unconstrained) second-order differential operator, and the inertia[1] of a particular matrix (3×3, in this case) constructed from solutions to certain boundary value problems.

This test for determining the index of the planar solutions is not useful in calculating the index of the nonplanar solutions because the boundary value problems defining the 3×3 matrix can not be solved in closed form. For these nontrivial solutions, the distinguished diagram theory developed in Chapter 3 is appropriately modified for this problem in order to determine how the index changes at folds. Further the index can be completely quantified because all nonplanar branches connect back to a planar solution on which the isoperimetric index has already been calculated.

In Section 6.2, we derive the second variation of (5.6) and the linearization of the constraints and boundary conditions. A method for eliminating the variations which do not respect the unit length constraint on the quaternions is described in Section 6.3. In Section 6.4, we present the second-order differential operator $\mathcal{S}$ associated with the quadratic form of the second variation. Section 6.5 contains the calculations necessary for analytically determining the index on the trivial branch. The results of the stability analysis on the trivial branches is presented in Section 6.6, and in Section 6.7, we describe the stability analysis of the nontrivial branches.

[1] The inertia of a matrix is a triplet of numbers corresponding to the number of positive, negative and zero eigenvalues of that matrix.

6.2 Derivation of the Second Variation

Calculation of the isoperimetric index requires second-order information, thus in this section, we calculate the second variation of (5.6) and evaluate the corresponding derivatives. By direct calculation:

$$\begin{aligned}\delta^2 J[\mathbf{h}] &= \frac{1}{2}\int_0^1 [\mathbf{h}' \cdot W_{\mathbf{q}'\mathbf{q}'}\mathbf{h}' + \mathbf{h} \cdot W_{\mathbf{q}\mathbf{q}}\mathbf{h} \\ &\quad -\mathbf{h} \cdot \hat{\mathbf{\Lambda}}\mathbf{h} + \mathbf{h} \cdot W_{\mathbf{q}\mathbf{q}'}\mathbf{h}' + \mathbf{h}' \cdot W_{\mathbf{q}'\mathbf{q}}\mathbf{h} + \mu\mathbf{h} \cdot \mathbf{h}'\Big]\ ds, \qquad (6.1)\end{aligned}$$

where

$$\hat{\mathbf{\Lambda}} = \frac{\partial^2 \mathbf{d}_3}{\partial \mathbf{q}^2} \cdot \boldsymbol{\lambda}_{\mathbf{0}},$$

$\mathbf{h} \in \mathbb{R}^4$ is the variation in the Euler parameters, and the subscripts on W represent partial derivatives. Here, we have denoted the equilibrium value of $\boldsymbol{\lambda}$ by $\boldsymbol{\lambda}_{\mathbf{0}}$.

We can eliminate the term involving μ as follows. An integration by parts on the term $\int_0^1 \mu\ \mathbf{h} \cdot \mathbf{h}'$ shifts the derivative to the multiplier μ; that is,

$$\int_0^1 \mu\ \mathbf{h} \cdot \mathbf{h}'\ ds \quad = \quad -\frac{1}{2}\int_0^1 \mu'\ \mathbf{h} \cdot \mathbf{h}\ ds.$$

We are assuming that $\mathbf{q} + \epsilon\mathbf{h}$ satisfy the same initial conditions as $\mathbf{q}$, so $\mathbf{h}(0) = \mathbf{h}(1) = \mathbf{0}$, and the boundary terms in the integration by parts vanish. Hence, the second variation becomes

$$\begin{aligned}\delta^2 J[\mathbf{h}] &= \frac{1}{2}\int_0^1 [\mathbf{h}' \cdot W_{\mathbf{q}'\mathbf{q}'}\mathbf{h}' + \mathbf{h} \cdot W_{\mathbf{q}\mathbf{q}}\mathbf{h} \\ &\quad -\mathbf{h}\Lambda\mathbf{h} + \mathbf{h}W_{\mathbf{q}\mathbf{q}'}\mathbf{h}' + \mathbf{h}'W_{\mathbf{q}'\mathbf{q}}\mathbf{h} - 2\mu'\mathbf{h} \cdot \mathbf{h}]\ ds.\end{aligned}$$

By Equation (5.11), $\mu' = 0$ and the second variation takes the form:

$$\begin{aligned}\delta^2 J[\mathbf{h}] &= \frac{1}{2}\int_0^1 \mathbf{h}' \cdot W_{\mathbf{q}'\mathbf{q}'}\mathbf{h}' + \mathbf{h} \cdot W_{\mathbf{q}\mathbf{q}}\mathbf{h} \\ &\quad -\mathbf{h}\mathbf{\Lambda}\mathbf{h} + \mathbf{h}W_{\mathbf{q}\mathbf{q}'}\mathbf{h}' + \mathbf{h}'W_{\mathbf{q}'\mathbf{q}}\mathbf{h}\ ds. \qquad (6.2)\end{aligned}$$

The next section is dedicated to finding explicit formulas, via the chain rule, for the second derivatives: $W_{\mathbf{q}\mathbf{q}}, W_{\mathbf{q}\mathbf{q}'}, W_{\mathbf{q}'\mathbf{q}}, W_{\mathbf{q}'\mathbf{q}'}, \mathbf{\Lambda}$.

6.2.1 Derivatives of W

Recall that the strain energy density function, W, depends on the Euler parameters through its dependence on the strains, u_i, (cf. Equation (4.12)). In this section we calculate the second derivatives of W with respect to the Euler parameters in terms of the first and second derivatives of W with respect to the strains:

$$
\begin{aligned}
W_{\mathbf{qq}} &= \frac{4}{|\mathbf{q}|^4}\sum_{i,j=1}^{3} W_{u_iu_j}\Big[\mathbf{B}_i\mathbf{q}'\otimes\mathbf{B}_j\mathbf{q}' + u_j\mathbf{B}_i\mathbf{q}'\otimes\mathbf{q} + u_i\mathbf{q}\otimes\mathbf{B}_j\mathbf{q}' + u_iu_j\mathbf{q}\otimes\mathbf{q}\Big] \\
&\quad + \frac{2}{|\mathbf{q}|^4}\sum_{i=1}^{3} m_i\Big[2\mathbf{B}_i\mathbf{q}'\otimes\mathbf{q} + 2\mathbf{q}\otimes\mathbf{B}_i\mathbf{q}' + 4u_i\mathbf{q}\otimes\mathbf{q} - 2|\mathbf{q}|^2u_i\mathbf{I}\Big],
\end{aligned}
$$

$$
\begin{aligned}
(W_{\mathbf{qq}'})^T = W_{\mathbf{q}'\mathbf{q}} &= -\frac{4}{|\mathbf{q}|^4}\sum_{i,j=1}^{3} W_{u_iu_j}\left[\mathbf{B}_i\mathbf{q}\otimes\mathbf{B}_j\mathbf{q}' + u_j\mathbf{B}_i\mathbf{q}\otimes\mathbf{q}\right] \\
&\quad + \frac{2}{|\mathbf{q}|^4}\sum_{i=1}^{3} m_i\left[|\mathbf{q}|^2\mathbf{B}_i - 2\mathbf{B}_i\mathbf{q}\otimes\mathbf{q}\right],
\end{aligned}
$$

and

$$
W_{\mathbf{q}'\mathbf{q}'} = \frac{4}{|\mathbf{q}|^4}\sum_{i,j=1}^{3} W_{u_iu_j}\mathbf{B}_i\mathbf{q}\otimes\mathbf{B}_j\mathbf{q},
$$

where the $\mathbf{B}_i$ matrices are defined in (4.13), (4.14), (4.15) and $\otimes$ denotes the outer product. If we further assume that W is a quadratic function of the strains u_i (cf. Equation (5.7)), then

$$
W_{u_iu_j} = K_i\delta_{ij}, \quad m_i = K_i(u_i - \hat{u}_i),
$$

where δ_{ij} denotes the Kronecker delta. Note that in this section we also assume that $K_1 = K_2$ and $\hat{u}_i = 0$.

6.2.2 Second Derivative of $\mathbf{d}_3$

In this section, we calculate the term

$$
\begin{aligned}
\boldsymbol{\Lambda} &= \frac{\partial^2(\mathbf{d}_3\cdot\boldsymbol{\lambda})}{\partial\mathbf{q}\partial\mathbf{q}} \\
&= \lambda_1\frac{\partial^2(\mathbf{d}_3\cdot\mathbf{e}_1)}{\partial\mathbf{q}^2} + \lambda_2\frac{\partial^2(\mathbf{d}_3\cdot\mathbf{e}_2)}{\partial\mathbf{q}^2} + \lambda_3\frac{\partial^2(\mathbf{d}_3\cdot\mathbf{e}_3)}{\partial\mathbf{q}^2} \\
&= \lambda_1\boldsymbol{\Lambda}_{13} + \lambda_2\boldsymbol{\Lambda}_{23} + \lambda_3\boldsymbol{\Lambda}_{33},
\end{aligned}
$$

where each matrix $\boldsymbol{\Lambda}_{i3}$, $i = 1\ldots3$ is a 4×4 matrix. The entries of the matrices $\boldsymbol{\Lambda}_{13}, \boldsymbol{\Lambda}_{23}, \boldsymbol{\Lambda}_{33}$ are complicated and are explicitly written out in Appendix C. The 4×4 matrix $\boldsymbol{\Lambda}$ can be converted to a drastically simpler 3×3 matrix after an appropriate projection described in the next section.

6.3 Quaternion Projection

A necessary condition that (5.6) has a minimum is Legendre's strengthened condition, which requires that the matrix $W_{\mathbf{q}'\mathbf{q}'}$ be positive definite. The calculation in the previous section reveals that

$$W_{\mathbf{q}'\mathbf{q}'} = \begin{pmatrix} K_1 & 0 & 0 & 0 \\ 0 & K_2 & 0 & 0 \\ 0 & 0 & K_3 & 0 \\ 0 & 0 & 0 & 0 \end{pmatrix},$$

which is only positive semi-definite. This complication is an artifact of the unit length constraint on the Euler parameters. Therefore, the topic of this section is an explicit projection of variations $\mathbf{h} \in \mathbb{R}^4$ onto the variations $\boldsymbol{\zeta} \in \mathbb{R}^3$ which ensure that the pointwise constraint $|\mathbf{q}|^2 = 1$ is satisfied. The expressions for $\mathbf{d}_3$ (4.10) and the strains u_i (4.12) reveal that the second variation (6.2) is homogeneous of degree zero in $\mathbf{q}$. Therefore, the second variation $\delta^2 J$ will be identically zero when $\boldsymbol{\zeta}$ is in the direction of $\mathbf{q}$. This flat direction (which is an artifact of the four-parameter quaternion covering of $SO(3)$) is of no interest in the determination of stability; thus we restrict our attention to variations in the subspace of $\mathbb{R}^4$ orthogonal to $\mathbf{q}$ in a pointwise sense. There are many bases for $\mathbf{q}^{\perp}$; one such basis is $\{\mathbf{B}_1\mathbf{q}, \mathbf{B}_2\mathbf{q}, \mathbf{B}_3\mathbf{q}\}$ (cf. Equations (4.13), (4.14), (4.15)). Thus, an arbitrary variation $\mathbf{h} \in \mathbb{R}^4$ can be projected on to $\mathbf{q}^{\perp}$ by applying the matrix whose rows are $(\mathbf{B}_i\mathbf{q})^T$. This projection matrix will be used in the example of DNA presented in Chapter 8. For the example of the idealized twisted elastic loop, we use another projection matrix whose rows are given by $\{\mathbf{D}_3^1\mathbf{q}, \mathbf{F}_1\mathbf{q}, \mathbf{B}_3\mathbf{q}\}$ (cf. Equations (4.15), (4.16), (4.19)):

$$\boldsymbol{\Pi} = \begin{pmatrix} q_3 & q_4 & q_1 & q_2 \\ q_4 & -q_3 & q_2 & -q_1 \\ q_2 & -q_1 & q_4 & -q_3 \end{pmatrix}. \tag{6.3}$$

This projection has the advantage that the projected operator $\mathcal{S}$ has constant coefficients if the coefficients are evaluated on the planar solutions. The rows of $\boldsymbol{\Pi}$ correspond to infinitesimal rotations about the in-plane normal of the rod, the out-of-plane normal of the rod and the tangential component of the rod, respectively (cf. Maddocks [40]). The projected second variation has the property that $\mathbf{P}$ is positive definite, therefore Legendre's strengthened condition is satisfied.

In the next two subsections, we describe the application of this projection to the quadratic form of the second variation, the linearized constraints and the boundary conditions.

6.3.1 The Second Variation

After projecting the variations, $\mathbf{h} = \mathbf{\Pi}^T \boldsymbol{\zeta}$, the second variation (6.2) becomes

$$\begin{aligned}\delta^2 J[\boldsymbol{\zeta}] \;=\; & \frac{1}{2}\int_0^1 \boldsymbol{\zeta}' \cdot \mathbf{\Pi} W_{\mathbf{q}'\mathbf{q}'} \mathbf{\Pi}^T \boldsymbol{\zeta}' + \boldsymbol{\zeta}' \cdot \left[\mathbf{\Pi} W_{\mathbf{q}'\mathbf{q}'} \mathbf{\Pi'}^T + \mathbf{\Pi} W_{\mathbf{q}'\mathbf{q}} \mathbf{\Pi}^T\right] \boldsymbol{\zeta} \\ & + \boldsymbol{\zeta} \cdot \left[\mathbf{\Pi}' W_{\mathbf{q}'\mathbf{q}'} \mathbf{\Pi}^T + \mathbf{\Pi} W_{\mathbf{q}\mathbf{q}'} \mathbf{\Pi}^T\right] \boldsymbol{\zeta}' + \boldsymbol{\zeta} \cdot \left[\mathbf{\Pi}' W_{\mathbf{q}'\mathbf{q}'} \mathbf{\Pi'}^T + \mathbf{\Pi} W_{\mathbf{q}\mathbf{q}} \mathbf{\Pi}^T \right. \\ & \left. - \mathbf{\Pi} \Lambda \mathbf{\Pi}^T + \mathbf{\Pi} W_{\mathbf{q}\mathbf{q}'} \mathbf{\Pi'}^T + \mathbf{\Pi}' W_{\mathbf{q}'\mathbf{q}} \mathbf{\Pi}^T\right] \boldsymbol{\zeta} \quad ds. \end{aligned} \tag{6.4}$$

6.3.2 Boundary Conditions and Constraints

The boundary conditions and the constraints also have to be linearized and projected. The three isoperimetric linearized constraints projected onto the three dimensional subspace are given by

$$\int_0^1 \left(\frac{\partial \mathbf{d}_3}{\partial \mathbf{q}} \cdot \mathbf{e}_i\right) \cdot \mathbf{\Pi}^T \boldsymbol{\zeta} \; ds$$

which when evaluated on the trivial solution (5.12) become

$$\int_0^1 \zeta_1 \; ds = 0 \qquad \int_0^1 \cos(2\pi n s)\zeta_2 \; ds = 0 \qquad \int_0^1 \sin(2\pi n s)\zeta_2 \; ds = 0. \tag{6.5}$$

The linearized projected boundary conditions are

$$\boldsymbol{\zeta}(0) = \mathbf{0}, \quad \boldsymbol{\zeta}(1) = \mathbf{0}. \tag{6.6}$$

6.4 The Operator $\mathcal{S}$

An important component of the stability analysis is the second-order operator associated with the second variation. The quadratic form of the second variation

$$\delta^2 J[\boldsymbol{\zeta}] \;=\; \frac{1}{2}\int_0^1 \left[\boldsymbol{\zeta}' \cdot \mathbf{P}\boldsymbol{\zeta}' + \boldsymbol{\zeta} \cdot \mathbf{C}\boldsymbol{\zeta}' + \boldsymbol{\zeta}' \cdot \mathbf{C}^T \boldsymbol{\zeta} + \boldsymbol{\zeta} \cdot \mathbf{Q}\boldsymbol{\zeta}\right] ds,$$

can be rewritten after integrating by parts in the form:

$$\delta^2 J[\boldsymbol{\zeta}] \;=\; \langle \boldsymbol{\zeta}, \mathcal{S}\boldsymbol{\zeta}\rangle$$

where $\mathcal{S}$ is defined to be

$$\mathcal{S}\boldsymbol{\zeta} \equiv -\frac{d}{ds}\left[\mathbf{P}\boldsymbol{\zeta}' + \mathbf{C}^T \boldsymbol{\zeta}\right] + \mathbf{C}\boldsymbol{\zeta}' + \mathbf{Q}\boldsymbol{\zeta} \tag{6.7}$$

and

$$\begin{aligned} & \mathbf{P} = \mathbf{\Pi} W_{\mathbf{q}'\mathbf{q}'} \mathbf{\Pi}^T, \\ & \mathbf{Q} = \mathbf{\Pi}' W_{\mathbf{q}'\mathbf{q}'} \mathbf{\Pi'}^T + \mathbf{\Pi} W_{\mathbf{q}\mathbf{q}} \mathbf{\Pi}^T - \mathbf{\Pi} \Lambda \mathbf{\Pi}^T + \mathbf{\Pi} W_{\mathbf{q}\mathbf{q}'} \mathbf{\Pi'}^T + \mathbf{\Pi}' W_{\mathbf{q}'\mathbf{q}} \mathbf{\Pi}^T, \\ & \mathbf{C} = \mathbf{\Pi}' W_{\mathbf{q}'\mathbf{q}'} \mathbf{\Pi}^T + \mathbf{\Pi} W_{\mathbf{q}\mathbf{q}'} \mathbf{\Pi}^T. \end{aligned} \tag{6.8}$$

6.5 Bifurcation Analysis and Stability Calculations

In this section, we reproduce the Lagrangian (or variational) form of the bifurcation analysis performed by Li and Maddocks [37] on the circular solution. This bifurcation analysis is intimately connected to the stability analysis of the planar equilibria. The formula for calculating the constrained index of the planar solutions requires the number of zero and negative eigenvalues of the 3×3 matrix and also the number of zero and negative eigenvalues of the operator $\mathcal{S}$. These calculations are performed in this section, the results appear in Tables 6.1 and 6.2 and are discussed in Section 6.6.

We begin with defining a bifurcation point. A necessary condition for there to be a bifurcation is that the linearization of the Euler-Lagrange equations is singular. That is, there is a nontrivial solution to the system

$$\mathcal{S}\boldsymbol{\zeta} + \sum_{i=1}^{n} \bar{\lambda}_i \mathbf{T}_i = 0, \tag{6.9}$$

which also satisfies the linearized constraints (6.5), and the boundary conditions (6.6). Following Maddocks [41], the bifurcation points are classified as either *type 1 bifurcations*, if $\bar{\boldsymbol{\lambda}} = \mathbf{0}$, or *type 2 bifurcations*, if $\bar{\boldsymbol{\lambda}} \neq \mathbf{0}$. Here, the coefficients of operator $\mathcal{S}$ evaluated on the trivial solution (5.12) are

$$\mathbf{P} = \begin{pmatrix} K_1 & 0 & 0 \\ 0 & K_1 & 0 \\ 0 & 0 & K_3 \end{pmatrix}, \quad \mathbf{Q} = \begin{pmatrix} 0 & 4\alpha K_3 & 8K_3 n\pi \\ -4\alpha K_3 & 0 & 0 \\ -8K_3 n\pi & 0 & 0 \end{pmatrix},$$

$$\mathbf{C} = \begin{pmatrix} 0 & 4\alpha K_3 & 8K_3 n\pi \\ -4\alpha K_3 & 0 & 0 \\ -8K_3 n\pi & 0 & 0 \end{pmatrix}.$$

The notation $\bar{\lambda}_i$ denotes the variations of the multipliers, and

$$\mathbf{T}_i \equiv \mathbf{\Pi} \frac{\partial(\mathbf{d}_3 \cdot \mathbf{e}_i)}{\partial \mathbf{q}},$$

which evaluates to

$$\mathbf{T}_1 = \begin{pmatrix} -\frac{1}{2}\frac{\bar{\lambda}_1}{K_1} \\ 0 \\ 0 \end{pmatrix}, \quad \mathbf{T}_2 = \begin{pmatrix} 0 \\ \frac{1}{2}(\frac{\bar{\lambda}_2}{K_1}\cos(2n\pi s)) \\ 0 \end{pmatrix}, \quad \mathbf{T}_3 = \begin{pmatrix} 0 \\ \frac{1}{2}\frac{\bar{\lambda}_3}{K_1}\sin(2n\pi s) \\ 0 \end{pmatrix}, \tag{6.10}$$

on the trivial solution (5.12). Explicitly, Equation (6.9) is

$$\begin{aligned} -\zeta_1'' + 4(\gamma - 1)n^2\pi^2\zeta_1 + \alpha\gamma\zeta_2' + 2\gamma n\pi\zeta_3' &= -\frac{1}{2}\frac{\bar{\lambda}_1}{K_1}, \\ -\zeta_2'' - \alpha\gamma\zeta_1' &= \frac{1}{2}\frac{(\bar{\lambda}_2\cos(2n\pi s) + \bar{\lambda}_3\sin(2n\pi s))}{K_1}, \\ -\zeta_3'' - 2n\pi\zeta_1' &= 0, \end{aligned} \tag{6.11}$$

where $\gamma = \frac{K_3}{K_1}$ and the variations in the multipliers produce the inhomogeneities on the right hand side of the equations.

6.5.1 Type 1 Bifurcation Points

Type 1 bifurcations occur at non-trivial solutions to the homogeneous system defined by setting $\bar{\lambda}_i = 0$ in (6.11). The general solution is

$$\zeta(s) = c_1 \begin{pmatrix} 0 \\ 0 \\ 1 \end{pmatrix} + c_2 \begin{pmatrix} 0 \\ 1 \\ 0 \end{pmatrix} + c_3 \left[\begin{pmatrix} -\gamma \\ 0 \\ 0 \end{pmatrix} + s \begin{pmatrix} 0 \\ 0 \\ 2\pi n(\gamma - 1) \end{pmatrix} \right] \tag{6.12}$$

$$+ c_4 \left[\begin{pmatrix} -\alpha\gamma \\ 0 \\ 0 \end{pmatrix} + s \begin{pmatrix} 0 \\ 4(\gamma-1)n^2\pi^2 \\ 0 \end{pmatrix} \right] + c_5 \begin{pmatrix} -1 \\ \frac{\alpha i \gamma}{\sigma} \\ \frac{2\pi n i}{\sigma} \end{pmatrix} e^{-i\sigma s} + c_6 \begin{pmatrix} -1 \\ -\frac{\alpha i \gamma}{\sigma} \\ -\frac{2\pi n i}{\sigma} \end{pmatrix} e^{i\sigma s},$$

where $\sigma^2 = 4\pi^2 n^2 + \alpha^2\gamma^2$. The coefficients $\{c_1, c_2, c_3, c_4, c_5, c_6\}$ are determined by enforcing the linearized boundary conditions $\boldsymbol{\zeta}(0) = \mathbf{0}$ and $\boldsymbol{\zeta}(1) = \mathbf{0}$. The coefficients are the solutions to the following homogeneous linear system:

$$\begin{pmatrix} 0 & 0 & -\gamma & -\alpha\gamma & -1 & -1 \\ 0 & 1 & 0 & 0 & \frac{\alpha i \gamma}{\sigma} & -\frac{\alpha i \gamma}{\sigma} \\ 1 & 0 & 0 & 0 & \frac{2\pi n i}{\sigma} & -\frac{2\pi n i}{\sigma} \\ 0 & 0 & -\gamma & -\alpha\gamma & -e^{-i\sigma} & -e^{i\sigma} \\ 0 & 1 & 0 & 4(\gamma-1)n^2\pi^2 & \frac{\alpha i \gamma}{\sigma} e^{-i\sigma} & -\frac{\alpha i \gamma}{\sigma} e^{i\sigma} \\ 1 & 0 & 2\pi n(\gamma-1) & 0 & \frac{2\pi n i}{\sigma} e^{-i\sigma} & -\frac{2\pi n i}{\sigma} e^{i\sigma} \end{pmatrix} \begin{pmatrix} c_1 \\ c_2 \\ c_3 \\ c_4 \\ c_5 \\ c_6 \end{pmatrix} = \begin{pmatrix} 0 \\ 0 \\ 0 \\ 0 \\ 0 \\ 0 \end{pmatrix},$$

which has a nontrivial solution provided that the determinant of the matrix vanishes, i.e.

$$\frac{8\, in\pi\ (\gamma-1)\left[(\alpha^2\gamma + 4\, n^2\pi^2)\gamma(1-\cos(\sigma)) - 2\, n^2\pi^2(\gamma-1)\sin(\sigma)\sigma\right]}{\sigma} = 0. \tag{6.13}$$

This equation has two families of solutions. The first solution is $\sigma = p$, where p satisfies the equation

$$p = \frac{2\pi^2 n^2(\gamma-1)}{(\alpha^2\gamma + 4n^2\pi^2)\gamma} \tan(\frac{p}{2}).$$

The solutions generated from $\sigma = p$ do not satisfy the integral constraints (6.5), and therefore do not correspond to type 1 bifurcation points. These solutions are in the null space of $\mathcal{S}$, however, which will be important in Section 6.6.

The second solution to (6.13) is $\sigma = 2\pi k$, k a non-zero integer, with the corresponding solution vector:

$$\begin{aligned} \zeta_1(s) &= 2\sin(2\pi k s), \\ \zeta_2(s) &= \frac{\alpha\gamma}{k\pi}\left(-1 + \cos(2\pi k s)\right), \\ \zeta_3(s) &= \frac{2n}{k}\left(-1 + \cos(2\pi k s)\right). \end{aligned}$$

This solution satisfies the linearized constraints (6.5), thus are type one bifurcation points for $\alpha^2\gamma^2 = 4\pi^2(k^2 - n^2)$, $k > n$.

6.5.2 Type 2 Bifurcation Points

In this section we present the analysis of the type 2 bifurcation points, which is intimately tied to the stability analysis of the planar equilibria. The type 2 bifurcation analysis requires the solution to the nonhomogeneous problem $\mathcal{S}\boldsymbol{\eta}_i = \mathbf{T}_i$, where $\mathbf{T}_i$ is defined by (6.10). The solutions $\boldsymbol{\eta}_i$ are computed using the homogeneous solution of the previous section and a particular solution for each $\mathbf{T}_i$, then applying the boundary conditions (6.6). Since the multipliers $\boldsymbol{\lambda}$ are constant (see Equation (4.3)), the variations in the multipliers $\bar{\boldsymbol{\lambda}}$ are constant as well. Since $\bar{\boldsymbol{\lambda}}_i$ appears as a scalar multiple of each solution $\boldsymbol{\eta}_i$, the basis of the nonhomogeneous solutions $\boldsymbol{\eta}_i$ is determined by the choice of constant. For this analysis, we choose $\bar{\lambda}_i = 1$.

A type 2 bifurcation point is a solution $\boldsymbol{\eta}_i$ that satisfies the constraints (6.5). An equivalent formulation constructs the matrix $\mathbf{N} = \{\mathcal{S}\boldsymbol{\eta}_i, \boldsymbol{\eta}_j\} = \{\mathbf{T}_i, \boldsymbol{\eta}_j\}$, which will also be used in the stability analysis of the trivial branches. Type 2 bifurcation points occur when the determinant of $\mathbf{N}$ vanishes. For the idealized loop problem, the entries of the matrix $\mathbf{N}$ are

$$
\begin{aligned}
\langle \mathbf{T}_1, \boldsymbol{\eta}_1 \rangle &= \frac{\left(\kappa_1 K_1 \sin(\frac{\sigma}{2})\sigma^2 - 1\right)}{16\, {K_1}^2 n^2 \pi^2 \,(\gamma - 1)}, & \langle \mathbf{T}_1, \boldsymbol{\eta}_2 \rangle &= 0, \\
\langle \mathbf{T}_1, \boldsymbol{\eta}_3 \rangle &= -\frac{\kappa_3 \, \sin(\frac{\sigma}{2})\sigma^2}{8\, K_1 \,\pi\, n \alpha \gamma}, & \langle \mathbf{T}_2, \boldsymbol{\eta}_1 \rangle &= 0, \\
\langle \mathbf{T}_2, \boldsymbol{\eta}_2 \rangle &= 0, & \langle \mathbf{T}_2, \boldsymbol{\eta}_3 \rangle &= 0, \\
\langle \mathbf{T}_3, \boldsymbol{\eta}_1 \rangle &= -\frac{\kappa_1\, \alpha\gamma\, \sigma^2\, (-1)^n \sin(\frac{\sigma}{2})}{8\, K_1\, n\pi\, \gamma^2 \alpha^2}, & \langle \mathbf{T}_3, \boldsymbol{\eta}_2 \rangle &= 0, \\
\langle \mathbf{T}_3, \boldsymbol{\eta}_3 \rangle &= \frac{\sigma^2 \kappa_3\, (-1)^n \sin(\frac{\sigma}{2})\, (\gamma - 1)}{4\, K_1\, \alpha^2 \gamma^2}, & &
\end{aligned}
$$

where

$$
\kappa_1 = \frac{1}{K_1 \left[(\alpha^2\gamma + 4\, n^2\pi^2)\gamma \sin(\frac{\sigma}{2}) + 2\, n^2\pi^2\sigma(\gamma - 1)\cos(\frac{\sigma}{2})\right]},
$$

and

$$
\kappa_3 = \frac{(-1)^n}{\left[\,(\alpha^2\gamma + 4\, n^2\pi^2)\gamma \sin(\frac{\sigma}{2}) + 2\, n^2\pi^2(\gamma - 1)\cos(\frac{\sigma}{2})\sigma\right]}.
$$

Since the second row and second column vanish, the determinant of $\mathbf{N}$ vanishes identically. The determinant vanishes identically due to the non-isolation of the circular equilibria. Each circular equilibrium can undergo a rigidbody rotation to produce another equilibrium configuration. Since the force is necessarily perpendicular to the plane of the circle, the force is also changing. Type 2 bifurcation points occur when the determinant of $\mathbf{N}$ vanishes, and in this case, since the determinant of $\mathbf{N}$ vanishes identically, there is a type 2 bifurcation point point everywhere as a consequence of the rotational symmetry of the circular equilibria. A suitable choice of boundary conditions can factor out this (and other) symmetries of the rod and lead to isolated equilibria [37], which is necessary for the numerical computation of the solution set. The formulation of the problem that was used for the stability analysis does not use this choice of boundary conditions.

Here, we merely recognize the zero eigenvalue of $\mathbf{N}$ generated by symmetry and consider a reduced 2×2 matrix

$$n = \begin{pmatrix} \langle \mathbf{T}_1, \boldsymbol{\eta}_1 \rangle & \langle \mathbf{T}_1, \boldsymbol{\eta}_3 \rangle \\ \langle \mathbf{T}_3, \boldsymbol{\eta}_1 \rangle & \langle \mathbf{T}_3, \boldsymbol{\eta}_3 \rangle \end{pmatrix} = \begin{pmatrix} \frac{\left(\kappa_1\, K_1 \sin(\frac{\sigma}{2})\sigma^2 - 1\right)}{16\, {K_1}^2 n^2 \pi^2 (\gamma - 1)} & -\frac{\kappa_3\, \sin(\frac{\sigma}{2})\sigma^2}{8\, K_1\, \pi\, n \alpha\gamma} \\ -\frac{\kappa_1\, \alpha\gamma\, \sigma^2 (-1)^n \sin(\frac{\sigma}{2})}{8\, K_1\, n\pi\, \gamma^2 a^2} & \frac{\sigma^2 \kappa_3\, (-1)^n \sin(\frac{\sigma}{2})(\gamma - 1)}{4\, K_1\, \alpha^2 \gamma^2} \end{pmatrix}.$$

The determinant of n:

$$|n| = -\frac{\sigma^2 \kappa_3 (-1)^n \sin(\sigma/2)}{K_1 n^2 \pi^2 \alpha^2 \gamma^2}$$

only vanishes at type 1 bifurcation points $\sigma = 2\pi k$.

The planar stability analysis also requires the number of negative eigenvalues of $\mathbf{N}$. To this end, we consider the eigenvalues of n

$$\theta_1 = \frac{1}{4} \frac{1}{8n^2\pi^2\alpha^2\gamma^2(\gamma - 1)} \left[\beta + \sqrt{\beta^2 + 16\left[\sigma^2 \chi (\gamma - 1)^2 n^2 \pi^2 \alpha^2 \gamma^2\right]}\right]$$

and

$$\theta_2 = \frac{1}{4} \frac{1}{8n^2\pi^2\alpha^2\gamma^2(\gamma - 1)} \left[\beta - \sqrt{\beta^2 + 16\left[\sigma^2 \chi (\gamma - 1)^2 n^2 \pi^2 \alpha^2 \gamma^2\right]}\right],$$

where

$$\beta = \left[\sigma^2 \chi (\alpha^2\gamma^2 + 4n^2\pi^2(\gamma - 1)^2) - \alpha^2\gamma^2\right],$$

and

$$\chi = \frac{\sin(\frac{\sigma}{2})}{\left[\, (\alpha^2\gamma + 4\, n^2\pi^2)\gamma \sin(\frac{\sigma}{2}) - 2\, n^2\pi^2(\gamma - 1)\cos(\frac{\sigma}{2})\sigma \right]}.$$

6.5.3 The Eigenvalues of $\mathcal{S}$

To determine the stability of the trivial branches, the number of negative eigenvalues of $\mathcal{S}$ needs to be determined. The number of negative eigenvalues of $\mathcal{S}$ corresponds to the number of (unconstrained) conjugate points of $\mathcal{S}$ in the interval $(0, 1)$ (cf. Morse [47]). The operator $\mathcal{S}$ is said to have an unconstrained conjugate point at $s = p$ provided there is a solution to the initial value problem $\mathcal{S}\boldsymbol{\zeta} = \mathbf{0}$, $\boldsymbol{\zeta}(0) = \mathbf{0}$, that also satisfies the boundary condition $\boldsymbol{\zeta}(p) = \mathbf{0}$. To analytically determine conjugate points of $\mathcal{S}$, we apply the boundary conditions at $s = 0$ to the homogeneous solution (6.12). Enforcing the homogeneous Dirichlet boundary conditions at $s = 0$ allows the six coefficients $(c_1, c_2, c_3, c_4, c_5, c_6)$ to be written in terms of three coefficients (ν_1, ν_2, ν_3):

$$\begin{pmatrix} c_1 \\ c_2 \\ c_3 \\ c_4 \\ c_5 \\ c_6 \end{pmatrix} = \begin{pmatrix} \frac{2\pi n i}{\sigma}(\gamma\nu_1 + \alpha\gamma\nu_2 + 2\nu_3) \\ \frac{a i \gamma}{\sigma}(\gamma\nu_1 + \alpha\gamma\nu_2 + 2\nu_3) \\ \nu_1 \\ \nu_2 \\ -\gamma\nu_1 - \alpha\gamma\nu_2 - \nu_3 \\ \nu_3 \end{pmatrix}.$$

Applying the boundary condition $\boldsymbol{\zeta}(p) = \mathbf{0}$ to the solutions $\boldsymbol{\zeta}$ which also satisfy $\boldsymbol{\zeta}(0) = \mathbf{0}$ yields a 3×3 linear system of equations for ν_i. There exists a solution provided there exists a $p > 0$ satisfying

$$p\left[(\alpha^2\gamma^2 + 4n^2\pi^2\gamma)(1 - \cos(p\sigma)) - 2\,\pi^2 n^2 p(\gamma - 1)\,\sin(p\sigma)\sigma\right] = 0, \tag{6.14}$$

which is exactly the condition for a type 1 bifurcation point (cf. Equation (6.13)). Thus, each candidate for a type 1 bifurcation point correspond to a conjugate point, and thus, a negative eigenvalue. Representative graphs of (6.14) for $\alpha = 0.5$ are depicted in Figure 6.1 for $\gamma = 1.1$ and Figure 6.2 for $\gamma = 0.9$. In each graph $p(\alpha^2\gamma^2 + 4n^2\pi^2\gamma)(1 - \cos(p\sigma))$ and $2\,\pi^2 n^2 p^2(\gamma - 1)\,\sin(p\sigma)\sigma$ are plotted, so that intersections in the graphs correspond to solutions of (6.14), and thus, to conjugate points. The results are shown in Tables 6.1 and 6.2, respectively. Note that for $\gamma < 1$ and $\gamma > 1$ the operator $\mathcal{S}$ has different numbers of conjugate points, and thus, different numbers of negative eigenvalues.

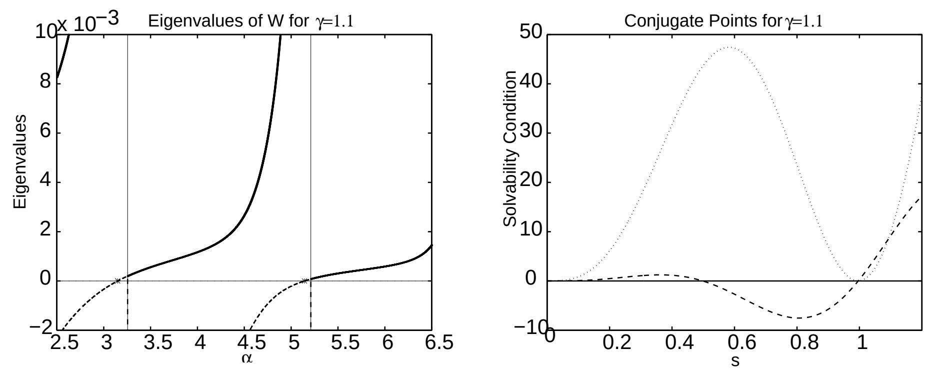

Figure 6.1: The graph on the left plots the eigenvalues of $\mathbf{N}$ as a function of the angle α plotted in terms of multiples of π. For each value of α, there are three eigenvalues, namely, the dotted line, the solid line, and the zero eigenvalue. The number of non-positive eigenvalues can be determined for each value of the parameter α. In the graph on the right, the dotted line indicates the graph of $p(\alpha^2\gamma^2 + 4n^2\pi^2\gamma)(1 - \cos(p\sigma))$ and the dashed line indicates the graph of $2\,\pi^2 n^2 p^2(\gamma - 1)\,\sin(p\sigma)\sigma$, thus, intersections of the dotted line with the dashed line in the interval $(0, 1)$ correspond to solutions of Equation (6.14), or conjugate points of $\mathcal{S}$. The number of conjugate points indicates the number of negative eigenvalues of the operator $\mathcal{S}$.

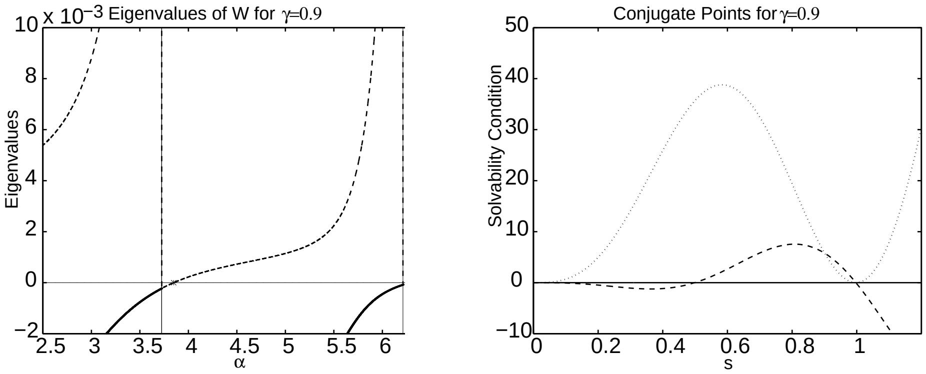

Figure 6.2: The graph on the left plots the eigenvalues of $\mathbf{N}$ as a function of the angle α plotted in terms of multiples of π. For each value of α, there are three eigenvalues, namely, the dotted line, the solid line, and the zero eigenvalue. The number of non-positive eigenvalues can be determined for each value of the parameter α. In the graph on the right, the dotted line indicates the graph of $p(\alpha^2\gamma^2 + 4n^2\pi^2\gamma)(1 - \cos(p\sigma))$ and the dashed line indicates the graph of $2\,\pi^2 n^2 p^2(\gamma - 1)\,\sin(p\sigma)\sigma$, thus, intersections of the dotted line with the dashed line in the interval $(0, 1)$ correspond to solutions of Equation (6.14), or conjugate points of $\mathcal{S}$. intersections of the dotted line with the dashed line in the interval $(0, 1)$ correspond to conjugate points of $\mathcal{S}$, which in turn indicates the number of negative eigenvalues.

6.6 Stability Analysis of Planar Equilibria

The stability analysis of the planar equilibria is based on a test originating in the theory of restricted quadratic forms, using the idea of $\mathcal{S}$-orthogonal subspaces (see [23, 39, 41]). In the context of constrained variational principles, the test was formulated by Maddocks [41] and is encapsulated in the formula:

$$\mathbf{d}^{-}(\mathbf{C}) = \mathbf{d}^{-}(\mathcal{H}) + \dim N(\mathcal{S}) - \delta(\mathbf{N}) - \nu(\mathbf{N}), \tag{6.15}$$

where $\mathbf{d}^{-}(\mathbf{C})$ is the number of negative eigenvalues of $\mathcal{S}$ on the subspace of interest (i.e., the isoperimetric index), $\mathbf{d}^{-}(\mathcal{H})$ is the number of negative eigenvalues of $\mathcal{S}$ on the whole space, $\dim N(\mathcal{S})$ denotes the dimension of the kernel of $\mathcal{S}$, $\delta(\mathbf{N})$ denotes the number of zero eigenvalues of the matrix $\mathbf{N}$, and $\nu(\mathbf{N})$ denotes the number of negative eigenvalues of $\mathbf{N}$. An equilibrium is stable provided the index is zero, i.e., the number of non-positive eigenvalues of the operator on the whole space equals the number of non-positive eigenvalues of $\mathbf{N}$.

The values of the individual terms appearing in this formula were calculated in the previous section and depend on whether $\gamma > 1$ or $\gamma < 1$, but the stability conclusions are the same for both cases. The results for $\gamma > 1$ can be seen in Table 6.1 and the results for $\gamma < 1$ can be seen in Table 6.2. The entries in the tables for the number of non-positive eigenvalues of $\mathbf{N}$ are determined from the graphs of the eigenvalues, the graphs on the left of Figures 6.1 and 6.2. Although the graphs are for fixed values of γ, namely, $\gamma = 1.1$ and $\gamma = 0.9$, the determinant of w is zero only at type 1 bifurcation points independent of γ. Therefore, $\mathbf{N}$ has the same number of non-positive eigenvalues for $\gamma > 1$ as for $\gamma = 1.1$ and similarly for $\gamma < 1$. The entries in the tables for the number of negative eigenvalues of $\mathcal{S}$ are determined by counting the intersections, or conjugate points, in the graphs on the right of Figures 6.1 and 6.2. The null space of $\mathcal{S}$ contains the candidates for type one bifurcation points which did not satisfy the constraints.

The constrained index can be determined by applying (6.15) using the entries in Tables 6.1 and 6.2. The numbers given in Tables 6.1 and 6.2 confirm that the planar single-covered circular solution is stable until the first bifurcation point and then unstable, with the isoperimetric index increasing by two at each bifurcation point. The table for the double-covered circles is the same as Tables 6.1 and 6.2 without the entries for $\alpha_0 < \alpha < \alpha_1$ and $\alpha_1 < \alpha < \alpha_2$. Thus for $n > 1$, since the index is greater than 2, the planar n-covered circles are unstable. These results have been confirmed by the conjugate point test, which produced the color coding of the index in Figure 5.2.

These results are only valid if $\alpha \neq 0$ and $\gamma \neq 1$, but similar calculations can be performed for $\alpha = 0$ and $\gamma = 1$.

6.7 Stability Analysis of Nonplanar Equilibria

In this section, stability results are presented for the nonplanar equilibria of the twisted elastic loop. The direct approach using Equation (6.15) is not feasible for analyzing the nontrivial branches because the operator $\mathcal{S}$ has non-constant

α	$\delta(\mathbf{N})+\nu(\mathbf{N})$	$\mathbf{d}^-(\mathcal{H})$	$\dim N(\mathcal{S})$	$d^-(C)$
$\alpha_0 < \alpha < \alpha_1$	1	0	1	0
$\alpha_1 < \alpha < \alpha_2$	2	1	1	0
$\alpha_2 < \alpha < \alpha_3$	1	2	1	2
$\alpha_3 < \alpha < \alpha_4$	2	3	1	2
$\alpha_4 < \alpha < \alpha_5$	1	4	1	4

Table 6.1: This table illustrates the use of Equation (6.15) for $\gamma > 1$ to determine stability of the twisted elastic loop for regions defined by: $\alpha_0 = 0$, $\alpha_1 = \pi\sqrt{m_1^2 - 4n^2}/\gamma$, $\alpha_2 = 2\pi\sqrt{2^2 - n^2}/\gamma$, $\alpha_3 = \pi\sqrt{m_2^2 - 4n^2}/\gamma$, $\alpha_4 = 2\pi\sqrt{3^2 - n^2}/\gamma$, etc. For n=1, the constrained index, $d^-(C)$ shown in the last column, is zero until the first bifurcation point α_2 and then non-zero. For $n > 1$, the constrained index is always greater than zero.

α	$\delta(\mathbf{N})+\nu(\mathbf{N})$	$\mathbf{d}^-(\mathcal{H})$	$\dim N(\mathcal{S})$	$d^-(C)$
$\alpha_0 < \alpha < \alpha_1$	2	1	1	0
$\alpha_1 < \alpha < \alpha_2$	3	2	1	0
$\alpha_2 < \alpha < \alpha_3$	2	3	1	2
$\alpha_3 < \alpha < \alpha_4$	3	4	1	2
$\alpha_4 < \alpha < \alpha_5$	2	5	1	4

Table 6.2: This table illustrates the use of Equation (6.15) for $\gamma < 1$ to determine stability of the twisted elastic loop for regions defined by: $\alpha_0 = 0$, $\alpha_1 = \pi\sqrt{m_1^2 - 4n^2}/\gamma$, $\alpha_2 = 2\pi\sqrt{2^2 - n^2}/\gamma$, $\alpha_3 = \pi\sqrt{m_2^2 - 4n^2}/\gamma$, $\alpha_4 = 2\pi\sqrt{3^2 - n^2}/\gamma$, etc. For n=1, the constrained index is zero until the first bifurcation point α_2 and then non-zero. For $n > 1$, the constrained index is always greater than zero.

coefficients. Instead, an indirect approach which uses the distinguished diagram theory presented in Chapter 3 is used to determine stability properties.

Unfortunately, the general theory discussed in Chapter 3 is not applicable to the twisted elastic loop problem without some modification. Distinguished diagram theory requires the zero eigenvalue of (3.3) at the fold to be simple. For the idealized elastic loop problem, however, the second variation has zero eigenvalues along the entire branch. These null directions are a consequence of symmetries: one is generated by translation in arc-length, and one by a coupling of rotational symmetry in space with a rotation about the centerline of the rod (cf. [37]). Consequently, for the example of the twisted elastic loop, the second variation operator has a zero eigenvalue of multiplicity three at a fold. For non-simple eigenvalues, the calculations of Chapter 3 can be repeated except instead of concluding that $\dot{\mathbf{q}}$ defined by Equation (3.4) is the eigenvector associated with the zero eigenvalue, one can only conclude that it is in the null space of $\mathcal{S}$; that is, $\dot{\mathbf{q}} = \sum_{i=1}^{3} c_i \boldsymbol{\eta}_i$, where $\boldsymbol{\eta}_i$ form a basis for the null space. The other steps are essentially the same as outlined in Chapter 3, and the following expression can be deduced:

$$\sum_{i=1}^{3} \dot{\mu}_i = -\ddot{\alpha}\frac{d}{d\tau}\left[W_{\mathbf{q}'} \cdot \frac{d\mathbf{f}}{d\alpha}\right]\bigg|_{s=1} . \tag{6.16}$$

Equation (6.16) reveals only that the sign of the sum of the derivatives of the critical eigenvalues can be determined at a fold. For the elastic loop problem, however, two of the three eigenvalues which are zero at a fold are zero on the entire branch, since they are a consequence of symmetries. Therefore because the two persistent zero eigenvalues have vanishing derivatives, $\dot{\mu}_1' = \dot{\mu}_2' = 0$, Equation (6.16) does characterize $\dot{\mu}_3$. A sufficient condition for applying distinguished diagram theory in the presence of multiple zero eigenvalues is that it is known that only one eigenvalue changes sign at the fold. Thus, the general formula (6.16) reduces to (3.12) and the theory described in Chapter 3 still applies. The abscissa and ordinate of the distinguished diagram are determined by applying (3.12) to the twisted elastic loop problem

$$\begin{aligned} \dot{\mu} &= -\ddot{\alpha}\frac{d}{d\sigma}\left\{W_{\mathbf{q}'} \cdot \frac{d\mathbf{f}}{d\alpha}\right\}\bigg|_{s=1} \\ &= -\ddot{\alpha}\frac{d}{d\sigma}\left\{m_3\right\}\big|_{s=1} , \end{aligned} \tag{6.17}$$

i.e. the distinguished diagram is a plot of twist moment against angle.

The distinguished projection of the bifurcation diagram allows conclusions to be made about how the index changes at a fold in the bifurcation parameter. For a fold opening to the right (left), if the lower (upper) branch has index I, then the upper (lower) branch has index $I + 1$ (see Figure 3.1). In order to actually quantify the index along the branch of solutions, the index of one solution along the branch must be known. For the idealized elastic rod, this information can be generated from the planar configurations at either end of the branch. For the elastic loop, each bifurcation point has a pitchfork structure (cf. Figure 7.1) and can be classified as either subcritical or supercritical (see Chapter 7). A pitchfork bifurcation point is called subcritical (supercritical) if the nontrivial branch occurs (at least locally) for values of the parameter α for which the trivial solution is stable (unstable) [21, p. 34]. This classification of bifurcation points gives additional information about the stability properties of solutions near that point [24, p. 24]. Nontrivial solutions near a subcritical bifurcation point are unstable and nontrivial solutions near a supercritical bifurcation point are stable. This definition relies on the fact that the solutions on one side of the bifurcation point have constrained index zero, which is only true for the $(1, 1, +)$ and $(1, 1, -)$ bifurcation points. All other bifurcation points can be classified as subcritical or supercritical in a more general sense. At each bifurcation point the constrained index increases by two. Suppose at bifurcation point $(n, m, +)$ the constrained index increases from i to $i+2$. Then this bifurcation point is labeled subcritical (supercritical) if the nontrivial branch occurs for values of the parameter for which the trivial solution has the index i (index $i+2$). Similarly, nontrivial solutions near a supercritical bifurcation point have index i and nontrivial solutions near a subcritical bifurcation point have index $i+1$. This more general definition is consistent with conjugate point calculations and reduces to the definition in [21, p. 34] for $i = 0$. For $i > 0$, the nontrivial branches have index at least two, and thus cannot correspond to stable equilibria even in the presence of folds.

Figure 6.3 depicts the distinguished diagrams of the first nontrivial branch of the elastic loop for three different values of γ. In all three figures, the straight lines correspond to the trivial branches of planar single covered circles. The curved branch which emanates from these straight lines corresponds to the first nontrivial branch which connects the $(1, 1, +)$ bifurcation point to the $(1, 1, -)$ bifurcation point. For $\gamma = 1.3$, the bifurcation points $(1, 1, , +)$ and $(1, 1, -)$ are subcritical and the solutions nearby are unstable. The nontrivial branch which is unstable near the bifurcation point has one negative eigenvalue because there are three zero eigenvalues at the bifurcation point and two along the nontrivial branch. Thus, there can be at most one negative eigenvalue along the first nontrivial branch. Additionally, since there are no folds along branch, the stability is the same for all solutions along the branch. For $\gamma = 1.7$, the bifurcation points are supercritical and solutions nearby are stable. The nontrivial branch contains two folds and the branch comprises stable solutions from the bifurcation points to the fold, and unstable solutions between the folds. For $\gamma = 2.1$ the bifurcation points are supercritical and there are no folds along the branch, thus, the entire branch is composed of stable solutions. In the diagrams, the red portions correspond to stable solutions, and the green and blue portions correspond to unstable solutions. Additionally, the colors indicate the value of the constrained index of the solution: red is index zero, green is index one, and yellow is index two.

The distinguished diagram for the solution set that appeared in Figure 5.2 is shown in Figure 6.4, for values of γ ranging from 1.0 to 2.1. Since stability results have already been discussed for the first nontrivial branch, here we focus on the other nontrivial branches. The only portion of the trivial branches which corresponds to stable equilibria is the piece of the branch of single covered circles before the first bifurcation points. The analytic results of Section 6.6 predict that all other segments of the trivial branches correspond to unstable equilibria, in fact, equilibria with index at least two. For all bifurcation points except $(1, 1, +)$ and $(1, 1, -)$, a nontrivial branch leaves the bifurcation point with at least two negative eigenvalues and, thus, correspond to unstable equilibria. Although folds do appear on the higher order branches, there are no stable equilibria on those branches because there are at least two negative eigenvalues on each branch and at most one positive eigenvalue can be gained at folds. Accordingly, no higher-order nontrivial branches contains stable equilibria. These results have been reproduced by the conjugate point test described in Chapter 2. The colors red, blue and green indicate the same index as was specified in Figure 6.3, and all other colors in Figure 6.4 represent index greater than two.

In contrast to the calculation of equilibria where the parameter γ played a non-essential role, the stability properties of the non-trivial equilibria do depend on γ. For example, the shape of the branches in the distinguished bifurcation diagram depends on the value of γ, where as the shape of the branches other projections of the bifurcation diagram do not (see for example Figure 5.2 which plots m_3 versus λ_1). Changing the value of the ratio of twisting stiffness to bending stiffness only changes the rate at which the directors $\mathbf{d}_1$ and $\mathbf{d}_2$ rotate about $\mathbf{d}_3$. Thus the angle α depends on γ, but other quantities such as λ_1 and m_3 do not.

We remark that according to the theory of linear elasticity for a transversely isotropic rod, the ratio γ of twist to bending stiffness satisfies $\gamma = (1+\nu)^{-1}$, where ν is the Poisson ratio for the material. For common materials, $0 < \nu < 0.5$, so $\frac{2}{3} < \gamma < 1$, which is outwith the range of interesting stability exchange results. However, the accepted range of γ values in DNA models is $0.7 < \gamma < 1.5$, [54]. Moreover, Kehrbaum and Maddocks [30] have shown that a rode whose cross-section is anisotropic but which is rapidly twisting in the unstressed state can be approximated by an effectively isotropic rod in which the ratio of the effective twist and bending stiffnesses can be much larger than 1.

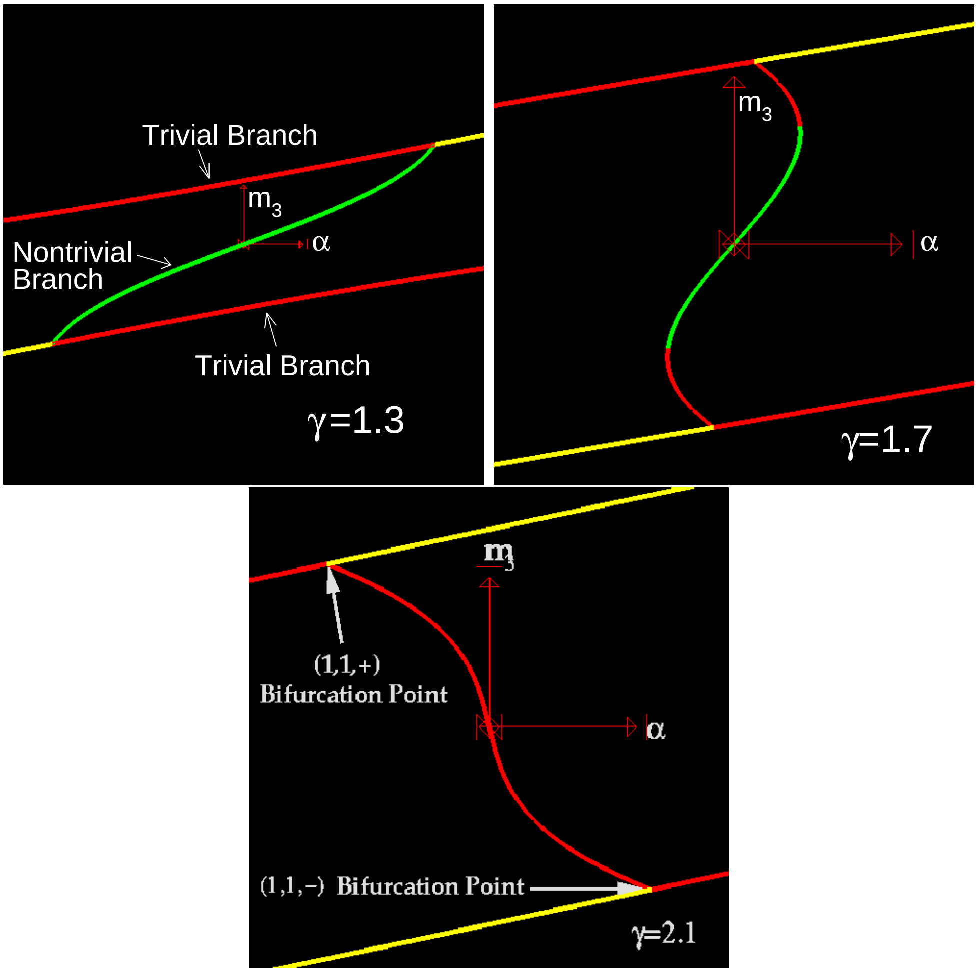

Figure 6.3: The twisted elastic loop distinguished diagram, which plots m_3. vs. α, is shown for three values of γ, the ratio of twisting stiffness to bending stiffness. For $\gamma = 1.3$, the entire first nontrivial branch correspond to unstable equilibria. When γ is increased to 1.7, the nontrivial branch has folds which correspond to stability exchanges and the red portion of the branch consists of stable solutions. For $\gamma = 2.1$, the first nontrivial branch is stable.

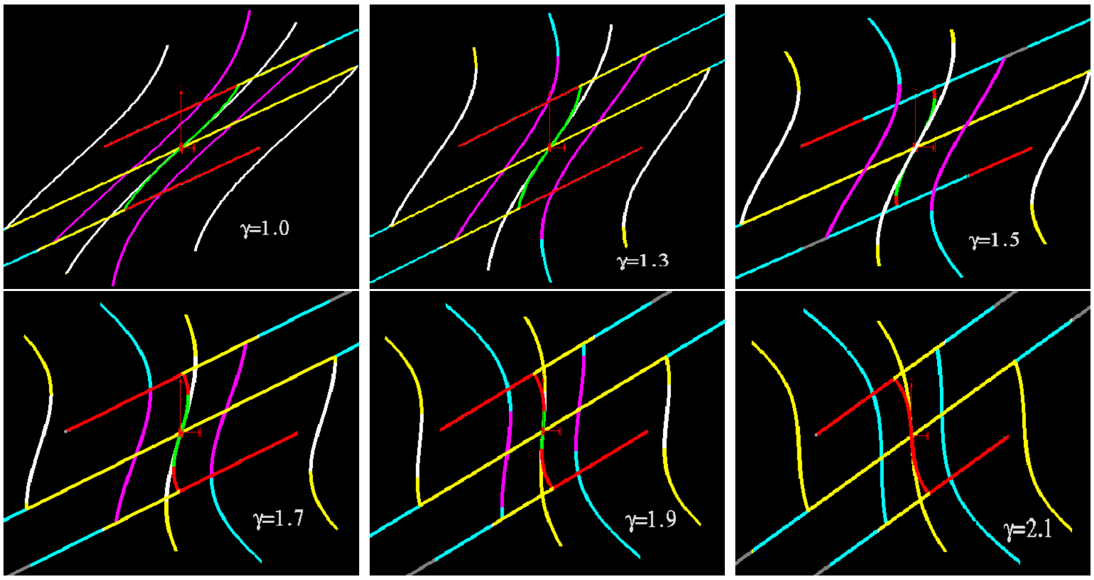

Figure 6.4: This sequence of illustrations depicts the distinguished diagram for the solution set that appeared in Figure 5.2 for varying values of γ. Stability exchanges occur at folds in the distinguished diagram, and the color indicates the constrained index (red=0, green=1, yellow=2, white=3, cyan=4, magenta=5, gray=6).

Chapter 7

Transition of Bifurcation Points

7.1 Introduction

In Chapter 6, we presented stability results for idealized twisted elastic loop equilibrium configurations. Analytic results on the trivial branches identified the bifurcation points and determined the constrained index for each critical point. Distinguished diagram theory predicted the index on the nontrivial branches, whose shape, and thus stability properties, varied with γ. Numerical experiments revealed that for values of γ close to 1, the $(1, 1, +)$ and $(1, 1, -)$ bifurcation points are *subcritical*, and as γ increases these bifurcation points become *supercritical*. According to the definition of [21, p. 34], a pitchfork bifurcation point is called subcritical (supercritical) if the nontrivial branch occurs (at least locally) for values of the parameter α for which the trivial solution is stable (unstable). A more general classification for which the index is greater than zero on both sides of the bifurcation point was presented in Section 6.7. Explicitly, a bifurcation point is labeled subcritical (supercritical) if the nontrivial branch occurs for values of the parameter for which the trivial solution has the index i (index $i + 2$). Similarly, nontrivial solutions near a supercritical bifurcation point have index i and nontrivial solutions near a subcritical bifurcation point have index $i + 1$. The classification of the bifurcation points depends on the value of γ, and an analytical investigation of this phenomenon is the goal of this chapter.

We begin by demonstrating that the bifurcation points shown in Figure 5.2 are pitchfork bifurcation points. As shown in Figure 5.2, these points do not appear to have a pitchfork structure since there is only one branch which emanates from each bifurcation point. However, this one branch is actually double-covered, which is a consequence of the projection of the solution set. The software package PCR [13], [14] is capable of performing a small four-dimensional rotation, which breaks the symmetries that result in a double-covered branch. The result of such a rotation is shown in Figure 7.1 for the first nontrivial branch. Now the bifurcation points can be seen to have a pitchfork structure. The analysis presented in this section supports this conclusion.

The criticality of the bifurcation points can be numerically determined from the distinguished diagram. Consider the $(1, 1, +)$ and $(1, 1, -)$ bifurcation points in Figure 7.1 or 6.3. Notice that locally for $\gamma = 1.3$ the diagram of the first nontrivial branch occurs at values of the parameter which correspond to stable

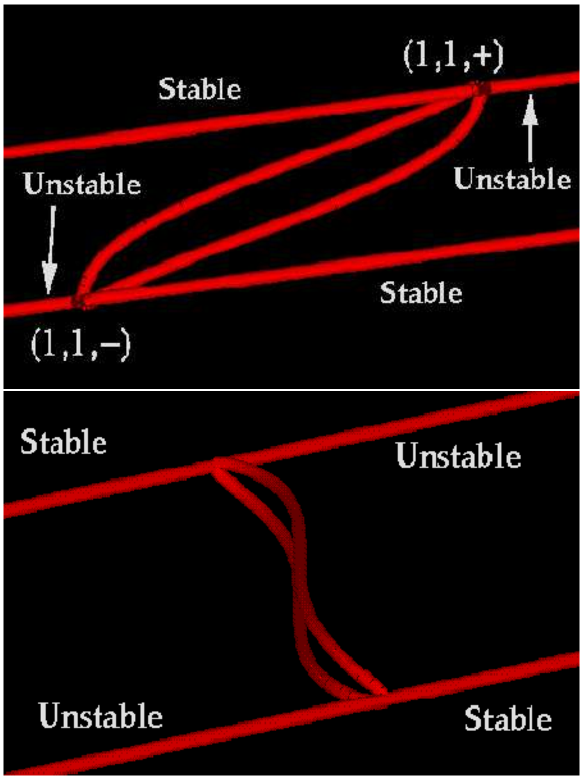

Figure 7.1: The top figure depicts the first nontrivial branch for $\gamma = 1.3$ and the bottom for $\gamma = 2.0$. A small rotation in the higher dimensional space is applied as a perturbation to reveal that the branches of nonplanar equilibria are in fact double covered in the projection used in Figure 5.2. The bifurcation points $(1, 1, +)$ and $(1, 1, -)$ (in the top figure) are subcritical bifurcation points because the nontrivial branches occur (at least locally) for values of the parameter for which the trivial branches are stable. The stable and unstable portions of the trivial branches are labeled in the diagram. The same bifurcation points are supercritical for $\gamma = 2.0$, because the nontrivial branches occur (at least locally) for values of the parameter for which the trivial branches are unstable.

trivial solutions so that $(1, 1, +)$ is subcritical. In contrast, for $\gamma = 1.7, 2.0, 2.1$, the first nontrivial branch occurs at values of the parameter which correspond to unstable trivial solutions so the bifurcation point is supercritical. The stability of the solutions on the nontrivial branch close to the bifurcation point follow from the classification of the bifurcation point. The nontrivial solutions close to a subcritical bifurcation point are unstable, and the nontrivial solutions close to a supercritical bifurcation point are stable [24, p. 24]. Accordingly, the value of γ for which the bifurcation point switches from being subcritical to being supercritical marks exactly the onset of stable solutions on the nontrivial branch.

In Section 7.2, we describe the perturbation method used to predict the value of γ for which each bifurcation point switches from being supercritical to subcritical. The implementation and results of the perturbation expansion applied to the twisted elastic loop example, and compares those results to the numerical observations in Section 7.3.

7.2 Perturbation Expansion

To analytically determine whether a bifurcation point is subcritical or supercritical, a perturbation expansion of the Euler-Lagrange equations is required. The general theory presented in this section is detailed in Antman [1, p. 166]. The theory presented in this section is not directly applicable to the idealized elastic loop problem, however, modifications are made in Section 7.3 to the formulation of the problem to mold it into the proper framework.

Consider a general equation of the form

$$\mathbf{f}[\alpha, \mathbf{u}] = \mathbf{0}, \quad \mathbf{f}[\cdot, \mathbf{0}] = \mathbf{0}. \tag{7.1}$$

We are interested in studying the non-trivial branch of solutions $\mathbf{u} \neq 0$ bifurcating from the trivial branch $\mathbf{u} = \mathbf{0}$ in a neighborhood of a bifurcation point α_0. Both the variables $\mathbf{u}$ and the parameter α are expanded:

$$\alpha(\epsilon) = \sum_{k=0}^{r-1} \frac{\alpha_k \epsilon^k}{k!} + O(\epsilon^r) \tag{7.2}$$

$$\mathbf{u}(\cdot, \epsilon) = \sum_{k=1}^{r-1} \frac{\mathbf{u}_k \epsilon^k}{k!} + O(\epsilon^r). \tag{7.3}$$

The equations for determining the pair $\{\mathbf{u}_k, \alpha_{k-1}\}$ are obtained by substituting the expansions (7.2) and (7.3) into the operator equation (7.1), and gathering terms of the same power of ϵ. For example, the 0^{th}-order expansion gives

$$\mathbf{f}[\alpha_0, \mathbf{0}] = \mathbf{0}. \tag{7.4}$$

The first-order expansion is simply the linearization of (7.4):

$$\left.\frac{\partial \mathbf{f}}{\partial \mathbf{u}}\right|_{[\alpha_0, \mathbf{0}]} \mathbf{u}_1 = \mathbf{0}, \tag{7.5}$$

where the term $\frac{\partial \mathbf{f}}{\partial \alpha}$ vanishes because $\mathbf{f}[\alpha, \mathbf{0}] = \mathbf{0}$ for all α. Similarly, the second-order expansion gives

$$\left.\frac{\partial \mathbf{f}}{\partial \mathbf{u}}\right|_{[\alpha_0,\mathbf{0}]} \mathbf{u}_2 = -\left.\frac{\partial^2 \mathbf{f}}{\partial \mathbf{u}\partial \mathbf{u}}\right|_{[\alpha_0,\mathbf{0}]} : \mathbf{u}_1\mathbf{u}_1 - 2\alpha_1 \left.\frac{\partial^2 \mathbf{f}}{\partial \alpha \partial \mathbf{u}}\right|_{[\alpha_0,\mathbf{0}]} : \mathbf{u}_1. \tag{7.6}$$

Finally, the third-order expansion gives

$$\begin{aligned}
\left.\frac{\partial \mathbf{f}}{\partial \mathbf{u}}\right|_{[\alpha_0,\mathbf{0}]} \mathbf{u}_3 \quad = \quad & -\left.\frac{\partial^3 \mathbf{f}}{\partial \mathbf{u}\partial \mathbf{u}\partial \mathbf{u}}\right|_{[\alpha_0,\mathbf{0}]} \therefore \mathbf{u}_1\mathbf{u}_1\mathbf{u}_1 - 3\left.\frac{\partial^2 \mathbf{f}}{\partial \mathbf{u}\partial \mathbf{u}}\right|_{[\alpha_0,\mathbf{0}]} : \mathbf{u}_1\mathbf{u}_2 \\
& -3\alpha_1 \left.\frac{\partial^3 \mathbf{f}}{\partial \alpha\partial \mathbf{u}\partial \mathbf{u}}\right|_{[\alpha_0,\mathbf{0}]} : \mathbf{u}_1\mathbf{u}_1 - 3\alpha_1^2 \left.\frac{\partial^3 \mathbf{f}}{\partial \alpha\partial \mathbf{u}\partial \mathbf{u}}\right|_{[\alpha_0,\mathbf{0}]} : \mathbf{u}_1 \\
& -3\alpha_1 \left.\frac{\partial^2 \mathbf{f}}{\partial \alpha}\partial \mathbf{u}\right|_{[\alpha_0,\mathbf{0}]} : \mathbf{u}_2 - 3\alpha_2 \left.\frac{\partial^2 \mathbf{f}}{\partial \alpha}\partial \mathbf{u}\right|_{[\alpha_0,\mathbf{0}]} : \mathbf{u}_1.
\end{aligned} \tag{7.7}$$

Here Antman's notation for tensor products has been adopted [1, Chapter XI]. The pair $\{\mathbf{u}_k, \alpha_{k-1}\}$ are determined in the following manner. The first order term $\mathbf{u}_1$ is determined by solving the Equation (7.5) subject to appropriate boundary conditions. The value of α_1 is determined from (7.6) by the solvability condition, that the right hand side of (7.6) is orthogonal to the null space of the adjoint of $\left.\frac{\partial \mathbf{f}}{\partial \mathbf{u}}\right|_{[\alpha_0,\mathbf{0}]}$. Once α_1 is found, Equation(7.6) can be solved for $\mathbf{u}_2$. Similarly, the value of α_2 is determined using the solvability condition of Equation (7.7). For the twisted elastic loop example, the bifurcation point is subcritical or supercritical depending on the sign of α_2.

7.3 Implementation and Results

There are several features of the twisted elastic loop problem which present difficulties in implementing the above perturbation method. The first difficulty involves the unit length constraint in the Euler parameters. The system of Euler-Lagrange equations (2.2) in terms of the variable $\mathbf{q}$ consist of four second-order equations subject to the constraint that $|\mathbf{q}|^2 = 1$. The formulation in Section 7.2 is not for a constrained system. An alternative formulation which avoids this difficulty is to express the Euler-Lagrange equations in terms of Euler angles (Θ, Φ, Ψ) [40]:

$$\begin{aligned}
-\Theta'' + (\Phi')^2 \sin\Theta\cos\Theta - \gamma(\Phi'\cos\Theta + \Psi')\Phi'\sin\Theta & \\
+ \lambda_1 \cos\Theta\cos\Phi + \lambda_2\cos\Theta\sin\Phi - \xi\sin\Theta &= 0, \\
-(\Phi'\sin^2\Theta)' - \gamma[\Phi'\cos\Theta + \Psi')\cos\Theta]' - \lambda_1\sin\Theta\sin\Phi + \lambda_2\sin\Theta\cos\Phi &= 0, \\
[\gamma(\Phi'\cos\Theta + \Psi')]' &= 0.
\end{aligned} \tag{7.8}$$

For the purposes of this perturbation expansion, we explicitly write out the constraints $\boldsymbol{\lambda}' = \mathbf{0}$ and $\mathbf{r}' - \mathbf{d}_3 = \mathbf{0}$

$$\lambda_1' = 0, \quad \lambda_2' = 0, \quad \xi' = 0, \tag{7.9}$$

$$r_1' - \sin\Theta\cos\Phi = 0, \quad r_2' - \sin\Theta\sin\Phi = 0, \quad r_3' - \cos\Theta = 0. \tag{7.10}$$

The second difficulty is that unlike (7.1), the solution about which we would like to expand is non-zero and depends on the bifurcation parameter. We overcome this using the following change of variables

$$\Theta \to \theta + \frac{\pi}{2}, \quad \Phi \to \phi + 2\pi n s, \quad \Psi' \to \psi' + \alpha, \quad \xi \to \lambda_3 - 2\pi n \alpha \gamma. \tag{7.11}$$

Applying this change of variables to (7.8), (7.9), and (7.10) gives the system:

$$\begin{gathered}
-\theta'' - (\phi' + 2\pi n)^2 \sin\theta \cos\theta - \gamma(\phi' + 2\pi n)\cos\theta(-(\phi' + 2\pi n)\sin\theta + \alpha + \psi') \\
-\lambda_1 \sin\theta \cos(\phi + 2\pi n s) - \lambda_2 \sin\theta \sin(\phi + 2\pi n s) - (\lambda_3 - \gamma 2\pi n \alpha)\cos\theta = 0, \\
-((\phi' + 2\pi n)\cos^2\theta)' + \gamma[(-(\phi' + 2\pi n)\sin\theta + \alpha + \psi')\sin\theta]' \\
-\lambda_1 \cos\theta \sin(\phi + 2\pi n s) + \lambda_2 \cos\theta \cos(\phi + 2\pi n s) = 0, \\
[\gamma(-(\phi' + 2\pi n)\sin\theta + \psi' + \alpha)]' = 0, \\
\lambda_1' = 0, \\
\lambda_2' = 0, \\
\lambda_3' = 0, \\
r_1' - \cos\theta \cos(\phi + 2\pi n s) = 0, \\
r_2' - \cos\theta \sin(\phi + 2\pi n s) = 0, \\
r_3' + \sin\theta = 0
\end{gathered} \tag{7.12}$$

subject to the boundary conditions

$$\theta(0) = \phi(0) = \psi(0) = \psi(1) = \mathbf{r}(0) = \mathbf{r}(1) = \lambda_1(0) = \lambda_2(0) = 0. \tag{7.13}$$

The trivial solution about we wish to expand is:

$$\begin{gathered}
\theta = \phi = \psi = \lambda_1 = \lambda_2 = \lambda_3 = 0, \\
r_1(s) = \frac{\sin(2\pi n s)}{2\pi n}, \quad r_2(s) = \frac{-\cos(2\pi n s) + 1}{2\pi n}, \quad r_3(s) = 0.
\end{gathered} \tag{7.14}$$

The variable transformation (7.11) effectively eliminates the dependence of the solution on the bifurcation parameter α, but unavoidably the solution (7.14) about which we want to linearize is not identically zero since $r_1(s) \not\equiv 0$, $r_2(s) \not\equiv 0$. The perturbation expansion is still valid for this case, provided the index in the variable expansion (7.3) is changed from $k = 1$ to $k = 0$. The term $\mathbf{u}_0$ is given by the solution (7.14).

At this point, we have effectively molded the twisted elastic loop problem to fit within the confines of this perturbation technique. The first-order equation (7.5) is obtained by linearizing (7.12)[1]:

$$\begin{gathered}
-\bar{\theta}'' - (2\pi n)^2 \bar{\theta} - \gamma[-(2\pi n)^2 \bar{\theta} + \bar{\phi}'\alpha + 2\pi n \bar{\psi}'] - \bar{\lambda}_3 = 0, \\
-(\bar{\phi}'' - \alpha\gamma\bar{\theta}') - \bar{\lambda}_1 \sin(2\pi n s) + \bar{\lambda}_2 \cos(2\pi n s) = 0,
\end{gathered}$$

[1] The computations detailed in this section were performed using the symbolic manipulation package Maple and the files are available upon request.

$$
\begin{aligned}
\gamma\left\{-2\pi n\bar{\theta}+\bar{\psi}'\right\}' &= 0,\\
\bar{\lambda}_1' &= 0,\\
\bar{\lambda}_2' &= 0,\\
\bar{\lambda}_3' &= 0,\\
\bar{r}_1'+\bar{\phi}\sin(2\pi ns) &= 0,\\
\bar{r}_2'-\bar{\phi}\cos(2\pi ns) &= 0,\\
\bar{r}_3'+\bar{\theta} &= 0,
\end{aligned}
$$

subject to the homogeneous Dirichlet boundary conditions (7.13). The solution to this system (called $\mathbf{u}_1$ in the variable expansion (7.3)) is:

$$
\begin{aligned}
\begin{pmatrix}\bar{\theta}\\ \bar{\phi}\\ \bar{\psi}\end{pmatrix} &= \begin{pmatrix}\sin(2\pi ks)\\ -\frac{\gamma\alpha}{2\pi k}(\cos(2\pi k)-1)\\ -\frac{n}{k}(\cos(2\pi ks)-1)\end{pmatrix}, \qquad \begin{pmatrix}\bar{\lambda}_1\\ \bar{\lambda}_2\\ \bar{\lambda}_3\end{pmatrix} = \begin{pmatrix}0\\0\\0\end{pmatrix},\\
\bar{r}_1 &= \frac{\alpha\gamma}{2\pi k}\left[-\frac{1}{2}\frac{\cos(2\pi(n+k)s)}{2\pi(n+k)}+\frac{1}{2}\frac{\cos(2\pi(k-n)s)}{2\pi(k-n)}+\frac{1}{2}\frac{\cos(2\pi ns)}{\pi n}\right]\\
&\quad -\frac{\alpha\gamma k^2}{4\pi^2 kn(k^2-n^2)},\\
\bar{r}_2 &= -\frac{\alpha\gamma}{4\pi k}\left[\frac{\sin(2\pi(k-n)s)}{2\pi(k-n)}+\frac{\sin(2\pi(k+n)s)}{2\pi(k+n)}-\frac{\sin(2\pi ns)}{\pi n}\right],\\
\bar{r}_3 &= \frac{\cos(2\pi ks)-1}{2\pi k}.
\end{aligned}
\tag{7.15}
$$

In order to determine α_1, we must determine the adjoint system $\mathcal{G}^* = \frac{\partial \mathbf{f}}{\partial \mathbf{u}}\Big|^*_{[\alpha_0,\mathbf{0}]}$. The adjoint operator $\mathcal{G}^*$ and adjoint boundary conditions are defined by $\langle \mathbf{x}, \mathcal{G}\mathbf{y}\rangle = \langle \mathcal{G}^*\mathbf{x}, \mathbf{y}\rangle$, where $\mathcal{G}$ denotes the operator corresponding to the linearized system and $\langle\cdot,\cdot\rangle$ denotes the L^2 inner product. The adjoint equations are

$$
\begin{aligned}
-\check{\theta}''-(2\pi n)^2\check{\theta}+\gamma(2\pi n)^2\check{\theta}-\alpha\gamma\check{\phi}'+2\pi n\gamma\check{\psi}'+\check{r}_3 &= 0\\
\gamma\alpha\check{\theta}'-\check{\phi}''+\check{r}_1\sin(2\pi ns)-\check{r}_2\cos(2\pi ns) &= 0,\\
2\pi n\gamma\check{\theta}'+\gamma\check{\psi}'' &= 0,\\
-\check{\lambda}_1'-\check{\phi}\sin(2\pi ns) &= 0,\\
-\check{\lambda}_2'+\check{\phi}\cos(2\pi ns) &= 0,\\
-\check{\lambda}_3'-\check{\theta} &= 0,\\
\check{r}_1' &= 0,\\
\check{r}_2' &= 0,\\
\check{r}_3' &= 0
\end{aligned}
$$

and the associated boundary conditions are

$$
\check{\theta},\check{\phi},\check{\psi}\Big|_0 = 0,\quad \check{\theta},\check{\phi},\check{\psi},\check{\theta}'\check{\phi}'\Big|_1 = 0,\quad \check{\lambda}_3\Big|_0 = 0,\quad \check{\lambda}_1,\check{\lambda}_2,\check{\lambda}_3\Big|_1 = 0.
$$

The null vector for the adjoint system is given by

$$\begin{aligned}
\begin{pmatrix}\check\theta\\ \check\phi\\ \check\psi\end{pmatrix} &= \begin{pmatrix} \frac{1}{2\pi\alpha\gamma}\left[-\frac{\sin(2\,\pi\,ks)}{k}+\frac{\sin(2\,\pi\,ns)}{n}\right] \\ \frac{1}{4\pi^2k^2}(\cos(2\,\pi\,ks)-1) \\ -\frac{n}{2\pi k^2\alpha\gamma}(\cos(2\,\pi\,ks)-1)-\frac{1}{2\pi n\gamma\alpha}(1-\cos(2\,\pi\,ns))\end{pmatrix}, \quad \begin{pmatrix}\check r_1\\ \check r_2\\ \check r_3\end{pmatrix}=\begin{pmatrix}0\\1\\0\end{pmatrix},\\
\check\lambda_1 &= \frac{\cos((2\,\pi\,n+2\,\pi\,k)\,s)}{(16\,\pi\,n+16\,\pi\,k)\,\pi^2k^2}+\frac{\cos((2\,\pi\,n-2\,\pi\,k)\,s)}{(16\,\pi\,n-16\,\pi\,k)\,\pi^2k^2}-\frac{\cos(2\,\pi\,ns)}{8\,\pi^3nk^2}\\
&\quad -\frac{1}{(16\,\pi\,n+16\,\pi\,k)\,\pi^2k^2}-\frac{1}{(16\,\pi\,n-16\,\pi\,k)\,\pi^2k^2}+\frac{1}{8\,\pi^3nk^2},\\
\check\lambda_2 &= \frac{\sin((2\,\pi\,n-2\,\pi\,k)\,s)}{(16\,\pi\,n-16\,\pi\,k)\,\pi^2k^2}+\frac{\sin((2\,\pi\,n+2\,\pi\,k)\,s)}{(16\,\pi\,n+16\,\pi\,k)\,\pi^2k^2}-\frac{\sin(2\,\pi\,ns)}{8\,\pi^3nk^2},\\
\check\lambda_3 &= -\frac{\cos(2\,\pi\,ks)}{4\,\pi^2k^2\alpha\,\gamma}+\frac{\cos(2\,\pi\,ns)}{4\,\pi^2n^2\gamma\,\alpha}+\frac{1}{4\,\pi^2k^2\alpha\,\gamma}-\frac{1}{4\,\pi^2n^2\gamma\,\alpha}.
\end{aligned}\tag{7.16}$$

The equation which determines α_1 is the solvability condition for (7.6), i.e. the L^2 inner product of (7.16) and the right hand side of (7.6) must be zero. The value of α_1 which satisfies the solvability condition for (7.6) is $\alpha_1 = 0$. This value is consistent with the fact that a pitchfork (and not transcritical) bifurcation occurs at the bifurcation point. The sign of the second order term α_2 determines whether the bifurcation point α_0 is subcritical or supercritical. This sign is determined by applying the solvability condition to the third order equations (7.7). To this end, we first must solve for $\mathbf{u}_2$, by solving (7.6)

$$\begin{gathered}
-\bar\theta''-(2\pi n)^2\bar\theta-\gamma[-(2\pi n)^2\bar\theta+\bar\phi'\alpha+2\pi n\bar\psi']-\bar\lambda_3 = \\
-\pi n\alpha_0\gamma(\gamma-2)(1-\cos(4\pi ks)),\\
-(\bar\phi''-\alpha\gamma\bar\theta')-\bar\lambda_1\sin(2\pi ns)+\bar\lambda_2\cos(2\pi ns) = -4\pi^2kn\sin(4\pi ks),\\
\gamma\left\{-2\pi n\bar\theta+\bar\psi'\right\}' = 2\alpha_0\gamma^2\pi k\sin(4\pi ks),\\
\bar\lambda_1' = 0,\\
\bar\lambda_2' = 0,\\
\bar\lambda_3' = 0,\\
\bar r_1'+\bar\phi\sin(2\pi ns) = -\frac{\cos(2\pi ns)}{2}\left[\frac{\alpha_0^2\gamma^2}{4\pi^2k^2}(1-\cos(2\pi ks))^2+\sin^2(2\pi ks)\right],\\
\bar r_2'-\bar\phi\cos(2\pi ns) = -\frac{\sin(2\pi ns)}{2}\left[\frac{\alpha_0^2\gamma^2}{4\pi^2k^2}(1-\cos(2\pi ks))^2+\sin^2(2\pi ks)\right],\\
\bar r_3'+\bar\theta = 0,
\end{gathered}$$

subject to boundary conditions (7.13). The solution to this system is:

$$\begin{aligned}
\bar\theta &= \frac{\alpha\,\gamma\,n\cos(2\,\pi\,ks)}{4\,\pi\,k^2}-\frac{\alpha\,\gamma\,n\cos(4\,\pi\,ks)}{4\,\pi\,k^2}-\frac{\alpha\,\gamma\,(\gamma-2)}{4\,\pi\,n\,(\gamma-1)}\\
&+ \frac{\alpha\,\gamma^2}{4\,\pi\,n\,(\gamma-1)}-\frac{\alpha\,\gamma}{2\,\pi\,n\,(\gamma-1)},\\
\bar\phi &= \frac{\alpha^2\gamma^2\sin(2\,\pi\,ks)n}{8\,\pi^2k^3}-\left(\frac{\alpha^2\gamma^2n}{k}+4\,\pi^2kn\right)\frac{\sin(4\,\pi\,ks)}{16\pi^2k^2},
\end{aligned}$$

$$
\begin{aligned}
\bar{\psi} &= \frac{n^2 \sin(2\,\pi\,ks)\alpha\,\gamma}{4\,\pi\,k^3} + \left(-\frac{2\,\pi\,n^2\gamma^2\alpha}{k} - 2\,\alpha\,\gamma^2\pi\,k\right)\frac{\sin(4\,\pi\,ks)}{16\gamma\pi^2k^2},\\
\bar{\lambda}_1 &= 0,\\
\bar{\lambda}_2 &= 0,\\
\bar{\lambda}_3 &= n\pi\alpha\gamma(\gamma-2),\\
\bar{r}_1 &= -\frac{\sin(2\,\pi\,ns)}{8\,\pi\,n} - \frac{\sin((-2\,\pi\,n+2\,\pi\,k)\,s)\alpha^2\gamma^2n}{(-32\,\pi\,n+32\,\pi\,k)\,\pi^2k^3} + \frac{\sin((2\,\pi\,n+2\,\pi\,k)\,s)\alpha^2\gamma^2n}{(32\,\pi\,n+32\,\pi\,k)\,\pi^2k^3}\\
&- \frac{\sin((-2\,\pi\,n+2\,\pi\,k)\,s)\alpha^2\gamma^3}{(-32\,\pi\,n+32\,\pi\,k)\,\pi^2kn\,(\gamma-1)} + \frac{\sin((2\,\pi\,n+2\,\pi\,k)\,s)\alpha^2\gamma^3}{(32\,\pi\,n+32\,\pi\,k)\,\pi^2kn\,(\gamma-1)}\\
&+ \frac{\sin((-2\,\pi\,n+2\,\pi\,k)\,s)\alpha^2\gamma^2}{(-16\,\pi\,n+16\,\pi\,k)\,\pi^2kn\,(\gamma-1)} - \frac{\sin((2\,\pi\,n+2\,\pi\,k)\,s)\alpha^2\gamma^2}{(16\,\pi\,n+16\,\pi\,k)\,\pi^2kn\,(\gamma-1)}\\
&+ \frac{\sin((-2\,\pi\,n+2\,\pi\,k)\,s)\alpha\,\gamma}{(-8\,\pi\,n+8\,\pi\,k)\,\pi k}\left(\frac{\alpha\,\gamma^2}{4\,\pi\,n\,(\gamma-1)} - \frac{\alpha\,\gamma}{2\,\pi\,n\,(\gamma-1)}\right)\\
&- \frac{\sin((2\,\pi\,n+2\,\pi\,k)\,s)\alpha\,\gamma}{(8\,\pi\,n+8\,\pi\,k)\,\pi k}\left(\frac{\alpha\,\gamma^2}{4\,\pi\,n\,(\gamma-1)} - \frac{\alpha\,\gamma}{2\,\pi\,n\,(\gamma-1)}\right)\\
&+ \frac{\sin((-2\,\pi\,n+4\,\pi\,k)\,s)}{-16\,\pi\,n+32\,\pi\,k} + \frac{\sin((2\,\pi\,n+4\,\pi\,k)\,s)}{16\,\pi\,n+32\,\pi\,k}\\
&+ \frac{\sin((-2\,\pi\,n+4\,\pi\,k)\,s)\alpha^2\gamma^2n}{(-64\,\pi\,n+128\,\pi\,k)\,\pi^2k^3} - \frac{\sin((2\,\pi\,n+4\,\pi\,k)\,s)\alpha^2\gamma^2n}{(64\,\pi\,n+128\,\pi\,k)\,\pi^2k^3}\\
&+ \frac{\sin((-2\,\pi\,n+4\,\pi\,k)\,s)n}{(-16\,\pi\,n+32\,\pi\,k)\,k} - \frac{\sin((2\,\pi\,n+4\,\pi\,k)\,s)n}{(16\,\pi\,n+32\,\pi\,k)\,k} - \frac{3\,\sin(2\,\pi\,ns)\alpha^2\gamma^2}{32\,\pi^3nk^2}\\
&+ \frac{\sin((-2\,\pi\,n+2\,\pi\,k)\,s)\alpha^2\gamma^2}{(-16\,\pi\,n+16\,\pi\,k)\,\pi^2k^2} + \frac{\sin((2\,\pi\,n+2\,\pi\,k)\,s)\alpha^2\gamma^2}{(16\,\pi\,n+16\,\pi\,k)\,\pi^2k^2}\\
&- \frac{\sin((-2\,\pi\,n+4\,\pi\,k)\,s)\alpha^2\gamma^2}{(-64\,\pi\,n+128\,\pi\,k)\,\pi^2k^2} - \frac{\sin((2\,\pi\,n+4\,\pi\,k)\,s)\alpha^2\gamma^2}{(64\,\pi\,n+128\,\pi\,k)\,\pi^2k^2},\\
\bar{r}_2 &= -\frac{1}{8\,\pi\,n} - \frac{\cos((2\,\pi\,n+4\,\pi\,k)\,s)}{16\,\pi\,n+32\,\pi\,k} + \frac{1}{16\,\pi\,n+32\,\pi\,k} - \frac{1}{-16\,\pi\,n+32\,\pi\,k}\\
&+ \frac{\cos(2\,\pi\,ns)}{8\,\pi\,n} - \frac{n}{(16\,\pi\,n+32\,\pi\,k)\,k} - \frac{n}{(-16\,\pi\,n+32\,\pi\,k)\,k}\\
&+ \frac{\alpha^2\gamma^2}{(-64\,\pi\,n+128\,\pi\,k)\,\pi^2k^2} - \frac{3\,\alpha^2\gamma^2}{32\,\pi^3nk^2} - \frac{\alpha^2\gamma^2}{(-16\,\pi\,n+16\,\pi\,k)\,\pi^2k^2}\\
&+ \frac{\alpha^2\gamma^2}{(16\,\pi\,n+16\,\pi\,k)\,\pi^2k^2} + \frac{\cos((2\,\pi\,n+4\,\pi\,k)\,s)n}{(16\,\pi\,n+32\,\pi\,k)\,k} + \frac{\cos((-2\,\pi\,n+4\,\pi\,k)\,s)n}{(-16\,\pi\,n+32\,\pi\,k)\,k}\\
&+ \frac{3\,\cos(2\,\pi\,ns)\alpha^2\gamma^2}{32\,\pi^3nk^2} - \frac{\cos((2\,\pi\,n+2\,\pi\,k)\,s)\alpha^2\gamma^2}{(16\,\pi\,n+16\,\pi\,k)\,\pi^2k^2}\\
&+ \frac{\cos((-2\,\pi\,n+2\,\pi\,k)\,s)\alpha^2\gamma^2}{(-16\,\pi\,n+16\,\pi\,k)\,\pi^2k^2} + \frac{\cos((2\,\pi\,n+4\,\pi\,k)\,s)\alpha^2\gamma^2}{(64\,\pi\,n+128\,\pi\,k)\,\pi^2k^2}\\
&- \frac{\cos((-2\,\pi\,n+4\,\pi\,k)\,s)\alpha^2\gamma^2}{(-64\,\pi\,n+128\,\pi\,k)\,\pi^2k^2} + \frac{\cos((-2\,\pi\,n+4\,\pi\,k)\,s)}{-16\,\pi\,n+32\,\pi\,k}\\
&- \frac{\alpha^2\gamma^2}{(64\,\pi\,n+128\,\pi\,k)\,\pi^2k^2} + \frac{\alpha^2\gamma^3}{(32\,\pi\,n+32\,\pi\,k)\,\pi^2kn\,(\gamma-1)}
\end{aligned}
$$

$$
\begin{aligned}
&+ \frac{\alpha^2\gamma^3}{(-32\,\pi\,n+32\,\pi\,k)\,\pi^2 kn\,(\gamma-1)} - \frac{\alpha^2\gamma^2}{(16\,\pi\,n+16\,\pi\,k)\,\pi^2 kn\,(\gamma-1)} \\
&- \frac{\alpha^2\gamma^2}{(-16\,\pi\,n+16\,\pi\,k)\,\pi^2 kn\,(\gamma-1)} + \frac{\alpha^2\gamma^2 n}{(32\,\pi\,n+32\,\pi\,k)\,\pi^2 k^3} \\
&+ \frac{\alpha^2\gamma^2 n}{(-32\,\pi\,n+32\,\pi\,k)\,\pi^2 k^3} - \frac{\alpha^2\gamma^2 n}{(-64\,\pi\,n+128\,\pi\,k)\,\pi^2 k^3} \\
&- \frac{\alpha^2\gamma^2 n}{(64\,\pi\,n+128\,\pi\,k)\,\pi^2 k^3} - \frac{\cos((2\,\pi\,n+2\,\pi\,k)\,s)\alpha^2\gamma^3}{(32\,\pi\,n+32\,\pi\,k)\,\pi^2 kn\,(\gamma-1)} \\
&- \frac{\cos((-2\,\pi\,n+2\,\pi\,k)\,s)\alpha^2\gamma^3}{(-32\,\pi\,n+32\,\pi\,k)\,\pi^2 kn\,(\gamma-1)} + \frac{\cos((2\,\pi\,n+2\,\pi\,k)\,s)\alpha^2\gamma^2}{(16\,\pi\,n+16\,\pi\,k)\,\pi^2 kn\,(\gamma-1)} \\
&+ \frac{\cos((-2\,\pi\,n+2\,\pi\,k)\,s)\alpha^2\gamma^2}{(-16\,\pi\,n+16\,\pi\,k)\,\pi^2 kn\,(\gamma-1)} - \frac{\cos((2\,\pi\,n+2\,\pi\,k)\,s)\alpha^2\gamma^2 n}{(32\,\pi\,n+32\,\pi\,k)\,\pi^2 k^3} \\
&- \frac{\cos((-2\,\pi\,n+2\,\pi\,k)\,s)\alpha^2\gamma^2 n}{(-32\,\pi\,n+32\,\pi\,k)\,\pi^2 k^3} + \frac{\cos((-2\,\pi\,n+4\,\pi\,k)\,s)\alpha^2\gamma^2 n}{(-64\,\pi\,n+128\,\pi\,k)\,\pi^2 k^3} \\
&+ \frac{\cos((2\,\pi\,n+4\,\pi\,k)\,s)\alpha^2\gamma^2 n}{(64\,\pi\,n+128\,\pi\,k)\,\pi^2 k^3} \\
&- \frac{\alpha\,\gamma}{(8\,\pi\,n+8\,\pi\,k)\,\pi k}\left(\frac{\alpha\,\gamma^2}{4\,\pi\,n\,(\gamma-1)} - \frac{\alpha\,\gamma}{2\,\pi\,n\,(\gamma-1)}\right) \\
&- \frac{\alpha\,\gamma}{(-8\,\pi\,n+8\,\pi\,k)\,\pi k}\left(\frac{\alpha\,\gamma^2}{4\,\pi\,n\,(\gamma-1)} - \frac{\alpha\,\gamma}{2\,\pi\,n\,(\gamma-1)}\right) \\
&+ \frac{\cos((2\,\pi\,n+2\,\pi\,k)\,s)\alpha\,\gamma}{(8\,\pi\,n+8\,\pi\,k)\,\pi k}\left(\frac{\alpha\,\gamma^2}{4\,\pi\,n\,(\gamma-1)} - \frac{\alpha\,\gamma}{2\,\pi\,n\,(\gamma-1)}\right) \\
&+ \frac{\cos((-2\,\pi\,n+2\,\pi\,k)\,s)\alpha\,\gamma}{(-8\,\pi\,n+8\,\pi\,k)\,\pi k}\left(\frac{\alpha\,\gamma^2}{4\,\pi\,n\,(\gamma-1)} - \frac{\alpha\,\gamma}{2\,\pi\,n\,(\gamma-1)}\right),
\end{aligned}
$$

$$
\begin{aligned}
\bar{r}_3 &= -\frac{\sin(2\,\pi\,ks)\alpha\,\gamma\,n}{8\,\pi^2 k^3} + \frac{\sin(4\,\pi\,ks)\alpha\,\gamma\,n}{16\,\pi^2 k^3} + \frac{\alpha\,\gamma\,(\gamma-2)\,s}{4\,\pi\,n\,(\gamma-1)} \\
&- \left(\frac{\alpha\,\gamma^2}{4\,\pi\,n\,(\gamma-1)} - \frac{\alpha\,\gamma}{2\,\pi\,n\,(\gamma-1)}\right) s.
\end{aligned}
$$

Then α_2 is determined by the condition that the right hand side of (7.7) is orthogonal to the adjoint null-vector Equation (7.16). This orthogonality condition reduces to

$$
\frac{-3\,\pi\,n^4 + n^2\pi\,k^2 + 2\,n^2\pi\,k^2\gamma + \gamma\,\alpha_2\,k^2\sqrt{-\,(n-k)\,(n+k)} - 2\,\pi\,k^4\gamma + 2\,\pi\,k^4}{4\,\pi\,\sqrt{-\,(n-k)\,(n+k)}k^3} = 0.
$$

The value of γ at which α_2 switches sign, i.e. $\alpha_2 = 0$, is given by

$$
\gamma = 1 + \frac{3n^2}{2(n+m)^2},
$$

where m indexes the bifurcation points on the trivial branch corresponding to the n-covered circular solutions. This formula agrees with numerical determinations of the criticality of the bifurcation points (cf. Table 7.1).

Bifurcation Point	Numerical Approximation	Analytical Prediction
$(1, 1, \pm)$	$\gamma = 1.35 - 1.40$	$\gamma = 1.375$
$(1, 2, \pm)$	$\gamma = 1.15 - 1.20$	$\gamma = 1.166$
$(2, 1, \pm)$	$\gamma = 1.65 - 1.70$	$\gamma = 1.666$
$(3, 1, \pm)$	$\gamma = 1.80 - 1.85$	$\gamma = 1.844$
$(1, 3, \pm)$	$\gamma = 1.05 - 1.10$	$\gamma = 1.094$

Table 7.1: For each bifurcation point, this table compares the numerical approximation and the analytic prediction of the value of γ at which the bifurcation points switch from being subcritical to supercritical. The numerical approximation and the analytical predictions agree to the accuracy at which the numerical approximation was made.

Chapter 8

DNA Example

8.1 Introduction

DNA (*deoxyribonucleic acid*) consists of two sugar-phosphate chains which wind around each other in a double helix. When an elastic rod model is adopted as a model of DNA, the centerline $\mathbf{r}(s)$ runs through the middle of the double helix, and the normal vector $\mathbf{d}_1(s)$ serves to locate the sugar-phosphate chains. Unlike the twisted elastic rod with straight unstressed state presented in the previous chapter, the unstressed configuration of the model of DNA has inherent curvature and twist. These input parameters to the model were previously determined from experimental DNA data by Manning et al. [45], where the equilibrium configurations of this model were also calculated. There are no 'trivial solutions' to this problem, and accordingly, the solution set cannot be broken into trivial and nontrivial solutions. Consequently, the analytic restricted quadratic form theory test used in Chapter 6 cannot be applied. The distinguished diagram results presented in Chapter 3 can be applied to this problem to predict changes in isoperimetric index at folds, but without the analytic calculations of the index at one point on the branch, the index cannot be completely quantified. Instead, the isoperimetric conjugate point test described in Chapter 2 is applied to this problem to determine the isoperimetric index for any equilibrium along the branch. Thus, the combination of the distinguished diagram theory and the conjugate point test provides an efficacious and complete characterization of the index of equilibria.

Section 8.2 describes the variational formulation of the elastic rod model of DNA minicircles and the calculation of equilibria. Section 8.3 discusses the second variation for this problem, and finally, Section 8.4 reports the results of the isoperimetric index calculation.

8.2 The Elastic Rod Model of DNA

The specific variational problem of the isoperimetric form (2.9) relevant for modeling DNA is to minimize (5.6) with strain energy (4.6), or explicitly:

$$\begin{gathered}
J[\mathbf{q}] = \int_0^1 \left[\sum_{i=1}^{3} \left(\frac{1}{2} K_i (u_i - \hat{u}_i)^2 \right) - \boldsymbol{\lambda} \cdot \mathbf{d}_3 + \mu \, \mathbf{q} \cdot \mathbf{q}' \right] \, ds, \\
\int_0^1 \mathbf{d}_3 \, ds = 0, \\
\mathbf{q}(0) = (0,0,0,1), \quad \mathbf{q}(1) = \pm(0,0,\sin(\alpha/2),\cos(\alpha/2)).
\end{gathered} \tag{8.1}$$

The positive *stiffnesses* (K_1, K_2, K_3) and the unstressed strains $\hat{u}_i$ are required input parameters to the model, whose values have previously been computed from experimental data [45]. Despite local DNA anisotropy, we still assume that $K_1 = K_2$, since the rapid intrinsic twist of DNA allows unequal bending stiffnesses to be averaged to yield an effectively isotropic rod for sufficiently large length scales [30].

Of particular interest in this molecular biology application are the truly cyclized DNA [27]; that is, the rod configurations for which both the centerline and directors close:

$$\mathbf{r}(0) = \mathbf{r}(1), \quad \mathbf{d}_i(0) = \mathbf{d}_i(1). \tag{8.2}$$

The boundary conditions specified in (8.1) do not correspond to cyclized DNA because the normal directors $\mathbf{d}_1(0)$ and $\mathbf{d}_1(1)$ are not equal, but instead form an angle α as depicted in Figure 5.1. Nevertheless, it is computationally convenient to study the one-parameter family of problems (8.1) and simply identify the cyclized DNA as those with $\alpha = 2\pi n$, rather than attempt to compute the isolated cyclized equilibria. This more general computation also allows comparison between the constrained index computed using conjugate points and distinguished diagram theory.

The solution set of critical points of (8.1), as previously computed in [45] using parameter continuation, is illustrated in Figure 8.1, which plots energy vs. twist moment m_3. Issues regarding the numerical techniques for symmetry breaking are addressed in [45] and [37]. Unlike the idealized elastic rod, for which a trivial solution was known for all values of α, the introduction of unstressed curvature and twist removes the possibility of finding a closed-form solution. Instead, a homotopy parameter ω is introduced by replacing $\hat{u}_i$ with $\omega \hat{u}_i$. Hence, $\omega = 0$ corresponds to the idealized problem, for which the solution set has already been computed, and $\omega = 1$ corresponds to the rod model of DNA which includes unstressed curvature. For a fixed value of α, parameter continuation in ω leads to a single solution of (8.1) when $\omega = 1$, at which point $\omega = 1$ is held fixed and the parameter α is varied.

Unlike the solution set of the idealized problem that is entirely connected, the solution set of the model of DNA contains many components, as seen in Figure 8.1. The circles in this diagram indicate the cyclized configurations. The

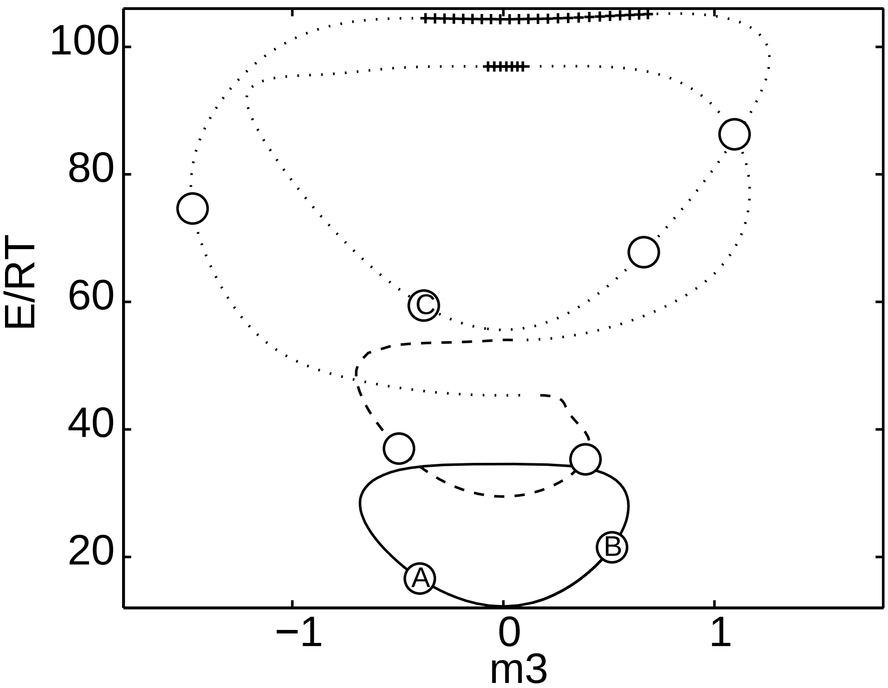

Figure 8.1: Bifurcation diagram for $\gamma = 1.7$, with the isoperimetric index indicated by line style (solid line= 0, dashed line= 1, dotted line= 2, crosses= 3). In this diagram, branches of equilibria as α varies are represented in a plot of the energy versus the twist moment $m_3(0)$. Cyclized DNA configurations (equilibria with $\alpha = 2n\pi$ and therefore $\mathbf{d}_1(0) = \mathbf{d}_1(1)$) are indicated with circles. The bifurcation diagram shown here contains only the two lowest-energy components of the complete solution set. Each component is a simple closed loop, and there are no bifurcation points (intersections of branches). The crossings seen in the figure are merely a consequence of the particular 2D projection chosen.

equilibria represented by this solution set are perturbations of the idealized elastic rod equilibria discussed in Section 5.5. The perturbed planar circle, perturbed nonplanar circle, and perturbed double-covered circles shown in Figure 8.3 are examples of equilibria for this problem. Unlike the idealized elastic rod, for which equilibria at different values of γ can be easily related (they differ only by a uniform rotation of $\mathbf{d}_1(s)$ about $\mathbf{d}_3(s)$), the solution set of the model of DNA must be recomputed (using parameter continuation in γ) for each value of γ. In the molecular biology literature, the value of $\gamma = K_3/K_1$ for DNA ranges between 0.7 and 1.5.

The goal of this chapter is to determine the isoperimetric index of each of these equilibria.

8.3 Second Variation

The second variation of (8.1) is of the form (6.1), with derivatives $W_{\mathbf{qq}}$,$W_{\mathbf{qq}'}$,$W_{\mathbf{q}'\mathbf{q}'}$, and $\mathbf{\Lambda}$ as defined in Section 6.2. As before, this second variation is formulated in terms of Euler parameters (6.1), and thus has a flat direction which we eliminate using a projection (see Section 6.3). Previously, the projection was specifically chosen so that Jacobi's equations $\mathcal{S}\boldsymbol{\zeta} = \mathbf{0}$ had constant coefficients. For this example, the index will be determined numerically, so any basis for the subspace of variations which respect the unit length constraint can be used. We chose the basis $\{\mathbf{B}_1\mathbf{q}_0, \mathbf{B}_2\mathbf{q}_0, \mathbf{B}_3\mathbf{q}_0\}$ (cf. [10]). Hence we take $\boldsymbol{\zeta} = \mathbf{\Pi}\boldsymbol{\eta}$, where $\boldsymbol{\eta}(s)$ is a variation in $\mathbb{R}^3$ and

$$\mathbf{\Pi} = \begin{bmatrix}\mathbf{B}_1\mathbf{q}_0 & \mathbf{B}_2\mathbf{q}_0 & \mathbf{B}_3\mathbf{q}_0\end{bmatrix}^T \in \mathbb{R}^{3\times 4}. \tag{8.3}$$

The resulting second variation is of the form (6.7) with coefficients (6.8) and projection matrix Π defined by (8.3).

In addition, the IVP (2.33) involves the linearization of the constraints, namely $\int_0^1 \mathbf{T}_i \cdot \boldsymbol{\zeta}\, ds$ in which:

$$\mathbf{T}_i = \mathbf{\Pi}\frac{\partial(\mathbf{d}_3 \cdot \mathbf{e}_i)}{\partial \mathbf{q}}(\mathbf{q}_0), \quad i = 1, 2, 3, \tag{8.4}$$

where $\mathbf{d}_3$ is given by (4.10).

8.4 Stability Results

We are now in a position to implement the conjugate point test as described in Sections 2.2 and 2.3 to the quadratic form and constraints defined in Equation (6.8), with $p = n = 3$. We solve the IVP system (2.33) numerically using an Adams-PECE adaptive step-size integrator [57]. It takes approximately 10 seconds on a Dec Alpha 3000 to solve this IVP system for each equilibrium solution. (This time is somewhat inflated by the fact that our $\hat{u}_i$ functions are only C^1, which causes the adaptive-step-size integrator to take small steps in some regions; if $\hat{u}_i \in C^\infty$, the time per equilibrium drops to about 3 seconds.)

The value of $\det \mathcal{M}$ is evaluated on a grid of s values in $(0, 1)$ in order to track its zeros (i.e., conjugate points). For example, Figure 8.2 shows plots of $\det \mathcal{M}$ as a function of arclength for three equilibria. Since $\mathcal{M}(0)$ is the six-by-six zero matrix, $\det \mathcal{M}$ is very small for $s \approx 0$. The asymptotic analysis in [46] assures us that $\det \mathcal{M}(s) \neq 0$ for $s > 0$ sufficiently small, as predicted by Property 2.5.

We applied the conjugate point test to a model of a DNA minicircle containing a natural bend of approximately 110 degrees (the molecule 05T05 described in [45]). The set of equilibria as the angle α is varied lie on several different components; the two lowest-energy components are shown in Figure 8.1 for $\gamma = K_3/K_1 = 1.7$. The results of the stability computations are shown in Figure 8.1 by the line styles of the bifurcation diagrams, which denote the isoperimetric index. For this particular value of γ (which is slightly above the range

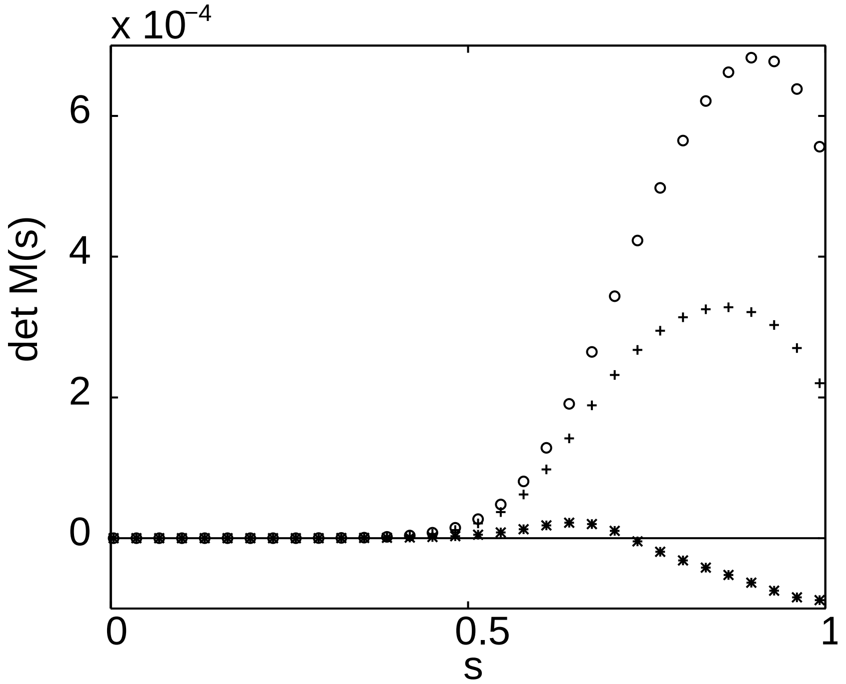

Figure 8.2: Graphs of the determinant of $\mathcal{M}$ versus arclength for three equilibrium solutions. For $s = 0$, $\mathcal{M}$ is the zero matrix, and for s close to zero, the determinant is very small but non-zero. Values of $s > 0$ where $\det \mathcal{M} = 0$ are conjugate points. The curves represent three solutions near a fold point. The curves of circles ($\circ$) and crosses ($+$) have no conjugate points and thus correspond to stable solutions with isoperimetric index zero. The curve of stars ($*$) has one conjugate point, and thus corresponds to an unstable solution with isoperimetric index one.

of generally accepted values for DNA), the entire low-energy component is stable, while the other component is entirely unstable, but of varying isoperimetric index.

The true cyclized equilibria (those with closed centerlines *and* closed double-helices) are labeled with circles in Figure 8.1. There are two such equilibria on the low-energy component, labeled A and B, and their physical configurations are shown in Figure 8.3. The other component contains several cyclized equilibria (and indeed there are many more on higher-energy components not shown here), but none are stable, and hence will presumably not be seen experimentally.

For all values of γ studied, the higher-energy component is entirely unstable, so it will not be displayed further. However, the stability properties of the lower-energy component do change with γ, as did the stability properties of the idealized elastic rod in Chapter 6. This lower energy component is shown in Figure 8.4 for three values of γ, with the cyclized equilibria again marked with circles and labeled as in Figure 8.1. Note the appearance of a region of instability at the top of the diagram, but that the two equilibria labeled A and B remain stable throughout. In addition, if γ is sufficiently small, two new cyclized equilibria emerge, one stable (labeled D) and one unstable (labeled E).

Like the formulation of the idealized elastic loop, the variational formulation

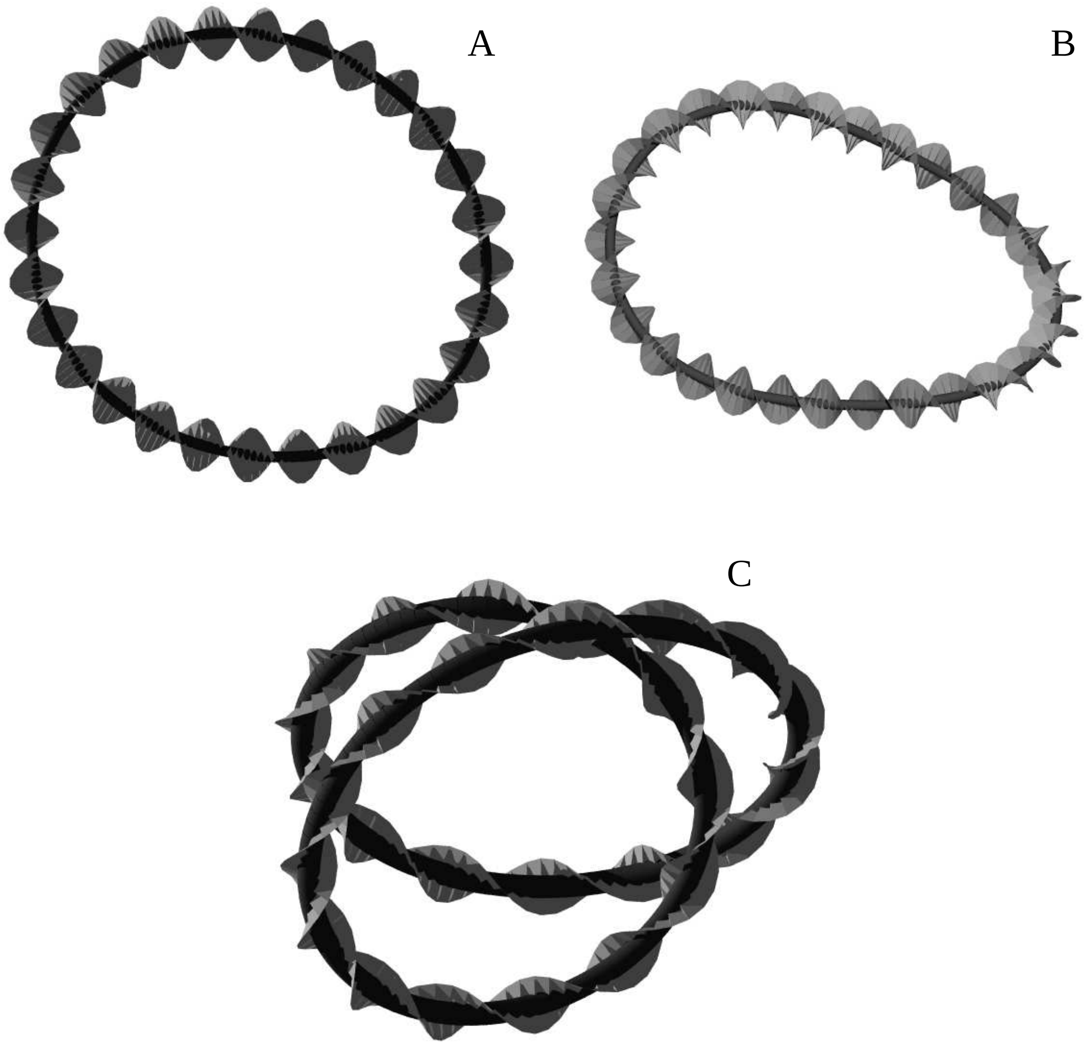

Figure 8.3: DNA configurations corresponding to the points A, B, and C on the bifurcation diagram in Figure 8.1. The centerline is indicated by a tube, and the twist of the double helices by a ribbon. Configurations A and B are stable, with roughly circular centerlines, although configuration A is nearly planar and configuration B is quite non-planar. Configuration C is unstable; its centerline is a perturbation of a double covered circle.

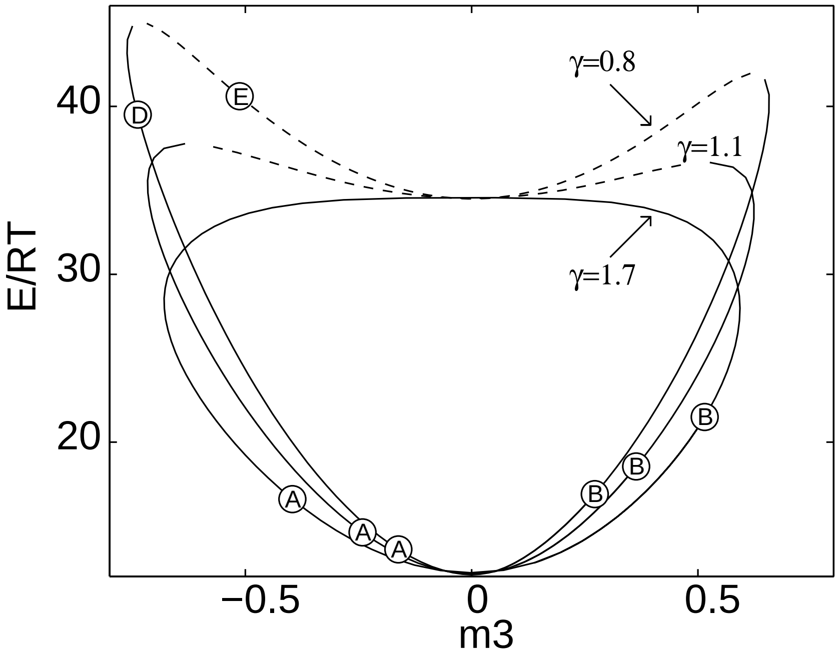

Figure 8.4: Bifurcation diagrams for DNA cyclization for three values of γ, with isoperimetric index indicated by line style (solid index 0;, dashed index 1) ; energy is plotted against twist moment as in Figure 8.1. The curve with $\gamma = 1.7$ consists only of stable equilibria. The curves with $\gamma = 1.1$ and $\gamma = 0.8$ have regions of unstable equilibria near the top. Cyclized DNA configurations (equilibria with $\mathbf{d}_1(0) = \mathbf{d}_1(1)$) are indicated with circles. Note that the $\gamma = 0.8$ diagram contains two additional such solutions, labeled D and E. The solution sets shown here are each the lowest-energy component of the complete bifurcation diagram for the labeled value of γ.

of the DNA example is parameter-dependent. The conjugate point test described in Chapter 2 was used to calculate the isoperimetric index, although this method does not exploit the structure of the resulting solution set. The distinguished diagram results should however predict changes in the index, calculated using the conjugate point method. For the DNA example, a distinguished diagram is provided by a plot of twist moment m_3 versus angle α, and the direction of stability exchange is as depicted in Figure 3.1. Figure 8.5 depicts this distinguished projection of the solution branches previously shown in Figure 8.4. The changes in isoperimetric index computed with the constrained conjugate point test agree with the index exchange predictions of distinguished diagram theory.

In a more speculative vein, we believe that critical points of the DNA variational principle with non-zero isoperimetric index may also be of physical interest. The families of critical points shown in Fig. 8.1 include branches of trefoil-like solutions approaching self-intersection with isoperimetric index at least two.

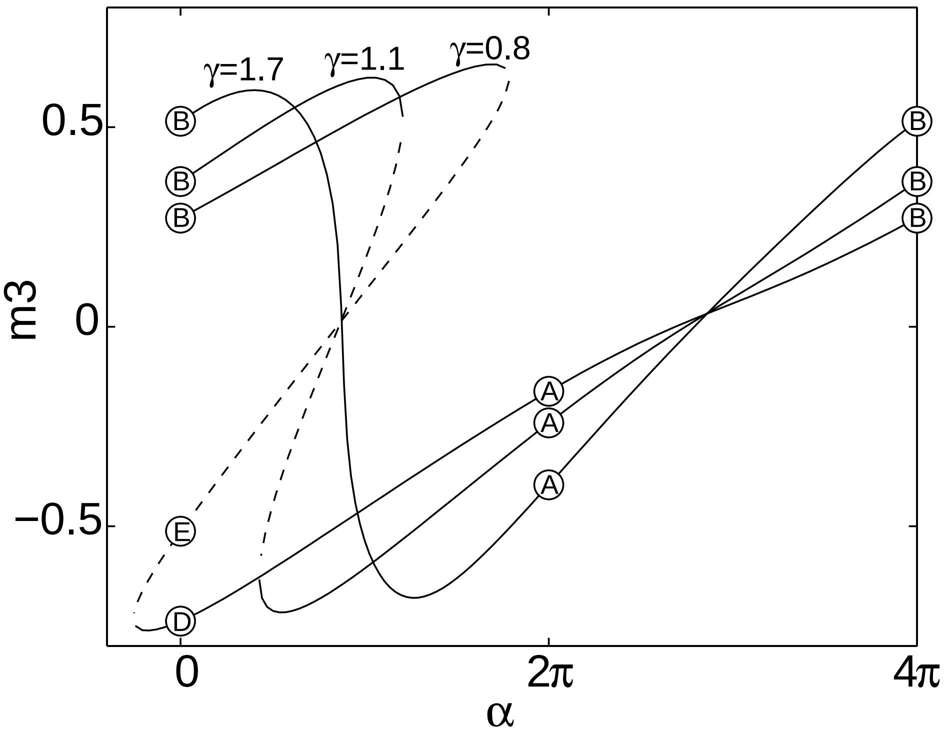

Figure 8.5: Bifurcation diagrams for DNA cyclization for three values of γ, with isoperimetric index indicated by line style (solid index 0, dashed index 1). The branches of equilibria that are represented are the same ones as in Figure 8.4, but now with the twist moment m_3 at $s = 0$ plotted against the angle α. This projection is a distinguished diagram for this problem, so that stability exchanges occur at folds (i.e. at points with vertical tangents) in the specific manner shown in Figure 3.1. Cyclized DNA configurations (equilibria with $\mathbf{d}_1(0) = \mathbf{d}_1(1)$) are indicated with circles, labeled as in Figure 8.4.

Macroscopic experiments with twisted elastic wires reveal that when effects of self-contact are included, some trefoil-like configurations are physically stable. Thus it seems likely that the isoperimetric index computed here will be one ingredient in a stability analysis of critical points in a more sophisticated model encompassing effects of self-contact.

Chapter 9

Conclusion and Discussion

The goal of this dissertation was to obtain stability results for equilibrium configurations of the idealized twisted elastic loop and for the equilibria of a more general elastic rod model of DNA minicircles. This example is of scientific importance because of the widespread acceptance of the twisted elastic rod as a model for DNA. We will not attempt to present a review of this extensive body of literature, but instead defer to the comprehensive survey articles [54] and [49]. Li and Maddocks [37] present a treatment of the Hamiltonian formulation of the equilibrium conditions governing the twisted elastic rod, characterize the complete solution set of the problem, and describe an efficient numerical algorithm for computing the equilibrium configurations including symmetry breaking techniques. This article provides the starting point for the analysis presented in this dissertation. However, there are a number of closely related works. Early work of Benham [3, 4, 5] and LeBret [33, 34] predicts the first bifurcation point on the trivial branch comprising single covered circles. Zajac [70] also determined the first bifurcation point on the first trivial branch, but motivated by a problem concerning the twisting of submarine cables. Goriely and Tabor reproduced Zajac's calculation in their studies of instabilities in the linearized dynamics of a filament and extended it to include the n-covered circles [18, 19]. In [31], Langer and Singer showed that torus knots are the only closed solutions of the related problem of minimizing total squared curvature, where as in [32] they pursued the analogy of elastic curves with solutions to the Localized Inductions Equations. Li [36] used techniques from differential geometry to characterize the equilibria with fixed but not necessarily closed boundary conditions associated with minimizing the total energy. Starostin [64, 63] determined a general formula for the bifurcation points on the trivial branches and also found nonplanar solutions via parameter continuation. Wadati and Tsuru [67] set forth a variational formulation and provide analytical solutions corresponding to the circular and figure-eight solutions of the equilibrium equations. Jülicher [25] classifies the solution set as planar rings, nonplanar rings, self-interacting rings and interwound configurations. Shi and Hearst [59, 58] investigate the equilibrium configurations of the idealized elastic loop by transforming the equilibrium equations into nonlinear Schrödinger equations. Intrinsic curvature and twist was added to the elastic rod model in [2], [45], [65]. Although this body of literature effectively deals with the equilibrium configurations and the solution set, little attempt is made to analytically determine the stability properties of these solutions. Some literature exists in regards to numerically determining minimizers though Monte Carlo techniques (for example [35],[28]), by dint of the fact that the algorithm can only converge to local minimizers, but a complete classification of the critical points was an open problem.

In order to analyze stability properties of twisted loops, it was necessary to develop new techniques to determine the index of critical points of a constrained calculus of variations problem. One approach combined a technique that extends the concept of distinguished bifurcation diagram to calculus of variations problems in which the bifurcation parameter enters by way of the boundary conditions with a treatment of isoperimetrically constrained problems. This theory was used to predict stability exchanges on the nontrivial branches of the idealized elastic loop. When combined with analytical calculations of the constrained index on twisted circular equilibria of the idealized problem, the distinguished diagram theory allows stability properties of all nonplanar equilibria to be classified solely from stability exchange predictions. The distinguished diagram technique proved inconclusive for the model of DNA because analytical determination of stability of an equilibrium in each connecting component was no longer available. Instead, another approach was developed in which the ideas of conjugate points and index theory in the unconstrained calculus of variations were exploited to define an isoperimetric index determined by counting isoperimetric conjugate points.

For the idealized problem, the stability of the planar solution was determined using a test based on $\mathcal{S}$-orthogonal subspaces originating in the theory of restricted quadratic forms [41, 39]. Tables 6.1 and 6.2 in Chapter 6 reveal the results this analysis. The first trivial branch is stable until the first bifurcation point and then unstable, and the trivial branches which correspond to n-covered circular solutions for $n > 1$ are unstable. At each bifurcation point two negative eigenvalues are gained.

The bifurcation points on the trivial branches were classified in order to quantify the index of solutions near bifurcation points and allow stability conclusions to be drawn based on the shape of the branches. The pitchfork structure of the bifurcation points allows them to be classified as either subcritical or supercritical. In either case, the index of the nearby solutions on the nontrivial branches is known. Numerical results can approximate the value of γ for which each bifurcation point switches between subcritical and supercritical. Chapter 7 computes this critical value of γ analytically for the $(n, m)^{th}$ bifurcation point using a perturbation technique detailed in [1]. The value is

$$\gamma = 1 + \frac{3n^2}{2(n+m)^2}.$$

The constrained index of the nonplanar solutions on the nontrivial branches is determined using the distinguished bifurcation diagram described in Chapter 3. The distinguished diagram, m_3 *vs.* α, predicts that the index changes as folds in the solution branch are traversed. The criticality of the bifurcation points discussed in Chapter 7 quantifies the index of solutions near the bifurcation point, and thus allows complete stability conclusions based on the fold result. The shape of the branches, the criticality of the bifurcation point, and thus the stability properties of the equilibria, depend on γ. For $\gamma = 1.3$, the first nontrivial branch corresponds to unstable equilibria (see Figure 6.3). For $\gamma = 1.7$, the first nontrivial branch consists of stable solutions from the bifurcation points to a fold and unstable solutions between the folds. For $\gamma = 2.1$, the entire branch consists of stable solutions. The higher-order branches contain folds for varying values of γ, but do not contain any stable solutions (see Figure 6.4).

The elastic rod model of Manning et al. [45] uses experimentally motivated parameters to determine the unstressed state of the rod. For this problem, the distinguished diagram alone cannot be used to determine stability because the explicit calculations carried out on the trivial branches of the idealized problem are no longer viable. Folds in the distinguished diagram still correspond to changes in index, but the index cannot be quantified for any particular equilibrium to allow stability conclusions to be made. For these equilibria, we calculated the isoperimetric index of families of critical points using the constrained conjugate point technique described in Chapter 2. The results reveal that for the 11 DNA molecules considered in [45] there are always at least two local minima, which was an unanticipated conclusion.

The techniques for determining the index of critical points that have been developed are applicable in a more general sense than the particular examples presented here. The first technique extends distinguished diagram theory to include calculus of variations problems which contain the bifurcation parameter in the boundary conditions. For the unconstrained setting, Chapter 3 shows that the distinguished diagram plots $W_{\mathbf{q}'} \cdot \frac{d\mathbf{f}}{d\alpha}$ against α. In the presence of isoperimetric constraints, the fundamental setting of the distinguished diagram calculation changes. The analysis presented in Chapter 3 uses the projection operator $\mathcal{Q}$ described in Section 2.2.2 to constrain the domain of the second-order differential operator to the tangent space of the constraint manifold. However, the same distinguished diagram as in the unconstrained case still arises. An alternative method for connecting the constrained stability of equilibria with the distinguished diagram relies on extension of results concerning 'bordered matrices' (cf. Appendix A).

The stability analysis of the elastic rod model of DNA used the method of constrained conjugate points to derive the isoperimetric index, and this approach is generally applicable too. In addition, we described a practical numerical implementation for determining the isoperimetric index based on a count of the number of zeroes of the determinant of a certain constrained stability matrix. The absence of a constrained conjugate point (in the sense we use) was previously described by Bolza [7] (and attributed by him to Kneser and Weierstrass) as a necessary and sufficient condition for the second variation to be nonnegative. However, we believe the connection between constrained conjugate points and a projected eigenvalue problem, which is the viewpoint that allows a definition of the isoperimetric index, to be a new observation. In any case, the test of Bolza is apparently not widely disseminated in the contemporary literature, although it has been exploited by Benjamin [6] to study stability of solitary waves, and by Segercrantz [56] to demonstrate the existence of a minimizing curve in a model of a motor.

We remark that the isoperimetric index only provides information about necessary conditions for minima. Since stable solutions have index zero, $\delta^2 J[\boldsymbol{\zeta}] \geq 0$ for all $\boldsymbol{\zeta}$ in an admissible set. But non-negativity of the second variation is only a necessary condition for the extremal to be a minimum. A sufficient condition for a minimum in unconstrained calculus of variations problems is that the second variation be strongly positive; that is, there exists a constant k such that $\delta^2 J[\boldsymbol{\zeta}] \geq k||\boldsymbol{\zeta}||^2$, for some norm. In the unconstrained setting, this sufficient condition is implied by the strengthened Legendre's condition and strengthened Jacobi's condition. The literature concerning the necessary and sufficient conditions for a minimum in constrained calculus of variations problems is considerably more obscure. In the constrained setting, there is surprisingly little work on sufficient conditions for a minimum, beyond the necessary condition derived by Hestenes [23]. Vogel [66] addresses the sufficient conditions for a constrained minimum in the case of a single constraint.

Appendix A

Constrained Stability and the Bordered Operator

An alternative method for connecting the constrained stability of equilibria with the distinguished diagram is based upon an extension of the spectral theory of bordered matrices from finite dimensions to an infinite dimensional theory of bordered operators. Bordered operators arise in constrained problems when the Lagrange multipliers are regarded as dependent variables. We shall show that the distinguished diagram predicts index changes in the bordered operator which in turn yields the appropriate isoperimetric index. This approach is joint work with J.H. Maddocks and L. Greenberg.

In finite dimensional constrained optimization theory, it is known that a spectral analysis of the Kuhn-Tucker 'bordered matrix', here denoted $\mathbf{M}$, that arises as the Hessian of the objective function with respect to the extended variable $(\mathbf{x}, \boldsymbol{\lambda})$ provides information regarding the positivity or non-negativity of the quadratic form $\mathbf{x} \cdot \mathbf{S}\mathbf{x}$ on the tangent space to the constraints [8, 22, 43, 44, 61]. In this setting, $\mathbf{S}$ is the real symmetric matrix representing the Hessian of the objective function with respect to the $\mathbf{x}$ variable. In the finite dimensional context it is also known that

$$\sigma^-(\mathbf{M}) = \sigma^-(\mathbf{QSQ}) + n. \tag{A.1}$$

Here, the notation $\sigma^-(\cdot)$ represents the number of negative eigenvalues of the appropriate matrix, n is the number of linearly independent constraints, and $\mathbf{Q}$ is an appropriate projection onto the tangent space of the constraint surface. In this Appendix, we prove the infinite dimensional analogue of Equation (A.1), namely

$$\sigma^-(\mathcal{M}) = \sigma^-(\mathcal{QSQ}) + n, \tag{A.2}$$

where $\mathcal{Q}$ is the projection defined by Equation (2.12), $\mathcal{M}$ is the bordered operator defined below, $\mathcal{S}$ is the second variation operator defined by Equation (3.19), and n is the number of linearly independent constraints. Equation (A.2) then provides a test for the second order condition $\langle \mathcal{S}\boldsymbol{\zeta}, \boldsymbol{\zeta} \rangle \geq 0, \quad \forall \boldsymbol{\zeta} \in \mathcal{A}_d^{cons}$, or equivalently $\sigma^-(\mathcal{QSQ}) = 0$, namely $\sigma^-(\mathcal{M}) = n$.

As shown in Chapter 3, distinguished diagram theory predicts changes in the index of $\mathcal{QSQ}$ along families of critical points, and thus through Equation (A.2) predicts changes in index of $\mathcal{M}$. In fact, the distinguished diagram results could also be computed directly for the bordered operator $\mathcal{M}$. We believe that the relationship between the distinguished diagram and the spectrum of the bordered operator, even in the finite dimensional context, was previously unknown.

We begin by setting notation. Let $\mathbf{T}_i$, $i = 1...n$, as defined by Equation (3.18), denote the linearized constraints, and assume that the $\mathbf{T}_i$ are linearly independent as functions of s on all intervals $(0, \sigma)$, $0 < \sigma < 1$. In the case of the bordered operator, the Lagrange multipliers $\boldsymbol{\lambda}$ are considered to be dependent variables and accordingly, we define an extended variable $\mathbf{z} = (\boldsymbol{\zeta}, \boldsymbol{\lambda})^T$, where $\boldsymbol{\zeta} \in \mathcal{A}_d(\sigma)$, (cf. (2.15)), and $\boldsymbol{\lambda} \in \mathbb{R}^n$. The bordered operator $\mathcal{M}(\sigma) : \mathcal{A}_d(\sigma) \times \mathbb{R}^n \to L^2 \times \mathbb{R}^n$ acting on $\mathbf{z}$ is defined to be

$$\mathcal{M}(\sigma) = \begin{pmatrix} & \vdots & & \vdots \\ \mathcal{S} & \mathbf{T}_1 & \dots & \mathbf{T}_n \\ & \vdots & & \vdots \\ \mathcal{T}_1(\cdot) & & & \\ \vdots & & \mathbf{0} & \\ \mathcal{T}_n(\cdot) & & & \end{pmatrix},$$

where $\mathcal{T}_i(\boldsymbol{\zeta}) = \int_0^\sigma \mathbf{T}_i \cdot \boldsymbol{\zeta}\, ds$. The inner product on the space $L^2 \times \mathbb{R}^n$ is defined by $\langle \mathbf{z}, \mathcal{M}\mathbf{z} \rangle = \langle \boldsymbol{\zeta}, \mathcal{S}\boldsymbol{\zeta} \rangle + \sum_{i=1}^n 2\lambda_i \int_0^1 \boldsymbol{\zeta} \cdot \mathbf{T}_i\, ds$. Note that $\mathcal{M}(1)$ will be denoted $\mathcal{M}$. Also we recall the definitions of the spaces $\mathcal{T}$ from Equation (2.14), $\mathcal{A}_d^{cons}$ from Equation (2.10), $\mathcal{A}_d^{cons}(\sigma)$ from Equation (2.16), and $\mathcal{A}_d(\sigma)$ from Equation (2.15).

We wish to obtain Equation (A.2) and to this end, we prove the following lemmas:

Lemma A.1. *$\langle \mathbf{z}, \mathcal{M}\mathbf{z} \rangle = \langle \boldsymbol{\zeta}, \mathcal{S}\boldsymbol{\zeta} \rangle$ whenever $\mathbf{z} = (\boldsymbol{\zeta}, \boldsymbol{\lambda})^T$, with $\boldsymbol{\zeta}(s) \in \mathcal{A}_d^{cons}$ and $\boldsymbol{\lambda} \in \mathbb{R}^n$.*

Proof. Consider

$$\begin{aligned} \mathcal{M}\mathbf{z} &= \begin{pmatrix} \mathcal{S}\boldsymbol{\zeta} + \sum_{i=1}^n \lambda_i \mathbf{T}_i \\ \mathcal{T}_1(\boldsymbol{\zeta}) \\ \vdots \\ \mathcal{T}_n(\boldsymbol{\zeta}) \end{pmatrix}, \\ \langle \mathbf{z}, \mathcal{M}\mathbf{z} \rangle &= \langle \boldsymbol{\zeta}, \mathcal{S}\boldsymbol{\zeta} \rangle + \sum_{i=1}^n 2\lambda_i \int_0^1 \boldsymbol{\zeta} \cdot \mathbf{T}_i. \end{aligned}$$

The result follows since for $\boldsymbol{\zeta} \in \mathcal{A}_d^{cons}$, $\int_0^1 \boldsymbol{\zeta} \cdot \mathbf{T}_i\, ds = 0$. ☐

Lemma A.2. *If the $\mathbf{T}_i$ are linearly independent on all intervals $(0, \sigma)$, then $\mathbf{z} = (\mathbf{0}, \boldsymbol{\lambda})$ is not an eigenvector for $\mathcal{M}(\sigma)$.*

Proof.

$$\mathcal{M}(\sigma) \begin{pmatrix} \mathbf{0} \\ \boldsymbol{\lambda} \end{pmatrix} = \begin{pmatrix} \sum_{i=1}^n \lambda_i \mathbf{T}_i \\ \mathbf{0} \end{pmatrix} \neq \mathbf{0}$$

since the $\mathbf{T}_i$ are linearly independent for all intervals $(0, \sigma)$. ☐

Lemma A.3. *For all values of σ, $\mathcal{M}(\sigma)$ has at least n negative eigenvalues.*

Proof. Test functions of the form $(\mathbf{0}, \boldsymbol{\lambda})^T$ form an n-dimensional subspace on which the Rayleigh quotient

$$R(\mathcal{M}) = \frac{\langle \boldsymbol{\zeta}, \mathcal{S}\boldsymbol{\zeta}\rangle + 2\sum_{i=1}^{n} \lambda_i \langle \boldsymbol{\zeta}, \mathbf{T}_i\rangle}{\langle \mathbf{z}, \mathbf{z}\rangle}$$

vanishes, and by Lemma A.2 no element of the subspace is an eigenvector. Therefore the min max Rayleigh principle for the eigenvalues of $\mathcal{M}$, i.e. the $n+1^{st}$ eigenvalue is given by

$$\min_{\mathcal{B}\in\mathcal{B}_n} \max_{\mathbf{z}\in\mathcal{B}} R(\mathcal{M}).$$

Choosing $\mathcal{B} = \{(\mathbf{0}, \boldsymbol{\lambda})^T\}$, we can conclude that there are at least n negative eigenvalues. □

Lemma A.4. *For σ sufficiently small, $\sigma^-(\mathcal{M}(\sigma)) = n$.*

Proof. Lemma A.3 guarantees that $\mathcal{M}(\sigma)$ has at least n negative eigenvalues for all values of σ. For σ sufficiently small, we want to show there are at most n negative eigenvalues. The max min Rayleigh principle for the eigenvalues of $\mathcal{M}$, i.e. the $n+1^{st}$ eigenvalue is given by

$$\max_{\mathbf{b}_1,\ldots,\mathbf{b}_n} \min_{\substack{\mathbf{z}\in\mathbf{D} \\ \langle \mathbf{z}, \mathbf{b}_i\rangle = 0 \\ i=1,\ldots,n}} R(\mathbf{z}),$$

allows us to conclude that for σ sufficiently small, there are at most n negative eigenvalues. For vectors orthogonal to the n-dimensional space $(\mathbf{0}, \boldsymbol{\lambda})^T$ are of the form $(\boldsymbol{\zeta}, \mathbf{0})^T$, and vectors of the form $(\boldsymbol{\zeta}, \mathbf{0})^T$ have the Rayleigh quotient $\langle \boldsymbol{\zeta}, \mathcal{S}\boldsymbol{\zeta}\rangle$ is positive, since the differential operator $\mathcal{S}$ is positive definite for σ sufficiently small. □

Lemma A.5. *The eigenvalues $\rho_i(\sigma)$ of $\mathcal{M}(\sigma)$ are decreasing functions of σ.*

Proof. Consider $\sigma_1 < \sigma_2$. Let $\begin{pmatrix} \boldsymbol{\zeta}_k \\ \boldsymbol{\lambda}_k \end{pmatrix}$ be the (normalized) eigenvector of $\mathcal{M}(\sigma_1)$ associated with the eigenvalue $\rho_k(\sigma_1)$. Then define

$$\boldsymbol{\xi}_k = \begin{cases} \boldsymbol{\zeta}_k & 0 \le s \le \sigma_1 \\ \mathbf{0} & \sigma_1 < s \le \sigma_2 \end{cases}.$$

and denote $\boldsymbol{\psi}_k(s)$ to be

$$\boldsymbol{\psi}_k(s) = \begin{pmatrix} \boldsymbol{\xi}_k \\ \boldsymbol{\lambda}_k \end{pmatrix}.$$

As in the proof of Property 2.5 appearing in Chapter 2, insert the linear combination

$$\sum_{k=1}^{m} a_k \boldsymbol{\psi}_k$$

with the normalization $\sum_{k=1}^m a_k^2 = 1$ into the Rayleigh quotient analogous to (2.19) to yield

$$\rho_m(\sigma_2) \leq \frac{\langle \sum_{k=1}^m a_k \boldsymbol{\psi}_k, \mathcal{M}(\sigma_2) \sum_{k=1}^m a_k \boldsymbol{\psi}_k \rangle}{\langle \sum_{k=1}^m a_k \boldsymbol{\psi}_k, \sum_{k=1}^m a_k \boldsymbol{\psi}_k \rangle}.$$

The numerator becomes

$$\begin{aligned}
&\langle \sum_{k=1}^m a_k \boldsymbol{\psi}_k, \mathcal{M}(\sigma_2) \sum_{k=1}^m a_k \boldsymbol{\psi}_k \rangle \\
&= \int_0^{\sigma_2} \left(\sum_{k=1}^m a_k \boldsymbol{\xi}_k \right) \cdot \mathcal{S} \left(\sum_{k=1}^m a_k \boldsymbol{\xi}_k \right) \\
&\quad +2 \sum_{i=1}^n \left(\sum_{k=1}^m a_k (\boldsymbol{\lambda} \cdot \mathbf{e}_i)_k \right) \int_0^{\sigma_2} \left(\sum_{k=1}^m a_k \boldsymbol{\xi}_k \right) \cdot \mathbf{T}_i \, ds \\
&= \int_0^{\sigma_1} \left(\sum_{k=1}^m a_k \boldsymbol{\zeta}_k \right) \cdot \mathcal{S} \left(\sum_{k=1}^m a_k \boldsymbol{\zeta}_k \right) \\
&\quad +2 \sum_{i=1}^n \left(\sum_{k=1}^m a_k (\boldsymbol{\lambda} \cdot \mathbf{e}_i)_k \right) \int_0^{\sigma_1} \left(\sum_{k=1}^m a_k \boldsymbol{\zeta}_k \right) \cdot \mathbf{T}_i \, ds \\
&= \langle \sum_{k=1}^m a_k \boldsymbol{\psi}_k, \mathcal{M}(\sigma_1) \sum_{k=1}^m a_k \boldsymbol{\psi}_k \rangle \\
&= \sum_{k=1}^m a_k^2 \rho_k(\sigma_1),
\end{aligned}$$

since $\boldsymbol{\psi}_k$ is exactly the eigenvector $(\boldsymbol{\zeta}_k, \boldsymbol{\lambda}_k)^T$ on the interval $0 \leq s \leq \sigma_1$. The denominator evaluates to $\langle \sum_{k=1}^m a_k \boldsymbol{\psi}_k, \sum_{k=1}^m a_k \boldsymbol{\psi}_k \rangle = \sum_{k=1}^m a_k^2 = 1$, thus

$$\rho_m(\sigma_2) \leq \frac{\sum_{k=1}^m a_k^2 \rho_k(\sigma_1)}{\sum_{k=1}^m a_k^2} \leq \rho_m(\sigma_1).$$

$\square$

A conjugate point of $\mathcal{M}$ is a value of σ such that

$$\mathcal{M}(\sigma)\mathbf{z} = \mathbf{0},$$

has a nontrivial solution, i.e. a value of σ for which $\mathcal{M}(\sigma)$ has zero as an eigenvalue. It follows from Lemmas A.4 and A.5 that $\sigma^-(\mathcal{M})$ can be determined by counting the number of conjugate points $\sigma < 1$, and adding n.

Lemma A.6. *The conjugate points of $\mathcal{M}(\sigma)$ exactly coincide with conjugate points of $\mathcal{QSQ}$, as defined in Equation (2.22) to be a value of σ such that*

$$\mathcal{QSQ}\boldsymbol{\zeta} = \mathbf{0}, \;\; \boldsymbol{\zeta} \in \mathcal{A}_d^{cons}(\sigma)$$

has a nontrivial solution.

Proof.

$$\mathcal{M}\mathbf{z} = \mathbf{0}, \boldsymbol{\zeta} \in \mathcal{A}_d(\sigma)$$
$$\iff \begin{pmatrix} \mathcal{S}\boldsymbol{\zeta} + \sum_{i=1}^{n} \lambda_i \mathbf{T}_i \\ \mathcal{T}_1(\boldsymbol{\zeta}) \\ \vdots \\ \mathcal{T}_n(\boldsymbol{\zeta}) \end{pmatrix} = \mathbf{0}, \iff \mathcal{S}\boldsymbol{\zeta} + \sum_{i=1}^{n} \lambda_i \mathbf{T}_i = \mathbf{0}, \;\; \boldsymbol{\zeta} \in \mathcal{A}_d^{cons}(\sigma).$$

Lemma 2.23 guarantees the equivalence

$$\mathcal{S}\boldsymbol{\zeta} + \sum_{i=1}^{n} \lambda_i \mathbf{T}_i = \mathbf{0}, \;\; \boldsymbol{\zeta} \in \mathcal{A}_d^{cons}(\sigma) \iff \mathcal{Q}\mathcal{S}\mathcal{Q}\boldsymbol{\zeta} = \mathbf{0}, \;\; \boldsymbol{\zeta} \in \mathcal{A}_d^{cons}(\sigma).$$

□

The previous lemmas are used to prove the main result:

Theorem 0.1.

$$\sigma^-(\mathcal{M}) = \sigma^-(\mathcal{Q}\mathcal{S}\mathcal{Q}) + n,$$

Proof. The number of negative eigenvalues of $\mathcal{Q}\mathcal{S}\mathcal{Q}$ and $\mathcal{M}$ can be determined by counting the number of conjugate points. Lemma A.6 guarantees that conjugate points of $\mathcal{Q}\mathcal{S}\mathcal{Q}$ exactly coincide with conjugate points of $\mathcal{M}$ (Lemma A.6). In the limit of short intervals $\mathcal{Q}\mathcal{S}\mathcal{Q}$ is positive semi-definite (Property 2.5), while $\mathcal{M}$ has n negative eigenvalues (Lemma A.4). Since they initially differ by n eigenvalues and the conjugate points coincide, the number of negative eigenvalues of $\mathcal{M}$ and $\mathcal{Q}\mathcal{S}\mathcal{Q}$ will always differ by n. □

We have as a corollary:

Corollary A.1. $\langle \mathcal{S}\boldsymbol{\zeta}, \boldsymbol{\zeta} \rangle \geq 0, \;\; \forall \boldsymbol{\zeta} \in \mathcal{A}_d^{cons} \iff \sigma^-(\mathcal{M}) = n$

Proof 1: According to the definition of $\mathcal{Q}$ (cf. Section 2.2.2),

$$\langle \mathcal{S}\boldsymbol{\zeta}, \boldsymbol{\zeta} \rangle \geq 0, \;\; \forall \boldsymbol{\zeta} \in \mathcal{A}_d^{cons} \quad \iff \quad \langle \mathcal{Q}\mathcal{S}\mathcal{Q}\boldsymbol{\eta}, \boldsymbol{\eta} \rangle \geq 0, \;\; \forall \boldsymbol{\eta} \in \mathcal{A}_d^{cons},$$

and the equivalence

$$\langle \mathcal{Q}\mathcal{S}\mathcal{Q}\boldsymbol{\eta}, \boldsymbol{\eta} \rangle \geq 0, \;\; \forall \boldsymbol{\eta} \in \mathcal{A}_d^{cons} \quad \iff \quad \sigma^-(\mathcal{Q}\mathcal{S}\mathcal{Q}) = 0,$$

is guaranteed by the Rayleigh Principle (2.19). The result follows from applying Theorem 0.1. □

An alternative independent direct proof of Corollary A.1 is also possible:
Proof 2: Suppose $\langle \mathcal{S}\boldsymbol{\zeta}, \boldsymbol{\zeta} \rangle \geq 0, \;\; \forall \boldsymbol{\zeta} \in \mathcal{A}_d^{cons}$ and $\sigma^-(\mathcal{M}) = n + 1$. Then there exists a subspace $\mathcal{W}$ of the domain of $\mathcal{M}$ such that $\dim(\mathcal{W}) = n + 1$ and $\langle \mathcal{M}\mathbf{w}, \mathbf{w} \rangle < 0$ for $\mathbf{w} \in \mathcal{W}$. There must exist a $\mathbf{w}_0 \in \mathcal{W}$ such that $\mathbf{w}_0$ has the

form $\mathbf{w}_0 = (\boldsymbol{\zeta}, \boldsymbol{\lambda})^T$, $\mathbf{0} \neq \boldsymbol{\zeta} \in \mathcal{A}_d^{cons}$ (since $\mathcal{A}_d^{cons}$ only requires n orthogonality conditions, and the Rayleigh quotient vanishes for vectors of the form $(\mathbf{0}, \boldsymbol{\lambda})^T$). Since $\mathbf{w}_0 \in \mathcal{W}$, $\langle \mathcal{M}\mathbf{w}_0, \mathbf{w}_0 \rangle < 0$. But since $\boldsymbol{\zeta} \in \mathcal{A}_d^{cons}$, $\langle \mathcal{M}\mathbf{w}_0, \mathbf{w}_0 \rangle = \langle \mathcal{S}\boldsymbol{\zeta}, \boldsymbol{\zeta} \rangle$ (Lemma A.1) so that $\langle \mathcal{S}\boldsymbol{\zeta}, \boldsymbol{\zeta} \rangle < 0$, a contradiction.

Conversely, assume that $\sigma^-(\mathcal{M}) = n$ and $\exists \boldsymbol{\zeta}_0 \in \mathcal{A}_d^{cons}$ such that $\langle \mathcal{S}\boldsymbol{\zeta}_0, \boldsymbol{\zeta}_0 \rangle < 0$. Define $\mathcal{W}(\boldsymbol{\zeta}) = \mathcal{K} \oplus \mathcal{R}(\boldsymbol{\zeta}_0)$ with dimension $n+1$, where

$$\mathcal{K} = \{(\mathbf{0}, \mathbf{k}) : \mathbf{k} \in \mathbb{R}^n\}, \qquad \mathcal{R}(\boldsymbol{\zeta}) = \{(r\boldsymbol{\zeta}, \mathbf{0}) : r \in \mathbb{R}, \}.$$

Then $\langle \mathcal{M}(r\boldsymbol{\zeta}_0, \boldsymbol{\lambda}), (r\boldsymbol{\zeta}_0, \boldsymbol{\lambda}) \rangle = r^2 \langle \mathcal{S}\boldsymbol{\zeta}_0, \boldsymbol{\zeta}_0 \rangle \leq 0$. This implies that the $n+1^{st}$ eigenvalue of $\mathcal{M}$ is less than or equal to zero. If this eigenvalue is zero, then $\mathcal{W}$ contains the eigenvector corresponding to the zero eigenvalue. But $\langle \mathbf{z}, \mathcal{M}\mathbf{z} \rangle = r^2 \langle \mathcal{M}\boldsymbol{\zeta}_0, \boldsymbol{\zeta}_0 \rangle < 0$, unless $r = 0$, and we know from Lemma A.2 that $\mathcal{M}\mathbf{z} \neq \mathbf{0}$, if $r = 0$. Thus the $n+1^{st}$ eigenvalue of $\mathcal{M}$ is less than zero, which contradicts $\sigma^-(\mathcal{M}) = n$. $\square$

Appendix B

Lagrange Multiplier for the Unit Length Constraint

The value of the multiplier μ' in Equation (6.1) can be determined from the Euler-Lagrange equations. This value depends on the normalization factor assumed in the expression for the director $\mathbf{d}_3$ (4.10). This dissertation assumes a quadratic normalization

$$\mathbf{d}_3 = \frac{1}{|\mathbf{q}|^2} \begin{pmatrix} 2(q_1 q_3 + q_2 q_4) \\ 2(-q_1 q_4 + q_2 q_3) \\ -q_1^2 - q_2^2 + q_3^2 + q_4^2 \end{pmatrix}$$

for which $\mu' = 0$. However, an expression for μ' can be determined for arbitrary normalization factors, β:

$$\mathbf{d}_3 = \frac{1}{|\mathbf{q}|^\beta} \begin{pmatrix} 2(q_1 q_3 + q_2 q_4) \\ 2(-q_1 q_4 + q_2 q_3) \\ -q_1^2 - q_2^2 + q_3^2 + q_4^2 \end{pmatrix}$$

Lemma B.1.

$$\mu' = (2 - \beta)\, \boldsymbol{\lambda} \cdot \mathbf{d}_3$$

Proof. The Euler-Lagrange derivative of the Lagrangian

$$J = \int_{s=0}^{s=1} W(u_1, u_2, u_3, s) + \boldsymbol{\lambda} \cdot \mathbf{d}_3 + \mu\, \mathbf{q} \cdot \mathbf{q}'$$

is

$$\sum_{i=1}^{3} 2m_i' \frac{\mathbf{B}_i \mathbf{q}}{|\mathbf{q}|^2} = \sum_{i=1}^{3} m_i \left[-4 \frac{\mathbf{B}_i \mathbf{q}'}{|\mathbf{q}|^2} - 2u_i \frac{\mathbf{q}}{|\mathbf{q}|^2} \right] - \frac{\partial (\mathbf{d}_3 \cdot \boldsymbol{\lambda})}{\partial \mathbf{q}} - \mu' \mathbf{q}. \quad \text{(B.1)}$$

If the Euler-Lagrange derivative (B.1) is multiplied by $\mathbf{q}$, then the following expression arises

$$\mu' = -\frac{\partial (\mathbf{d}_3 \cdot \boldsymbol{\lambda})}{\partial \mathbf{q}} \cdot \mathbf{q}.$$

It is convenient for the calculation to rewrite this in the following form

$$\mu' = -\boldsymbol{\lambda} \cdot \frac{\partial \mathbf{d}_3}{\partial \mathbf{q}} \mathbf{q}.$$

The notation $\mathbf{d}_3$ is the third director normalized by $|\mathbf{q}|^\beta$, i.e.,

$$\mathbf{d}_3 = \frac{\hat{\mathbf{d}}_3}{|\mathbf{q}|^\beta}$$

where $\hat{\mathbf{d}}_3$ is the unnormalized director. This expression can be factored as follows

$$\mathbf{d}_3 = \frac{1}{|\mathbf{q}|^{\beta-2}} \frac{\hat{\mathbf{d}}_3}{|\mathbf{q}|^2}.$$

The derivative of the factored form of $\mathbf{d}_3$ is

$$\frac{\partial \mathbf{d}_3}{\partial \mathbf{q}} = \frac{1}{|\mathbf{q}|^{\beta-2}} \frac{\partial}{\partial \mathbf{q}} \left(\frac{\hat{\mathbf{d}}_3}{|\mathbf{q}|^2} \right) - \left(\frac{\hat{\mathbf{d}}_3}{|\mathbf{q}|^2} \right) (\beta - 2) \frac{\mathbf{q}}{|\mathbf{q}|^\beta}$$

so that

$$\frac{\partial \mathbf{d}_3}{\partial \mathbf{q}} \cdot \mathbf{q} = \frac{1}{|\mathbf{q}|^{\beta-2}} \frac{\partial}{\partial \mathbf{q}} \left(\frac{\hat{\mathbf{d}}_3}{|\mathbf{q}|^2} \right) \cdot \mathbf{q} - \left(\frac{\hat{\mathbf{d}}_3}{|\mathbf{q}|^2} \right) (\beta - 2) \frac{|\mathbf{q}|^2}{|\mathbf{q}|^\beta}.$$

Employing the expression for $\frac{\partial}{\partial \mathbf{q}} \left(\frac{\hat{\mathbf{d}}_3}{|\mathbf{q}|^2} \right)$ given in Equation (4.11),

$$\left(\frac{\partial \mathbf{d}_3}{\partial \mathbf{q}} \right)^T = \frac{2}{|\mathbf{q}|^2} \mathbf{B}_2 \mathbf{q} \otimes \mathbf{d}_1 - \frac{2}{|\mathbf{q}|^2} \mathbf{B}_1 \mathbf{q} \otimes \mathbf{d}_2$$

we get

$$\frac{1}{|\mathbf{q}|^{\beta-2}} \frac{\partial}{\partial \mathbf{q}} \left(\frac{\hat{\mathbf{d}}_3}{|\mathbf{q}|^2} \right) \cdot \mathbf{q} = 0$$

and

$$\frac{\partial \mathbf{d}_3}{\partial \mathbf{q}} = -(\beta - 2) \frac{\hat{\mathbf{d}}_3}{|\mathbf{q}|^\beta}.$$

The expression for μ' then becomes

$$\mu' = (\beta - 2)(\mathbf{d}_3 \cdot \boldsymbol{\lambda}).$$

$\square$

Appendix C

Second Derivative of $\mathbf{d}_3 \cdot \boldsymbol{\lambda}$

This appendix records the explicit forms of three 4×4 matrices $\boldsymbol{\Lambda}_{13} = \frac{\partial^2(\mathbf{d}_3 \cdot \mathbf{e}_1)}{\partial \mathbf{q} \partial \mathbf{q}}$, $\boldsymbol{\Lambda}_{23} = \frac{\partial^2(\mathbf{d}_3 \cdot \mathbf{e}_2)}{\partial \mathbf{q} \partial \mathbf{q}}$, and $\boldsymbol{\Lambda}_{33} = \frac{\partial^2(\mathbf{d}_3 \cdot \mathbf{e}_3)}{\partial \mathbf{q} \partial \mathbf{q}}$, appearing in Equation (6.1). These matrices are too large to write out in matrix form, therefore they are presented rowwise. The first row of $\boldsymbol{\Lambda}_{13}$ is

$$
\begin{aligned}
&[-8\,\frac{q_3\,q_1}{|\mathbf{q}|^4} + 16\,\frac{(\,q_1\,q_3 + q_2\,q_4\,)\,q_1^2}{|\mathbf{q}|^6} - 4\,\frac{q_1\,q_3 + q_2\,q_4}{|\mathbf{q}|^4}\,, \\
&-4\,\frac{q_4\,q_1}{|\mathbf{q}|^4} - 4\,\frac{q_3\,q_2}{|\mathbf{q}|^4} + 16\,\frac{(\,q_1\,q_3 + q_2\,q_4\,)\,q_2\,q_1}{|\mathbf{q}|^6}\,, \\
&2\,\frac{1}{|\mathbf{q}|^2} - 4\,\frac{q_1^2}{|\mathbf{q}|^4} - 4\,\frac{q_3^2}{|\mathbf{q}|^4} + 16\,\frac{(\,q_1\,q_3 + q_2\,q_4\,)\,q_3\,q_1}{|\mathbf{q}|^6}\,, \\
&-4\,\frac{q_2\,q_1}{|\mathbf{q}|^4} - 4\,\frac{q_3\,q_4}{|\mathbf{q}|^4} + 16\,\frac{(\,q_1\,q_3 + q_2\,q_4\,)\,q_4\,q_1}{|\mathbf{q}|^4}\,]\,.
\end{aligned}
$$

The second row of $\boldsymbol{\Lambda}_{13}$ is

$$
\begin{aligned}
&[-4\,\frac{q_4\,q_1}{|\mathbf{q}|^4} - 4\,\frac{q_3\,q_2}{|\mathbf{q}|^4} + 16\,\frac{(\,q_1\,q_3 + q_2\,q_4\,)\,q_2\,q_1}{|\mathbf{q}|^6}\,, \\
&-8\,\frac{q_4\,q_2}{|\mathbf{q}|^4} + 16\,\frac{(\,q_1\,q_3 + q_2\,q_4\,)\,q_2^2}{|\mathbf{q}|^6} - 4\,\frac{q_1\,q_3 + q_2\,q_4}{|\mathbf{q}|^4}\,, \\
&-4\,\frac{q_2\,q_1}{|\mathbf{q}|^4} - 4\,\frac{q_3\,q_4}{|\mathbf{q}|^4} + 16\,\frac{(\,q_1\,q_3 + q_2\,q_4\,)\,q_3\,q_2}{|\mathbf{q}|^6}\,, \\
&2\,\frac{1}{|\mathbf{q}|^2} - 4\,\frac{q_2^2}{|\mathbf{q}|^4} - 4\,\frac{q_4^2}{|\mathbf{q}|^4} + 16\,\frac{(\,q_1\,q_3 + q_2\,q_4\,)\,q_4\,q_2}{|\mathbf{q}|^6}].
\end{aligned}
$$

The third row $\boldsymbol{\Lambda}_{13}$ is

$$
\begin{aligned}
&[2\,\frac{1}{|\mathbf{q}|^2} - 4\,\frac{q_1^2}{|\mathbf{q}|^4} - 4\,\frac{q_3^2}{|\mathbf{q}|^2}^{2} + 16\,\frac{(\,q_1\,q_3 + q_2\,q_4\,)\,q_3\,q_1}{|\mathbf{q}|^6}\,, \\
&-4\,\frac{q_2\,q_1}{|\mathbf{q}|^4} - 4\,\frac{q_3\,q_4}{|\mathbf{q}|^4} + 16\,\frac{(\,q_1\,q_3 + q_2\,q_4\,)\,q_3\,q_2}{|\mathbf{q}|^6}\,, \\
&-8\,\frac{q_3\,q_1}{|\mathbf{q}|^4} + 16\,\frac{(\,q_1\,q_3 + q_2\,q_4\,)\,q_3^2}{|\mathbf{q}|^6} - 4\,\frac{q_1\,q_3 + q_2\,q_4}{|\mathbf{q}|^4}\,,
\end{aligned}
$$

$$-4\,\frac{q_3\,q_2}{|\mathbf{q}|^4} - 4\,\frac{q_4\,q_1}{|\mathbf{q}|^4} + 16\,\frac{(\,q_1\,q_3 + q_2\,q_4\,)\,q_4\,q_3}{|\mathbf{q}|^6}].$$

The fourth row of $\mathbf{\Lambda}_{13}$ is

$$[-4\,\frac{q_2\,q_1}{|\mathbf{q}|^4} - 4\,\frac{q_3\,q_4}{|\mathbf{q}|^4} + 16\,\frac{(\,q_1\,q_3 + q_2\,q_4\,)\,q_4\,q_1}{|\mathbf{q}|^6},$$
$$2\,\frac{1}{|\mathbf{q}|^2} - 4\,\frac{q_2^2}{|\mathbf{q}|^4} - 4\,\frac{q_4^2}{|\mathbf{q}|^4} + 16\,\frac{(\,q_1\,q_3 + q_2\,q_4\,)\,q_4\,q_2}{|\mathbf{q}|^6},$$
$$-4\,\frac{q_3\,q_2}{|\mathbf{q}|^4} - 4\,\frac{q_4\,q_1}{|\mathbf{q}|^4} + 16\,\frac{(\,q_1\,q_3 + q_2\,q_4\,)\,q_4\,q_3}{|\mathbf{q}|^6},$$
$$-8\,\frac{q_4\,q_2}{|\mathbf{q}|^4} + 16\,\frac{(\,q_1\,q_3 + q_2\,q_4\,)\,q_4^2}{|\mathbf{q}|^6} - 4\,\frac{q_1\,q_3 + q_2\,q_4}{|\mathbf{q}|^4}]$$

The first row of $\mathbf{\Lambda}_{23}$ is

$$= \quad [8\,\frac{q_4\,q_1}{|\mathbf{q}|^4} + 16\,\frac{(\,q_3\,q_2 - q_4\,q_1\,)\,q_1^2}{|\mathbf{q}|^6} - 4\,\frac{q_3\,q_2 - q_4\,q_1}{|\mathbf{q}|^4},$$
$$-4\,\frac{q_3\,q_1}{|\mathbf{q}|^4} + 4\,\frac{q_4\,q_2}{|\mathbf{q}|^4} + 16\,\frac{(\,q_3\,q_2 - q_4\,q_1\,)\,q_2\,q_1}{|\mathbf{q}|^6},$$
$$-4\,\frac{q_2\,q_1}{|\mathbf{q}|^4} + 4\,\frac{q_3\,q_4}{|\mathbf{q}|^4} + 16\,\frac{(\,q_3\,q_2 - q_4\,q_1\,)\,q_3\,q_1}{|\mathbf{q}|^6},$$
$$-2\,\frac{1}{|\mathbf{q}|^2} + 4\,\frac{q_1^2}{|\mathbf{q}|^4} + 4\,\frac{q_4^2}{|\mathbf{q}|^4} + 16\,\frac{(\,q_3\,q_2 - q_4\,q_1\,)\,q_4\,q_1}{|\mathbf{q}|^6}].$$

The second row of $\mathbf{\Lambda}_{23}$ is

$$[-4\,\frac{q_3\,q_1}{|\mathbf{q}|^4} + 4\,\frac{q_4\,q_2}{|\mathbf{q}|^4} + 16\,\frac{(\,q_3\,q_2 - q_4\,q_1\,)\,q_2\,q_1}{|\mathbf{q}|^6},$$
$$-8\,\frac{q_3\,q_2}{|\mathbf{q}|^4} + 16\,\frac{(\,q_3\,q_2 - q_4\,q_1\,)\,q_2^2}{|\mathbf{q}|^6} - 4\,\frac{q_3\,q_2 - q_4\,q_1}{|\mathbf{q}|^4},$$
$$2\,\frac{1}{|\mathbf{q}|^2} - 4\,\frac{q_2^2}{|\mathbf{q}|^4} - 4\,\frac{q_3^2}{|\mathbf{q}|^4} + 16\,\frac{(\,q_3\,q_2 - q_4\,q_1\,)\,q_3\,q_2}{|\mathbf{q}|^6},$$
$$4\,\frac{q_2\,q_1}{|\mathbf{q}|^4} - 4\,\frac{q_3\,q_4}{|\mathbf{q}|^4} + 16\,\frac{(\,q_3\,q_2 - q_4\,q_1\,)\,q_4\,q_2}{|\mathbf{q}|^6}].$$

The third row of $\mathbf{\Lambda}_{23}$ is

$$[-4\,\frac{q_2\,q_1}{|\mathbf{q}|^4} + 4\,\frac{q_3\,q_4}{|\mathbf{q}|^4} + 16\,\frac{(\,q_3\,q_2 - q_4\,q_1\,)\,q_3\,q_1}{|\mathbf{q}|^6},$$
$$2\,\frac{1}{|\mathbf{q}|^2} - 4\,\frac{q_2^2}{|\mathbf{q}|^4} - 4\,\frac{q_3^2}{|\mathbf{q}|^4} + 16\,\frac{(\,q_3\,q_2 - q_4\,q_1\,)\,q_3\,q_2}{|\mathbf{q}|^6},$$
$$-8\,\frac{q_3\,q_2}{|\mathbf{q}|^4} + 16\,\frac{(\,q_3\,q_2 - q_4\,q_1\,)\,q_3^2}{|\mathbf{q}|^6} - 4\,\frac{q_3\,q_2 - q_4\,q_1}{|\mathbf{q}|^4},$$
$$4\,\frac{q_3\,q_1}{|\mathbf{q}|^4} - 4\,\frac{q_4\,q_2}{|\mathbf{q}|^4} + 16\,\frac{(\,q_3\,q_2 - q_4\,q_1\,)\,q_4\,q_3}{|\mathbf{q}|^6}].$$

The fourth row of $\mathbf{\Lambda}_{23}$ is

$$
\begin{aligned}
= \quad [&-2\,\frac{1}{|\mathbf{q}|^2} + 4\,\frac{q_1^2}{|\mathbf{q}|^4} + 4\,\frac{q_4^2}{|\mathbf{q}|^4} + 16\,\frac{(\,q_3\,q_2 - q_4\,q_1\,)\,q_4\,q_1}{|\mathbf{q}|^6}\,,\\
&4\,\frac{q_2\,q_1}{|\mathbf{q}|^4} - 4\,\frac{q_3\,q_4}{|\mathbf{q}|^4} + 16\,\frac{(\,q_3\,q_2 - q_4\,q_1\,)\,q_4\,q_2}{|\mathbf{q}|^6}\,,\\
&4\,\frac{q_3\,q_1}{|\mathbf{q}|^4} - 4\,\frac{q_4\,q_2}{|\mathbf{q}|^4} + 16\,\frac{(\,q_3\,q_2 - q_4\,q_1\,)\,q_4\,q_3}{|\mathbf{q}|^6}\,,\\
&8\,\frac{q_4\,q_1}{|\mathbf{q}|^4} + 16\,\frac{(\,q_3\,q_2 - q_4\,q_1\,)\,q_4^2}{|\mathbf{q}|^6} - 4\,\frac{q_3\,q_2 - q_4\,q_1}{|\mathbf{q}|^4}].
\end{aligned}
$$

The first row of $\mathbf{\Lambda}_{33}$ is

$$
\begin{aligned}
[&-2\,\frac{1}{|\mathbf{q}|^2} + 8\,\frac{q_1^2}{|\mathbf{q}|^4} + 8\,\frac{(-q_1^2 - q_2^2 + q_3^2 + q_4^2)\,q_1^2}{|\mathbf{q}|^6} - 2\,\frac{(-q_1^2 - q_2^2 + q_3^2 + q_4^2)}{|\mathbf{q}|^4}\,,\\
&8\,\frac{q_2\,q_1}{|\mathbf{q}|^4} + 8\,\frac{(-q_1^2 - q_2^2 + q_3^2 + q_4^2)\,q_2\,q_1}{|\mathbf{q}|^6}\,,\\
&8\,\frac{(-q_1^2 - q_2^2 + q_3^2 + q_4^2)\,q_3\,q_1}{|\mathbf{q}|^6}\,, 8\,\frac{(-q_1^2 - q_2^2 + q_3^2 + q_4^2)\,q_4\,q_1}{|\mathbf{q}|^6}].
\end{aligned}
$$

The second row of $\mathbf{\Lambda}_{33}$ is

$$
\begin{aligned}
= \quad [&8\,\frac{q_2\,q_1}{|\mathbf{q}|^4} + 8\,\frac{(-q_1^2 - q_2^2 + q_3^2 + q_4^2)\,q_2\,q_1}{|\mathbf{q}|^6}\,,\\
&-2\,\frac{1}{|\mathbf{q}|^2} + 8\,\frac{q_2^2}{|\mathbf{q}|^4} + 8\,\frac{(-q_1^2 - q_2^2 + q_3^2 + q_4^2)\,q_2^2}{|\mathbf{q}|^6} - 2\,\frac{(-q_1^2 - q_2^2 + q_3^2 + q_4^2)}{|\mathbf{q}|^4}\,,\\
&8\,\frac{(-q_1^2 - q_2^2 + q_3^2 + q_4^2)\,q_3\,q_2}{|\mathbf{q}|^6}\,, 8\,\frac{(-q_1^2 - q_2^2 + q_3^2 + q_4^2)\,q_4\,q_2}{|\mathbf{q}|^6}].
\end{aligned}
$$

The third row of $\mathbf{\Lambda}_{33}$ is

$$
\begin{aligned}
[&8\,\frac{(-q_1^2 - q_2^2 + q_3^2 + q_4^2)\,q_3\,q_1}{|\mathbf{q}|^6}\,,\\
&8\,\frac{(-q_1^2 - q_2^2 + q_3^2 + q_4^2)\,q_3\,q_2}{|\mathbf{q}|^6}\,,\\
&2\,\frac{1}{|\mathbf{q}|^2} - 8\,\frac{q_3^2}{|\mathbf{q}|^4} + 8\,\frac{(-q_1^2 - q_2^2 + q_3^2 + q_4^2)\,q_3^2}{|\mathbf{q}|^6} - 2\,\frac{(-q_1^2 - q_2^2 + q_3^2 + q_4^2)}{|\mathbf{q}|^4},\\
&-8\,\frac{q_3\,q_4}{|\mathbf{q}|^4} + 8\,\frac{(-q_1^2 - q_2^2 + q_3^2 + q_4^2)\,q_4\,q_3}{|\mathbf{q}|^6}].
\end{aligned}
$$

The fourth row of $\mathbf{\Lambda}_{33}$ is

$$
\begin{aligned}
[&8\,\frac{(-q_1^2 - q_2^2 + q_3^2 + q_4^2)\,q_4\,q_1}{|\mathbf{q}|^6}\,, 8\,\frac{(-q_1^2 - q_2^2 + q_3^2 + q_4^2)\,q_4\,q_2}{|\mathbf{q}|^6}\,,\\
&-8\,\frac{q_3\,q_4}{|\mathbf{q}|^4} + 8\,\frac{(-q_1^2 - q_2^2 + q_3^2 + q_4^2)\,q_4\,q_3}{|\mathbf{q}|^6}\,,\\
&2\,\frac{1}{|\mathbf{q}|^2} - 8\,\frac{q_4^2}{|\mathbf{q}|^4} + 8\,\frac{(-q_1^2 - q_2^2 + q_3^2 + q_4^2)\,q_4^2}{|\mathbf{q}|^6} - 2\,\frac{(-q_1^2 - q_2^2 + q_3^2 + q_4^2)}{|\mathbf{q}|^4}].
\end{aligned}
$$

Bibliography

[1] S. S. Antman. *Nonlinear Problems of Elasticity.* Springer-Verlag, 1995.

[2] W. R. Bauer, R. A. Lund, and J. H. White. Twist and writhe of a DNA loop containing intrinsic bends. *Proc. Natl. Acad. Sci. USA*, 90:833–837, Feb 1993.

[3] C. J. Benham. Elastic model of supercoiling. *Proc. Natl. Acad. Sci. U.S.A.*, 74:2397–2401, 1977.

[4] C. J. Benham. An elastic model of the large-scale structure of duplex DNA. *Biopolymers*, 18:609–623, 1979.

[5] C. J. Benham. Geometry and mechanics of DNA superhelicity. *Biopolymers*, 22:2477–2495, 1983.

[6] T. B. Benjamin. The stability of solitary waves. *Proc. R. Soc. Lond. A.*, 328:153–183, 1972.

[7] O. Bolza. *Lectures on the Calculus of Variations.* Chelsea Publishing Company, 1973.

[8] R. Bott. Nondegenerate critical manifolds. *Annals of Mathematics*, 60(2):248–261, 1954.

[9] M. C. Crandall and P. H. Rabinowitz. Bifurcation, perturbation of simple eigenvalues and linearized stability. *Archive for Rational Mechanics and Analysis*, 52:160–192, 1973.

[10] D. J. Dichmann. *Hamiltonian Dynamics of a Spatial Elastica and the Stability of Solitary Waves.* PhD thesis, University of Maryland, College Park, 1994.

[11] D. J. Dichmann, Y. Li, and J. H. Maddocks. Hamiltonian formulations and symmetries in rod mechanics. In J. P. Mesirov, K. Schulten, and D. W. Sumners, editors, *Mathematical Approaches to Biomolecular Structure and Dynamics*, volume 82 of *The IMA Volumes in Mathematics and Its Applications*, pages 71–113, 1996.

[12] E. J. Doedel, H. B. Keller, and J. P. Kernévez. Numerical analysis and control of bifurcation problems, part II. *International Journal of Bifuration and Chaos*, 4:745–772, 1991.

[13] G. Domokos and R. C. Paffenroth. Case study: Visualization for boundary value problems. In R. D. Bergeron and A. E. Kaufman, editors, *IEEE Visualization '94 Conference Proceedings*, pages 345–348. IEEE Computer Society Press, 1994.

[14] G. Domokos and R. C. Paffenroth. *PCR* - a visualization tool for multi-point boundary value problems. Technical Report BN-1167, Institute for Physical Science and Technology, University of Maryland, College Park, 1994.

[15] G. M. Ewing. *Calculus of Variations with Applications.* Dover Publications, 1969.

[16] I. M. Gelfand and S. V. Fomin. *Calculus of Variations.* Prentice-Hall, 1963.

[17] H. Goldstein. *Classical Mechanics.* Addison-Wesley, 1980.

[18] A. Goriely and M. Tabor. Nonlinear dynamics of filaments I: Dynamical instabilities. *Physica D*, to appear.

[19] A. Goriely and M. Tabor. Nonlinear dynamics of filaments II: Nonlinear analysis. *Physica D*, to appear.

[20] J. Gregory and C. Lin. *Constrained Optimization in the Calculus of Variations and Optimal Control Theory.* Van Nostrand Reinhold, 1992.

[21] J. Hale and H. Koçak. *Dynamics and Bifurcations.* Springer-Verlag, New York, 1991.

[22] C. Hassell and E. Rees. The index of a constrained critical point. *Amer. Math. Monthly*, 100(8):772–778, 1993.

[23] M. R. Hestenes. *Calculus of Variations and Optimal Control Theory.* Robert E. Krieger Publishing Company, 1966.

[24] G. Iooss and D. Joseph. *Elementary Stability and Bifurcation Theory.* Springer-Verlag, 1980.

[25] F. Jülicher. Supercoiling transitions of a closed DNA. *Physical Review E*, 49, 1994.

[26] J. Junkins and J. Turner. *Optimal Spacecraft Rotational Maneuvers.* Elsevier, 1986.

[27] J. D. Kahn and D. M. Crothers. Protein-induced bending and DNA cyclization. *Proc. Natl. Acad. Sci. USA*, 89:6343–6347, 1992.

[28] J. D. Kahn and D. M. Crothers. Measurement of the DNA bend angle induced by the catabolite activator protein using monte carlo simulation of cyclized kinetics. *Journal of Molecular Biology*, submitted.

[29] T. Kato. *Perturbation Theory for Linear Operators.* Springer-Verlag, Berlin, 1984.

[30] S. Kehrbaum and J. H. Maddocks. Effective properties of elastic rods with high intrinsic twist. preprint.

[31] J. Langer and D. Singer. Knotted elastic curves in $\mathbf{R}^3$. *J. London Math. Soc.*, 2(30):512–520, 1984.

[32] J. Langer and D. Singer. Lagrangian aspects of the Kirchhoff elastic rod. *SIAM Review*, 38(4):605–618, 1996.

[33] M. LeBret. Relationship between the energy of superhelix formation, the shear modulus, and the torsional brownian motion of DNA. *Biopolymers*, 17:1939–1955, 1978.

[34] M. LeBret. Catastrophic variation of twist and writhing of circular DNA with constraint. *Biopolymers*, 18:1709–1725, 1979.

[35] S. D. Levene. Conformation and energetics of supercoiled DNA: Experimental and theoretical studies. In F. Eckstein and D. M. J. Lilley, editors, *Nucleic Acids and Molecular Biology*, volume 8, pages 119–132. Springer-Verlag, Berlin, 1994.

[36] H. Li. *Geometrically Constrained Curves and the Calculus of Variations.* PhD thesis, Rice University, 1986.

[37] Y. Li and J. H. Maddocks. On the computation of equilibria of elastic rods, part I: Integrals, symmetry and a hamiltonian formulation. *J. Comp. Physics*, to appear.

[38] A. E. H. Love. *A Treatise on the Mathematica Theory of Elasticity.* Dover, 1944.

[39] J. H. Maddocks. On second-order conditions in constrained variational principles. JOTA to appear.

[40] J. H. Maddocks. Stability of nonlinearly elastic rods. *Arch. Rational Mech. Anal.*, 85(4):180–198, 1984.

[41] J. H. Maddocks. Restricted quadratic forms and their application to bifurcation and stability in constrained variational principles. *SIAM J. Math. Anal.*, 16:47–68, 1985. Errata (1988) can be found in vol. 19, pp. 1256–1257.

[42] J. H. Maddocks. Stability and folds. *Arch. Rat. Mech. Anal.*, 99:301–328, 1987.

[43] J. H. Maddocks. Restricted quadratic forms, inertia theorems, and the Schur complement. *Linear Algebra and Appl.*, 1988.

[44] H. B. Mann. Quadratic forms with linear constraints. *Amer. Math. Monthly*, 50:430–433, 1943.

[45] R. S. Manning, J. H. Maddocks, and J. D. Kahn. A continuum model of sequence-dependent DNA structure. *J. Chemical Physics*, 105(13):5626–5646, 1996.

[46] R. S. Manning, K. A. Rogers, and J. H. Maddocks. Isoperimetric conjuate points and stability of DNA minicircles. in preparation.

[47] M. Morse. *Introduction to Analysis in the Large.* Institute for Advanced Study, 1951.

[48] A. Naylor and G. Sell. *Linear Operator Theory in Engineering and Science*, volume 40 of *Applied Mathematics Sciences.* Springer-Verlag, 1982.

[49] W. K. Olson. Simulating DNA at low resolution. *Current Opinion in Structural Biology*, 6:242–256, 1996.

[50] M. Reed and B. Simon. *Methods of Modern Mathematical Physics, IV: Analysis of Operators.* Academic Press, 1978.

[51] M. Renardy and R. Rogers. *An Introduction to Partial Differential Equations.* Springer-Verlag, New York, 1993.

[52] H. Sagan. *Introduction to the Calculus of Variations.* Dover Publications, 1969.

[53] D. H. Sattinger. Stability of solutions of nonlinear equations. *J. Math. Anal. & Appl.*, 39:1–12, 1972.

[54] T. Schlick. Modeling superhelical DNA: Recent analytical and dynamical approaches. *Current Opinion in Structural Biology*, 5:245–262, 1995.

[55] L. S. Schulman. *Techniques and Applications of Path Integration.* Wiley, New York, 1981.

[56] J. Segercrantz. On the existence of conjugate points for a constrained minimization problem. *J. Comput. Appl. Math.*, 10(3):385–386, 1984.

[57] L. F. Shampine and M. K. Gordon. *Computer Solution of Ordinary Differential Equations: The Initial Value Problem.* W. H. Freeman, San Francisco, 1975.

[58] Y. Shi, A. Borovik, and J. E. Hearst. An elastic rod model incorporating deformations of shear and extension: Novel closed-form solutions for the stationary states of supercoiled DNA. draft manuscript.

[59] Y. Shi and J. E. Hearst. The Kirchhoff elastic rod, the nonlinear Schrödinger equation, and DNA supercoiling. *J. Chemical Physics*, 101(6):5186–5200, 1994.

[60] M. D. Shuster. A survey of attitude representations. *Journal of Astronautical Sciences*, 1994.

[61] D. Spring. On the second derivative test for constrained local extrema. *Amer. Math. Monthly*, 1985.

[62] I. Stakgold. *Boundary Value Problems of Mathematical Physics*. MacMillan Company, 1967.

[63] E. L. Starostin. Three dimensional conformations of looped DNA in an elastomechanical approximation. In Chien Wei-zang, editor, *Proceedings of the 2nd International Conference on Nonlinear Mechanics*, pages 188–190, Beijing, China, 1993. Peking University Press.

[64] E. L. Starostin. Three-dimensional shapes of looped DNA. *Meccanica*, 31:235–271, 1996.

[65] I. Tobias and W. K. Olson. The effect of intrinsic curvature on supercoiling: Predictions of elasticity theory. *Biopolymers*, 33:639–646, 1993.

[66] T. Vogel. On constrained extrema. *Pacific Journal of Mathematics*, 176(2), 1996.

[67] M. Wadati and H. Tsuru. Elastic model of looped DNA. *Physica D*, 21:213–226, 1986.

[68] H. Weinberger. On the stability of bifurcating solutions. In *Nonlinear Analysis*. Academic Press, 1978.

[69] A. Weinstein and W. Stenger. *Methods of Intermediate Problems for Eigenvalues: Theory and Ramifications*. Academic Press, New York, 1972.

[70] E. E. Zajac. Stability of two planar loop elasticas. *Transactions of the ASME*, 29:136–142, March 1962.